Calhoun: The NPS Institutional Archive

DSpace Repository

Theses and Dissertations | 1. Thesis and Dissertation Collection, all items

2019-12

TRIBOELECTRIC GENERATOR FOR ENERGY HARVESTING

Mann, Katherine Y.

Monterey, CA; Naval Postgraduate School

http://hdl.handle.net/10945/64018

This publication is a work of the U.S. Government as defined in Title 17, United States Code, Section 101. Copyright protection is not available for this work in the United States.

Downloaded from NPS Archive: Calhoun

http://www.nps.edu/library

Calhoun is the Naval Postgraduate School's public access digital repository for research materials and institutional publications created by the NPS community. Calhoun is named for Professor of Mathematics Guy K. Calhoun, NPS's first appointed -- and published -- scholarly author.

Dudley Knox Library / Naval Postgraduate School
411 Dyer Road / 1 University Circle
Monterey, California USA 93943

NAVAL POSTGRADUATE SCHOOL

MONTEREY, CALIFORNIA

THESIS

TRIBOELECTRIC GENERATOR FOR ENERGY HARVESTING

by

Katherine Y. Mann

December 2019

Thesis Advisor: Young W. Kwon
Second Reader: Jarema M. Didoszak

Approved for public release. Distribution is unlimited.

THIS PAGE INTENTIONALLY LEFT BLANK

REPORT DOCUMENTATION PAGE			*Form Approved OMB No. 0704-0188*

Public reporting burden for this collection of information is estimated to average 1 hour per response, including the time for reviewing instruction, searching existing data sources, gathering and maintaining the data needed, and completing and reviewing the collection of information. Send comments regarding this burden estimate or any other aspect of this collection of information, including suggestions for reducing this burden, to Washington headquarters Services, Directorate for Information Operations and Reports, 1215 Jefferson Davis Highway, Suite 1204, Arlington, VA 22202-4302, and to the Office of Management and Budget, Paperwork Reduction Project (0704-0188) Washington, DC 20503.

1. AGENCY USE ONLY *(Leave blank)*	**2. REPORT DATE** December 2019	**3. REPORT TYPE AND DATES COVERED** Master's thesis

4. TITLE AND SUBTITLE TRIBOELECTRIC GENERATOR FOR ENERGY HARVESTING	**5. FUNDING NUMBERS**
6. AUTHOR(S) Katherine Y. Mann	
7. PERFORMING ORGANIZATION NAME(S) AND ADDRESS(ES) Naval Postgraduate School Monterey, CA 93943-5000	**8. PERFORMING ORGANIZATION REPORT NUMBER**
9. SPONSORING / MONITORING AGENCY NAME(S) AND ADDRESS(ES) N/A	**10. SPONSORING / MONITORING AGENCY REPORT NUMBER**

11. SUPPLEMENTARY NOTES The views expressed in this thesis are those of the author and do not reflect the official policy or position of the Department of Defense or the U.S. Government.

12a. DISTRIBUTION / AVAILABILITY STATEMENT Approved for public release. Distribution is unlimited.	**12b. DISTRIBUTION CODE** A

13. ABSTRACT (maximum 200 words)

The open ocean and coastal environments provide an abundant amount of unharvested energy. It would be powerful if the U.S. Navy could harness more of the ocean's tidal movements, wave oscillations, and vibrations to power its ports and vehicles. A linear sliding contact-mode triboelectric nanogenerator (TENG) consisting of two interdigitative copper electrodes and polytetrafluoroethylene (PTFE) adhesive tape was constructed on 3D printed material. To improve the TENG's performance in low frequency, ocean wave conditions, a gear system proved the concept that the relatively low frequencies of waves could be increased to produce more power from a sliding contact-mode TENG. Next, a tabletop system and wave tank apparatus, which included a spring and pulley, were developed to translate linear, reciprocating motion 90°. This system converted the vertical heaving motion of ocean waves to horizontal reciprocating linear motion at a safe distance from the harsh environment of the ocean surface. A frequency analysis was conducted on each experiment to investigate both the alternating current (AC) voltage and closed-circuit current of the TENG to quantify the potential power and power density.

14. SUBJECT TERMS triboelectric nanogenerator, TENG, ocean energy harvesting, energy production and storage, U.S. Navy energy	**15. NUMBER OF PAGES** 129
	16. PRICE CODE

17. SECURITY CLASSIFICATION OF REPORT Unclassified	**18. SECURITY CLASSIFICATION OF THIS PAGE** Unclassified	**19. SECURITY CLASSIFICATION OF ABSTRACT** Unclassified	**20. LIMITATION OF ABSTRACT** UU

NSN 7540-01-280-5500

Standard Form 298 (Rev. 2-89)
Prescribed by ANSI Std. 239-18

THIS PAGE INTENTIONALLY LEFT BLANK

Approved for public release. Distribution is unlimited.

TRIBOELECTRIC GENERATOR FOR ENERGY HARVESTING

Katherine Y. Mann
Lieutenant, United States Navy
BS, U.S. Naval Academy, 2013

Submitted in partial fulfillment of the
requirements for the degree of

MASTER OF SCIENCE IN MECHANICAL ENGINEERING

from the

NAVAL POSTGRADUATE SCHOOL
December 2019

Approved by: Young W. Kwon
Advisor

Jarema M. Didoszak
Second Reader

Garth V. Hobson
Chair, Department of Mechanical and Aerospace Engineering

THIS PAGE INTENTIONALLY LEFT BLANK

ABSTRACT

The open ocean and coastal environments provide an abundant amount of unharvested energy. It would be powerful if the U.S. Navy could harness more of the ocean's tidal movements, wave oscillations, and vibrations to power its ports and vehicles. A linear sliding contact-mode triboelectric nanogenerator (TENG) consisting of two interdigitative copper electrodes and polytetrafluoroethylene (PTFE) adhesive tape was constructed on 3D printed material. To improve the TENG's performance in low frequency, ocean wave conditions, a gear system proved the concept that the relatively low frequencies of waves could be increased to produce more power from a sliding contact-mode TENG. Next, a tabletop system and wave tank apparatus, which included a spring and pulley, were developed to translate linear, reciprocating motion 90°. This system converted the vertical heaving motion of ocean waves to horizontal reciprocating linear motion at a safe distance from the harsh environment of the ocean surface. A frequency analysis was conducted on each experiment to investigate both the alternating current (AC) voltage and closed-circuit current of the TENG to quantify the potential power and power density.

THIS PAGE INTENTIONALLY LEFT BLANK

TABLE OF CONTENTS

I. INTRODUCTION....1
A. MOTIVATION....1
B. LITERATURE REVIEW....3
1. TENG Modes, Designs and Characteristics....4
2. TENG Networks....16
3. Challenges....23
4. Potential of Blue Energy TENGs....26

II. EXPERIMENTATION PROCESS....29
A. DEVELOPMENT OF NPS TENG MODEL....29
1. NASA Ames Model....29
2. NPS TENG Model....32
B. USING GEAR BOX FOR FURTHER FREQUENCY ANALYSIS....40
1. Development of Gear Box....41
2. Converting Reciprocating Linear Wave Motion to One Direction Circular Motion....45
C. PULLEY SYSTEM TO FACILITATE HORIZONTAL MOTION AND WATER PROTECTION....48
1. Linear Motor, Tabletop System....50
2. Oscillating Column, Wave Tank System....51
D. MEASUREMENT SYSTEM....54

III. RESULTS FROM EXPERIMENTATION....57
A. EXPERIMENTAL RESULTS OF TENG FREQUENCY ANALYSIS WITH ATTACHED GEAR BOX AND CIRCULAR MOTION....57
1. Voltage Data....58
2. Current Data....59
3. Summary of Frequency Analysis Results....62
B. EXPERIMENTAL RESULTS OF PULLEY SYSTEM TENG USING LINEAR MOTOR....65
1. Voltage Data....66
2. Current Data....69
3. Summary of Tabletop Pulley....70
C. EXPERIMENTAL RESULTS OF PULLEY SYSTEM WAVETANK TENG USING WAVE TANK....72
1. Voltage Data....72

2. Current Data 74
3. Summary of WT Pulley 76

IV. CONCLUSION AND FUTURE WORK 79
A. CONCLUSION 79
B. RECOMMENDATIONS AND ERROR ANALYSIS 80
C. FUTURE WORK 81

APPENDIX A. TENG FREQUENCY ANALYSIS RESULTS 83

APPENDIX B. LINEAR RECIPROCATING MOTOR RESULTS 89

APPENDIX C. WAVE TANK RESULTS 99

LIST OF REFERENCES 105

INITIAL DISTRIBUTION LIST 109

LIST OF FIGURES

Figure 1. Fundamental Working Modes of TENGs. Source: [4]. 5

Figure 2. Floating Oscillator-Embedded Triboelectric Generator Source: [7]. 8

Figure 3. Structural Parameters Analyzed with FO-TENG. Source: [7]. 9

Figure 4. FO-TEG Potential under Various Input Vibration Types. Source: [7]. 10

Figure 5. Design and Composition of Floating TENG. Source: [1]. 11

Figure 6. TENG Network. Source: [1]. 12

Figure 7. Enclosed Ball TENG Source [1]. 13

Figure 8. Rolling Rod and Interdigitative Electrode TENG. Source [9]. 14

Figure 9. Electron Transfer on Interdigitative Electrodes. Source: [9]. 15

Figure 10. Voltage vs Copper Rod Displacement on Interdigitative Electrode. Source: [9]. 15

Figure 11. Air Driven TENG. Source: [10]. 16

Figure 12. Air Driven TENG in Ocean Waves. Source: [10]. 17

Figure 13. Spring Assisted TENG. Source: [5]. 19

Figure 14. Effects of Spring Rigidity on Spring Assisted TENG Source: [5]. 20

Figure 15. TENG Using Springs. Source: [5]. 20

Figure 16. Wavy-Structured, Direct Water-Wave-Impact TENG. Source: [13]. 22

Figure 17. Circuit Diagram of TENG Charging Capacitor. Source: [13]. 22

Figure 18. Voltage vs Relative Humidity for FO-TENG. Source: [14]. 26

Figure 19. TENG Powered by Blue Energy. Source:[26]. 27

Figure 20. NASA Ames 3D Printed TENG. Source: [28] 29

Figure 21. Charge Transfer across NASA Ames TENG Interdigitative Electrode. Source: [28]. 30

Figure 22. NASA Ames TENG: Vibration Frequency vs. Average Current Output at Various Amplitudes. Source: [28]. 31

Figure 23. NASA Ames TENG: Voltage and Current vs. Time at Various Frequencies 32

Figure 24. Machined Copper Electrode 33

Figure 25. Solidworks Designs For 3D Printed Electrode Cradle (a) and Track (b). Source: [29]. 34

Figure 26. Tracks Used by ENS Sarah Reilly [29] 34

Figure 27. Track for Triboelectric Material 36

Figure 28. Components of Oscillating Column as Designed in Solidworks. Source: [29]. 37

Figure 29. Complete Oscillating Column with Attached Electrode Side of NPS TENG. Source: [29]. 37

Figure 30. The OC in the NPS Wave Tank as Positioned Before Data Collection. Source: [29]. 38

Figure 31. Frequency vs Maximum Peak-to-Peak AC Voltage Output for TENG in Wave Tank. Source: [29]. 40

Figure 32. LEGO Mindstorm EV3 Intelligent Brick (left) and Medium Servo Motor (right) 42

Figure 33. MCM Working Mechanism 42

Figure 34. Driving Gear and Driven Gear for MCM 43

Figure 35. MCM Depicting Shafts 1, 2, and 3 44

Figure 36. Experimental Setup of MCM 45

Figure 37. MCS System 46

Figure 38. Complete MCM and MCS System 48

Figure 39. Conceptual Design of Tabletop and Wave Tank System 49

Figure 40. Components of Tabletop and Wave Tank Systems 51

Figure 41. Linear Motor Tabletop Assembly 51

Figure 42. Oscillating Column with TENG Pulley-Spring System 53

Figure 43. Pulley-Spring System for Wave Tank Assembly 53

Figure 44. MCM Voltage Testing with Teledyne Lecroy Oscilloscope 55

Figure 45. Bemonoc DIY Design DC 24V Linear Actuator Reciprocating Motor with a 70-Millimeter Stroke 56
Figure 46. Maximum Peak-Peak AC Voltage for Each Frequency Tested 59
Figure 47. Closed Circuit Current at 1:1 Gear Ratio and 0.408 Hertz 60
Figure 48. Closed Circuit Current at 1:3 Gear Ratio and 6.125 Hertz 60
Figure 49. Maximum Closed-Circuit Current during Frequency Analysis Testing 61
Figure 50. Averaged Maximum Peak-Peak AC Voltage vs. Frequency for NPS TENG 63
Figure 51. Averaged Maximum Closed-Circuit Current vs. Frequency for NPS TENG 63
Figure 52. The Potential Power Generated vs. Frequency 64
Figure 53. The Potential Power Density vs. Frequency 65
Figure 54. TENG Frequency and AC Peak-Peak Voltage for Tabletop Test 66
Figure 55. Track C: Peak-Peak AC Voltage at 0.696 Hertz 67
Figure 56. Track C: Peak-Peak AC Voltage at 1.320 Hertz 68
Figure 57. Track C: Peak-Peak AC Voltage at 2.168 Hertz 68
Figure 58. TENG Frequency and Closed Circuit for Tabletop Test 69
Figure 59. TENG Frequency and Potential Power Generated during Tabletop Test 70
Figure 60. TENG Frequency and Potential Power Density during Tabletop Test 71
Figure 61. TENG Frequency and AC Peak-Peak Voltage for Wave Tank Test 73
Figure 62. Peak-Peak AC Voltage at 1.147 Hertz in Wave Tank 74
Figure 63. TENG Frequency and Closed Circuit for Wave Tank Test 75
Figure 64. TENG Frequency and Potential Power Generated for Wave Tank Test 76
Figure 65. TENG Frequency and Potential Power Density for Wave Tank Test 77

THIS PAGE INTENTIONALLY LEFT BLANK

LIST OF TABLES

Table 1. Individual vs Network of Air Driven Oscillator TENGs. Source: [10]. 18

Table 2. Summary of OC and TENG Testing. Source: [29]. 39

Table 3. Frequencies Tested with MCM for Frequency Analysis 58

Table 4. Summary of Maximum, Averaged Peak-Peak AC Voltage and Closed-Circuit Current for Frequency Analysis Testing..... 62

Table 5. Summary of Maximum, Averaged Potential Power and Power Density for Frequency Analysis Testing 64

Table 6. Linear Motor Speed in Hertz..... 66

Table 7. Summary of AC Peak-Peak Voltage for Tabletop Test 66

Table 8. Summary of Closed Circuit Current for Tabletop Test..... 69

Table 9. Summary of Potential Power for Tabletop Test 71

Table 10. Summary of Potential Power Density for Tabletop Test 71

Table 11. Summary of AC Peak-Peak Voltage for Wave Tank Test 73

Table 12. Summary of Closed Circuit Current for Wave Tank Test 75

Table 13. Summary of Potential Power for Wave Tank Test..... 77

Table 14. Summary of Potential Power Density for Wave Tank Test..... 77

THIS PAGE INTENTIONALLY LEFT BLANK

LIST OF ACRONYMS AND ABBREVIATIONS

AC	alternating current
EMG	electromagnetic generator
FEP	fluorinated ethylene propylene
FO-TEG	floating oscillator-embedded triboelectric generator
IE-TENG	interfacial electrification enabled triboelectric nanogenerator
LED	light-emitting diode
MCM	motion conversion mechanism
MCS	motion conversion system
NASA	National Aeronautics and Space Administration
NOAA	National Oceanic and Atmospheric Administration
NPS	Naval Postgraduate School
OC	oscillating column
OWC	oscillating water column
PDMS	polydimethylsiloxane
PET	polyethylene terephthalate
PLA	polylactic acid
PMMA	polymethyl methacrylate
PTFE	polytetrafluoroethylene
PU	polyurethane
RPM	rotations per minute
SEM	scanning electron microscope
TENG	triboelectric nanogenerator

THIS PAGE INTENTIONALLY LEFT BLANK

ACKNOWLEDGMENTS

I would like to thank Dr. Young Kwon for his encouragement and guidance throughout my time here at the Naval Postgraduate School. During my first quarter, he exposed me to the TENG research at the NASA Ames Research Center and has since enlightened me on the incredible research being done throughout NPS and academia. I am very thankful to Professor Didoszak for his advice and support throughout my thesis process as well. Much gratitude to John Mobley of the Mechanical Engineering Machine Lab and STG1 Cauffiel in the RoboDojo, for their help in fabricating the various 3D-printed and machined pieces for this project. I am incredibly appreciative to Warren Rogers, Frank Levin, and Matthew Porter of the Electrical Engineering department for their many hours of patience and for their generosity with their time, space, and electrical equipment.

ENS Sarah Reilly, a recent NPS graduate, developed the wave column, TENG attachment, and facilitated all my follow-on research. I wish her the best of luck as she enters the Nuclear Navy as a Submarine Officer. Finally, I would like to thank my family—both near and far—for their endless help day in and day out while at graduate school. I am so grateful for my husband, Jay, and twin, Beth, both fellow NPS students, for their unwavering encouragement and inspiration.

THIS PAGE INTENTIONALLY LEFT BLANK

I. INTRODUCTION

A. MOTIVATION

As global energy demand increases, renewable energy sources are vital for the future sustainability and development of human civilization [1]. Fossil fuel supplies are definite and have fluctuating costs due to political conditions, natural disasters or transportation requirements. Since water covers over 70% of the earth's surface, harvesting its power has incredible potential. The kinetic energy produced by waves and tidal currents have less dependence on season, time of day, weather, or temperature compared to solar or wind energy. Since about 40% of the world's population lives within 100 km of coastlines, "blue energy" harvested by the ocean could be both generated and used within the same geographical area [1,2].

Electromagnetic generators (EMG) currently are the dominate method for converting mechanical energy to electricity. However, these generators are heavy, bulky, and very expensive to operate [1,3,4]. Hydroelectric plants and conventional power plants run by boilers both produce electricity using EMGs; however, hydroelectric plants use water instead of superheated steam to drive its turbine [1,5]. Hydroelectric plants are mostly commonly found along dammed rivers. The pressure of water being released at the foot of the dam in a controlled manner drives high power, high frequency turbines. A few coastal hydroelectric plants, such as the Annapolis Tidal Station in Nova Scotia, Canada, dam water at high tide in a basin and release it during low tide through EMGs. The Annapolis Tidal Station is particularly effective because the tide range in the Bay of Fundy can reach over 16 meters [6]. However, most coastal areas have neither a drastic range in tides nor such a large area in which to create a basin. The Tidal Station creates significant environmental concerns as it has trapped whales and fish inside its basin and has increased erosion along the nearby shoreline and channels [6]. Other blue energy sources such as underwater thermal vents and the osmosis process have not been extensively developed due to their relatively high engineering cost and low power conversion [7,8].

Triboelectric generation, which converts ambient mechanical energy into electrical energy, is a new and emerging technology with extraordinary potential [7]. Combining contact electrification and electrostatic induction, triboelectric generators create current and voltage when a repetitive mechanical force changes the displacement of the triboelectric layer of two materials. Each material's triboelectric layer contains strong fixed charges on its nanostructured surfaces. If the two materials have a large variance on the triboelectric scale, that is, one material has a high electron repulsion while the other has an electron affinity, the charge transfer and energy produced increases [7].

In contrast to the heavy, large volume and expensive EMGs, triboelectric nanogenerators (TENG) are inexpensive, lightweight, mobile, small, cost effective and benign to the ocean environment [1,4,5,8]. They have the unique capability to transform low frequency (< 5 Hz) mechanical energy into a substantial and sustainable amount of electricity [9,10]. Based on the conditions of a specific marine environment, a TENG's design parameters can be inexpensively adjusted to maximize the energy production [11]. Furthermore, TENGs have several working modes, high energy conversion rates and the potential for simple, large-scale fabrication and maintenance [8,12]. Since 2012, the instantaneous conversion efficiency has reached 50% and the output area power density of TENGs has been 500 W/ m^2, twice that of solar photovoltaic panels [4]. In the ocean environment, it is estimated that a TENG network could generate 1MW/km^2, a magnitude that could greatly improve with continued progress in materials and structure designs [4].

The U.S. Navy operates ocean-bound vessels and coastal bases all around the world. Energy, its cost, and its reliability are incredibly important for the U.S. Navy to effectively fulfill its missions around the globe. TENG technology can utilize the U.S. Navy's favorite and most abundant environment, the ocean. These generators could provide reliable, low-cost, mobile electricity to be both stored and instantaneously used in various capacities. This research investigates harvesting wave energy using a floating, oscillating column TENG.

B. LITERATURE REVIEW

Dr. Zhong Lin Wang from Georgia Institute of Technology, National Aeronautics and Space Administration (NASA) researchers, and professors and students from various universities in the United States, South Korea, and China have been doing extensive research and development in triboelectric nanogeneration. Various design parameters, materials, efficiencies, environments and modes of electrification have been analyzed [4].

Dr. Wang first proposed self-powering nanogenerators in 2006 with the discovery of piezoelectric nanogenerators which converted small mechanical energy into electricity using the piezoelectric effect [4]. The first TENG was designed and tested in 2012 to generate electricity from various sources such as wind, water and human motion [4,9]. Its practical use focused on powering small, portable, relatively low power microelectronics such as cell phones [4]. Professor Zhong Lin Wang's studies have established TENG theory and have investigated the power output and optimization of parameters for all modes of TENGs [4].

Triboelectric generators harness the energy created through the triboelectric effect [4]. When two different dielectrics come into contact, electrostatic charges move from one surface to the other surface, causing the surface charge density to increase. If the gap distance between the two materials continues to increase and decrease in a cyclic movement, a flow of free electrons, produces a current density through an external load. This current, dependent on the charge density of each dielectric surface and the speed at which the two materials are separated and contacted, can be converted to usable electrical energy [4].

Since displacement current enables the electricity transport, TENGs use capacitive conduction based on Maxwell's displacement current, Equation 1, and Ohm's Law, Equation 2, where J_D is displacement current density, ε_0 is the permittivity of free space, t is time, E is the electric field, P is the polarization field, and σ is the conductivity of the material.

$$\boldsymbol{J_D = \varepsilon_0 \frac{\delta E}{dt} + \frac{\delta P}{\delta t}} \qquad (1)$$

$$\boldsymbol{J_D = \sigma E} \quad (2)$$

In contrast to TENGs, electromagnetic generators use resistive conduction. The Lorentz force, *F*, Equation 3, explains why free electron flow depends on the moving speed, *v*, of the conductor across an electric field and a magnetic field, *B,* with a certain tensor resistance, *e*.

$$\boldsymbol{F = -ev \times B} \quad (3)$$

The transfer of charges in a TENG is maximized when a conductor makes frictional contact with an insulator [4]. The conductor gives up electrons while the insulator accepts them in return. Based on the design and durability requirements of a TENG, the materials used may vary but should have a large difference in electrostatic affinity [3].

Four major modes of operation, explained in the following sections, show the diversity of the new technology [4,9]. TENGs are relatively inexpensive, light weight, and easily manufactured [9]. They show significant promise for self-powered sensors or microelectronics which prioritize small size, functionality, wireless portability due to their lack of an external power supply [4]. Moreover, TENGs that can store or transfer the energy produced are being developed and tested for future large-scale energy production [9].

Although many studies to date have only focused on the design of a singular TENG, several research initiatives have developed networks or "farms" of TENGs. Individual TENGS could be connected in series or a single device could contain multiple TENGs to yield more energy [1,10].

1. TENG Modes, Designs and Characteristics

Utilizing the phenomena of triboelectrication through friction and polarization, several modes of movement have been developed; namely, vertical contact-separation mode, in-plane contact-sliding mode, single-electrode mode and freestanding triboelectric-layer mode [4]. In each mode, shown simply in Figure 1, energy is produced from the kinetic energy of beings, objects or forces of nature already in motion [4,9].

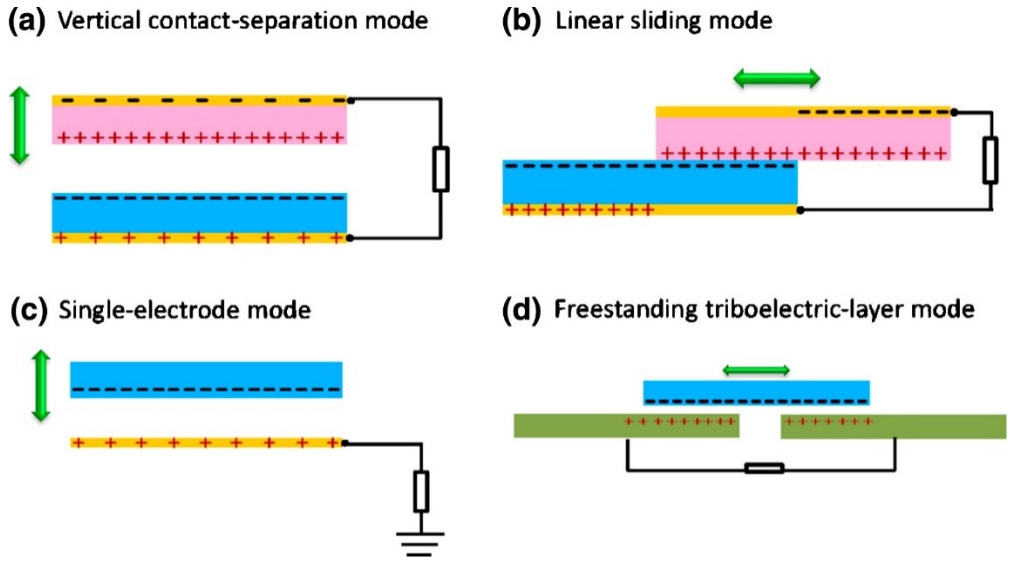

Figure 1. Fundamental Working Modes of TENGs. Source: [4].

a. Vertical Contact-Separation Mode

The first mode, vertical contact-separation mode, occurs when two dissimilar dielectric films undergo a cycle of contact and small vertical separation [3]. Due to their different material properties, the two dielectrics have opposite charged surfaces when connected. A polarization and electric potential drop caused by opposite charges occurs as an external force separates the two surfaces. If the two electrodes are connected electrically by a load, the free electrons flow from the negatively charged electrode to the positively charged electrode. As the two surfaces approach one another, closing the small gap between, the electrons flow in the opposite direction and the electrical potential ceases [3]. Examples of vertical contact-separation mode include the spring-levitated oscillating TENG, spring-assisted contact separation TENG and noncontact magnetic-assisted TENG [3–5, 8].

b. Lateral Sliding Mode

Some TENGs use polarization in the lateral direction and create triboelectric charges by sliding two dielectrics across each other [4]. The parallel surfaces create friction while in cylindrical rotation or lateral planar motion. When the dissimilar materials are designed in a way such that there is a periodic time of contact and separation, AC power is

generated. Wind, ocean waves, ocean currents or the rolling of a ball could produce AC power using laterally sliding mode TENGs [13]. The floating oscillator-embedded triboelectric generator (FO-TEG), the rolling rod/ interdigitative electrodes TENG, floating internal ball TENG, and desalination TENG, all use lateral sliding motion [1,4,7, 14].

c. Single Electrode Mode

The single-electrode mode creates power through the interaction of a single electrode on the TENG and the environment which acts as the grounded, second electrode [4]. If there is a cyclical approaching and departing of the two surfaces, power can be generated. This mode can be utilized in contact-separation motions such as the walking of a human's shoe (electrode 1) against the ground (electrode 2) or in contact-sliding mode such as the interaction of fluorinated ethylene propylene (FEP) thin film (electrode 1) and water waves (electrode 2) [4, 15].

d. Freestanding Triboelectric-Layer Mode

Finally, a freestanding triboelectric-layer mode operates in a manner similar to the sliding mode [4]. Unlike the sliding mode though, one electrode is not connected electrically to the other. Since moving objects in nature inherently possess surface electrical charges due to interactions with air or other objects, a TENG can be constructed using a gapped pair of symmetrical electrodes underneath a dielectric layer. When the moving object comes near or away from the electrodes, induction creates an asymmetric charge distribution. Electrons attempt to balance the potential difference between the moving object, producing AC current. Freestanding triboelectric-layer TENGs are advantageous because the entire system can be mobile during energy harvesting. Potential mechanical energy sources include human walking motion and the movement of an automobile [3, 4].

e. Common Materials Used in TENGs

As discussed, basic TENG designs require two electrodes, materials with significant disparity in the triboelectric spectrum, and a substantial outer casing to protect the electrodes from relative humidity and ionized water [13]. One of the advantages of TENG technology is its use of relatively common and inexpensive materials.

Due to their positivity in the triboelectric series, thin layers of copper and aluminum are the most common metal electrodes [1,5,8,11,13]. Gold and nickel are sometimes added to the cooper and aluminum to improve performance [13]. Polymers such as polytetrafluoroethylene (PTFE), polyethylene terephthalate (PET), polydimethylsiloxane (PDMS) and polyurethane (PU) are conventional as the material with negative triboelectric properties. They are inexpensive, abundant, and reliable as an outer casing [1,5,8,10,11,13]. For solid-liquid TENGs, FEP is routinely used as the polymer because of its hydrophobic properties [13]. The large difference in electron affinity of the two materials, a metal and a polymer, induces the electron flow.

Several designs have had nanostructures etched on its PTFE or polymer surface to increase surface area [1, 9, 10, 14].

f. Harvesting Sinusoidal and Impact Energy

One of the challenges and purposes of TENGs is to harvest the ambient "waste" energy in which other generation methods have not invested [7]. Examples include the motion of humans walking, excess vibration from mechanical motors, ocean wave motion, etc. This ambient energy can be categorized into two main groups, impulse excitement and sinusoidal vibration. Impulse excitement has a high amplitude and short duration while sinusoidal vibration has smaller amplitudes and higher frequency. It is important to note that TENG designs must be flexible in order to operate in the random and mixed form amplitudes and frequencies found in their target environments [7].

In 2015 scientists from the Department of Electrical Engineering at the Korea Advanced Institute of Science and Technology along with the NASA Ames Research Center in California, developed a floating oscillator-embedded triboelectric generator (FO-TEG) which simply and efficiently converts both impulse excitation and sinusoidal vibration into electrical energy [7]. An enclosed metal-lined tube has a polymer-coated metal-embedded oscillator which moves linearly as the FO-TEG experiences impulse excitation or sinusoidal vibration. Repulsive force magnets at each end of the tube and the external mechanical motion enable the oscillator to "float" and continue charge-producing

motion from friction between the polymer surface of the inner oscillator and metal surface of the outer tube, Figure 2 [7].

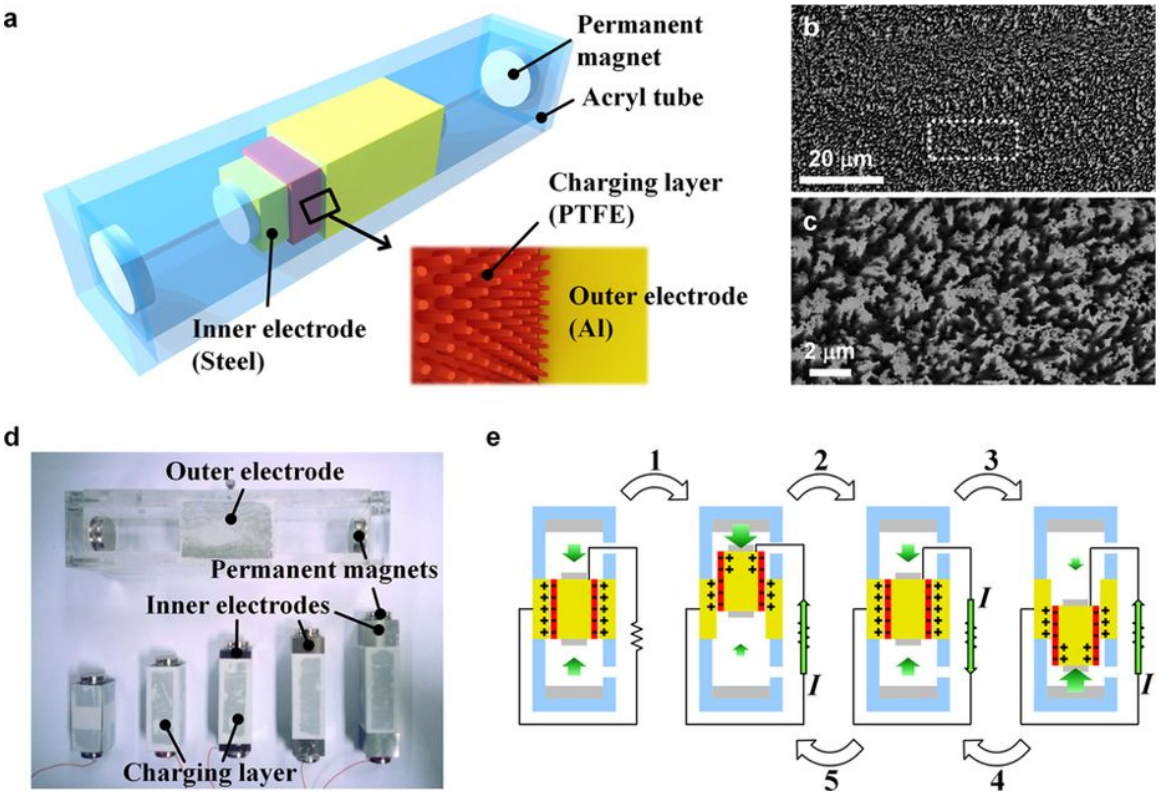

(a) Structure of FO-TEG (b-c) Scanning Electron Microscope (SEM) image and magnified SEM image of PTFE charging layer (d) FO-TEG components at various lengths (e) Operating principle of FO-TENG.

Figure 2. Floating Oscillator-Embedded Triboelectric Generator. Source: [7].

The inner electrode has a steel core and PTFE film outer coating which has a constant negative charge density [7]. The PTFE layer was modified with plasma etched nanostructures to increase surface area and charge transfer. When the inner electrode is completely aligned with the outer electrode, the PTFE has only its inherent negative charge while the outer electrode possesses excess negative charges by nature. Once the oscillator moves, the electrodes are no longer aligned and electron flow, or current, is produced from the disparity in the charges between the two materials. The repulsion from the permanent magnets assists returning the inner electrode to the center [7].

The scientists assessed various design parameters such as the mass of the inner oscillator, the natural airgap distance between inner oscillator and the ends of outer tube and material selection, Figure 3.

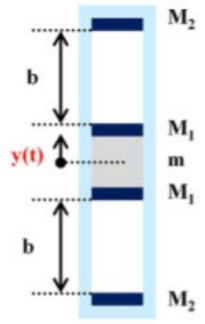

y(t)	Vertical displacement
m	Mass of cylinder
b	Neutral airgap distance
M_1, M_2	Magnetic moments
k	Drag coefficient

Figure 3. Structural Parameters Analyzed with FO-TENG.
Source: [7].

Despite the specific design parameters, larger amplitudes of impact produce greater current and increase damping exponentially [7]. As the mass of the oscillator increases, the oscillator frequency decreases which mitigates the damping. If the oscillator mass is too small, the inner electrode will not traverse the length of the FO-TEG effectively.

The air gap, determined by the length of the inner electrode versus the length of the total FO-TEG, needs to be able to both support a sufficient amplitude of movement and also to enable an adequate frequency of oscillation [7]. PTFE was chosen due to its low surface adhesion property and strong negative order of electrification. The outer electrode surface was polished to reduce the macro-scale friction during each oscillation [7].

Single step waves, produced by motions like stepping or hitting, double-pulsed square waves, made by motions like bouncing or jumping, and continuous sine waves, caused by motions such as humans running, water waves and machinery operations, were analyzed, Figure 4 [7]. Although damping caused oscillation to continue for a small time

after step and square waves, sine waves proved to be most productive because the continuous motion produces continuous electrical energy output. For a FO-TEG to be at its optimal effectiveness, the air gap and correlating frequency of oscillation must be optimized for the frequency of external mechanical generation. In other words, the average frequency of the sine waves which produce the internal oscillation between the electrodes must be known for the design parameters to be appropriate [7].

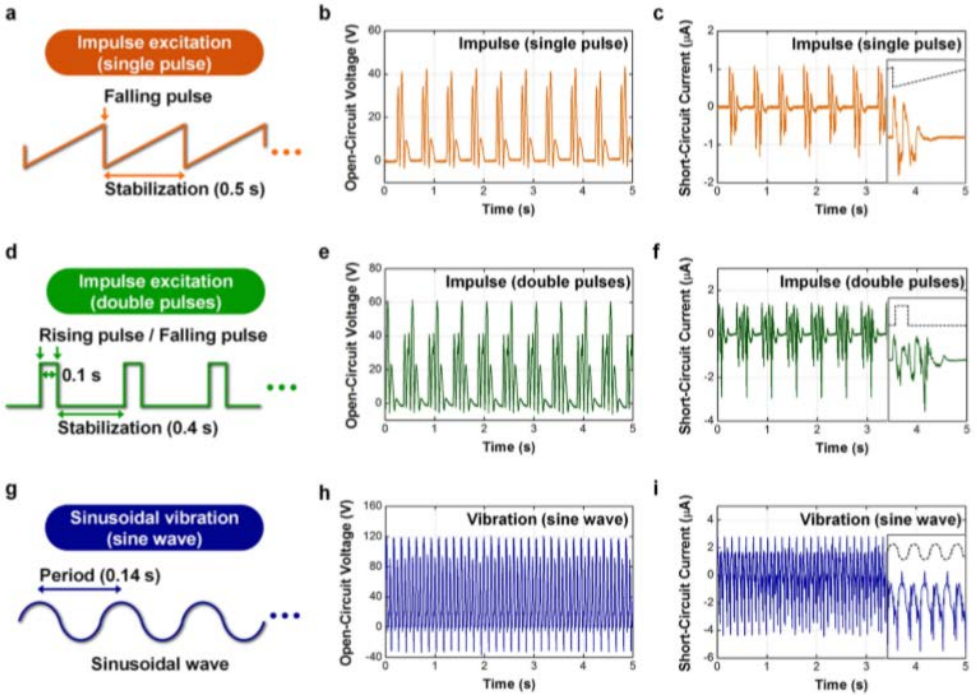

Figure 4. FO-TEG Potential under Various Input Vibration Types. Source: [7].

This project recognized how detrimental relative humidity is on triboelectric generation. Therefore, the scientists tested the FO-TEG in various humidity environments to ensure the design was air-tight [7].

g. TENG Designs

TENGs can produce sustainable, instantaneous power for micro-scale power sources such as LED lightbulbs and sensors. Their durability, small size and independence

make them an attractive energy source for remote pieces of equipment or lights that have relatively small energy demands.

However, in certain high-energy environments such as oceans or rivers, a network of TENGs could produce a magnitude of electricity that could power a substantial load instantaneously or be stored and transferred for use at a different time and location [3,11].

The modes of TENGs discussed are all examples of solid-solid contact electrification where two solid materials, which are triboelectrically different, produce electrical current through the cycle of contact and separation [9]. A team of scientists under Professor Zhong Lin Wang has designed multiple variations of TENGs which would harvest ocean movements via solid-solid contact electrification.

(1) Floating Internal Ball TENG

A floating, lightweight, inexpensive TENG design uses the wave movement on the ocean surface to induce the rolling of an enclosed ball [1]. This ball causes contact and separation between a polymer and a thin metal electrode. The design of this system, Figure 5, is advantageous because the freely moving ball can capture the random, all-directional oscillatory motions of the ocean surface [1].

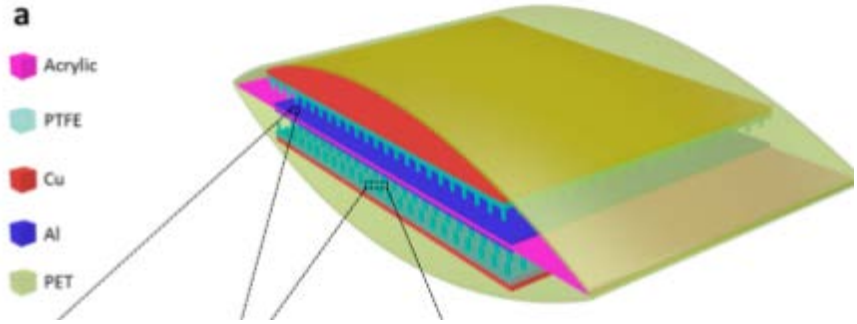

Figure 5. Design and Composition of Floating TENG. Source: [1].

A bent, heat-treated PET case covers the outside of the TENG while the PTFE film, deposited copper and aluminum thin film between the top and bottom layers comprise the functional core [1]. The kinetic energy from the ocean waves cause an internal rolling ball

to collide with the top plate of the unit which causes the two layers of PTFE to contact the aluminum electrode. Because PTFE is much more triboelectrically negative than aluminum, electrons move from the aluminum to the PTFE. Subsequently, free electrons move from the copper electrode to the now positively charged aluminum electrode so that the copper electrode becomes positive. When the separation between the upper plate and copper electrode is maximized, the dipole moment created weakens and free electrons flow back to the copper electrode. This alternating flow of electrons produces a current in an external circuit as the cycle repeats itself with each wave [1]. Scientists used resistors to measure the output power under controlled accelerations and displacements. For one unit, the maximum load resistance was 1 MΩ while the peak power density was 0.26mW/cm^2 [1].

In efforts to develop a TENG network, scientists tested this TENG model in a four unit system, Figure 6 [1].

(a) floating in water; (b) producing electricity to power LED lights; (c) TENG network

Figure 6. TENG Network. Source: [1].

Current amplitudes, peak current density, peak voltage density and charging accumulation rate all increased proportional with the number of TENG units in the system, Figure 7.

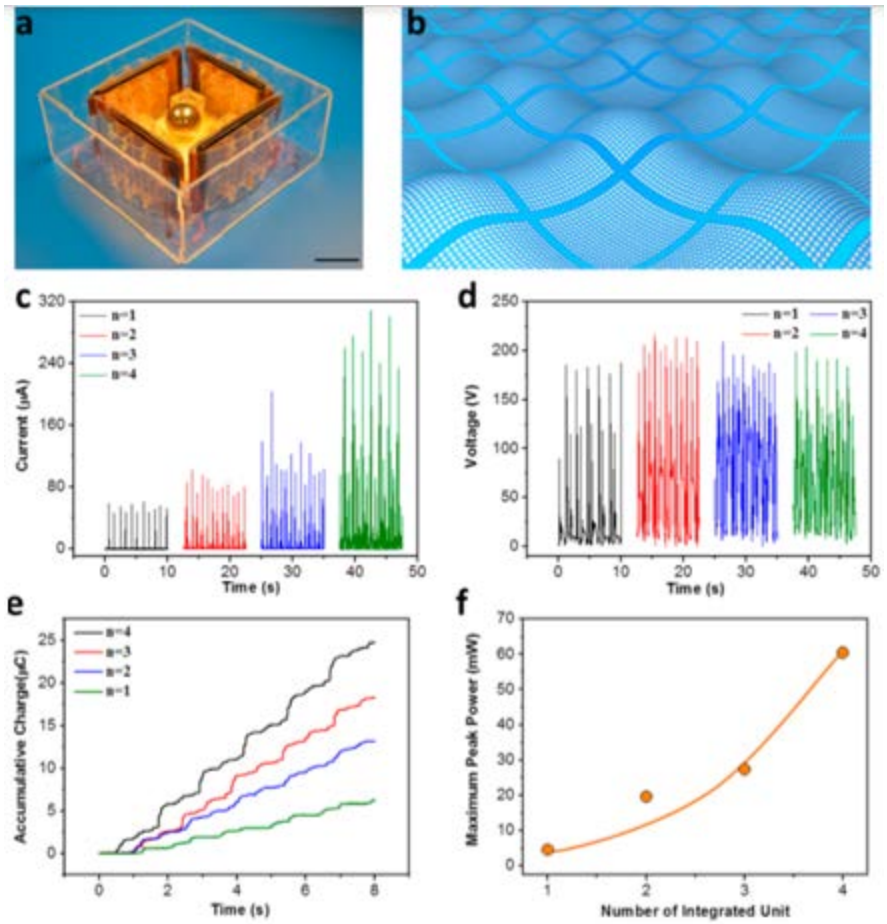

(a) Depiction of enclosed ball TENG; (b) TENG Network; (c-f) Current, Voltage, Accumulative Charge and Maximum Peak Power all increase with number of TENG units.

Figure 7. Enclosed Ball TENG. Source: [1].

Using a diode bridge, the output power frequency is controllable and tunable. Most importantly, the peak output power exponentially increases as the number of TENG units increase [1].

This experiment constructed a network of only 4 TENG units but argued that a large family of TENGs connected in series would produce reliable and practical amounts of current, voltage amplitude and voltage density. This TENG's light weight, anticorrosive, floating characteristics make it ideal for marine energy harvesting near or far from shore [1].

(2) Rolling Rod and Interdigitative Electrodes TENG

A coalition of engineers developed a TENG similar to the enclosed ball model. The movement of a cylindrical copper roller coated in a thin layer of polyurethane over a series of PTFE filmed interdigitative electrodes generates electric output [9]. In the model, the roller traverses over the 9 electrode pairs during one ocean wave impact, generating 9 pulses of electricity, Figure 8. Each wave interaction produces a power density of 1.1 W/m^2 which immediately powers a series of LED lights [9].

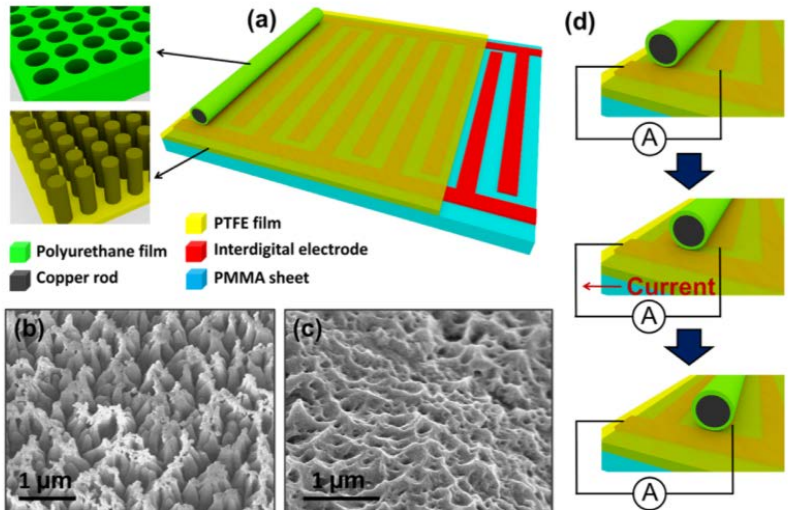

(a) Design of single-layered TENG with interdigitative electrodes and PU coated copper rod; (b-c) SEM images of PTFE and PU surfaces with nanowire arrays and porous structures; (d) mechanic operation of TENG over interdigitative electrodes.

Figure 8. Rolling Rod and Interdigitative Electrode TENG. Source: [9].

The TENG can generate as many pulses of electrical output as there are interdigitative electrodes. As the PU coated copper roller (electrode A) travels over a PTFE coated thin strip of aluminum (electrode B), electrons transfer from the PU surface to the PTFE surface [9]. The newly positive-charged PU-copper roller then gain electrons when it passes the next aluminum strip, Figure 9. Voltage and electric potential fluctuate each time the roller cycles over an electrode pair, Figure 10. The advantage of this design is that the TENG need only travel between each interdigitative electrode, not the entire length of

the unit, to generate electrical output. Therefore, if this TENG is placed in an ocean environment with fluctuating periods and amplitudes, the TENG will generate some magnitude of electricity as long as the roller can travel over one electrode pair [9].

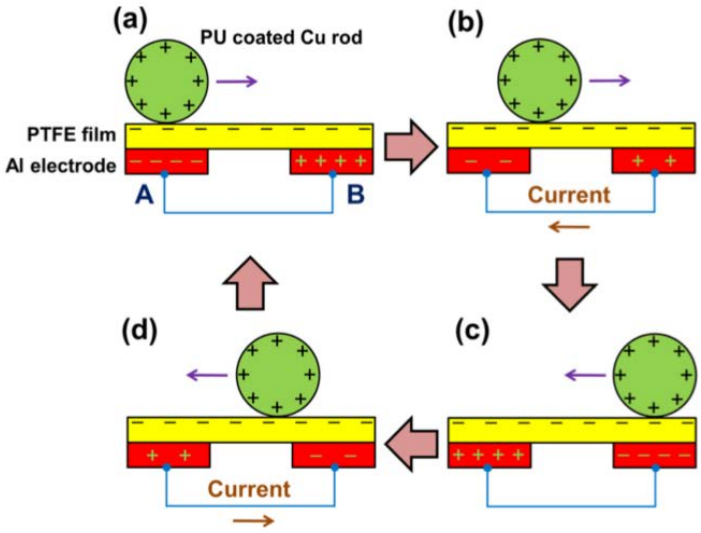

As PU coated Cu rod rolls over interdigitative electrodes, electrons transfer from PU surface to PTFE film on each AL electrode.

Figure 9. Electron Transfer on Interdigitative Electrodes. Source: [9].

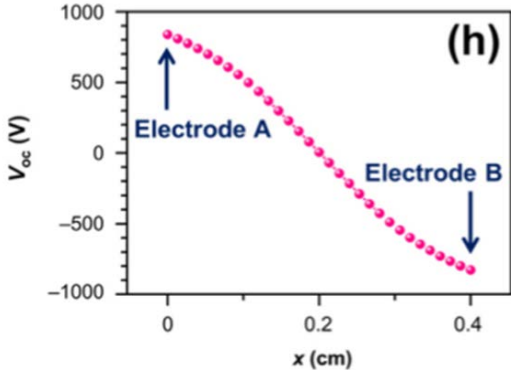

Figure 10. Voltage vs Copper Rod Displacement on Interdigitative Electrode. Source: [9].

There is an ideal number of interdigitative electrodes based on the scale of the TENG and each electrode width [9]. If too many interdigitative electrodes are present over

a short range, or the diameter of the roller is too large, the amount and efficiency of electron transfer decreases. During experimentation, an increase in tilt angle increased output current charge [9].

If additional layers were attached vertically to each TENG unit, more electricity could be generated. Further, for a given number of vertical electrode groups, there exists a resistance which maximizes instantaneous power density [9].

2. TENG Networks

a. Air Driven TENG

Another recent study involved a spring-levitated oscillator structure which interacts with ocean waves to generate a difference in internal air pressure [10]. This difference in pressure drives the TENG components to generate electricity through contact electrification and electrostatic induction, Figure 11 [10].

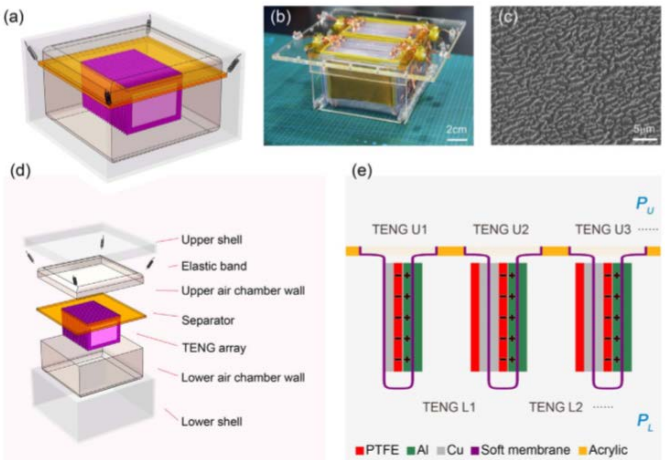

(a, b, d) Structure of Air-Driven TENG; (c) Nanostructures on PTFE surface; (e) Detailed view of TENG array. PU and PL represent pressure in upper and lower chambers, respectively.

Figure 11. Air Driven TENG. Source: [10].

As the vertical-contact mode TENG moves up and down in a wave, the pressure between the upper chamber and lower chamber inside the device changes and helps drive the oscillator up and down [10]. This motion produces a cycle of contact and separation

between the electrodes, which are located on both sides of the internal membrane. Aluminum foil was used for one electrode while PTFE wrapped around thin foil of copper, was used for the other. This electrostatic induction is harvested by connecting the Cu to the Al through an external circuit, Figure 12. The pressure difference between the upper and lower internal air chambers is crucial in the cycling of the oscillator because it ensures the complete contact and separation of the electrodes. This design is incredibly durable for the continuous nature of ocean waves [10].

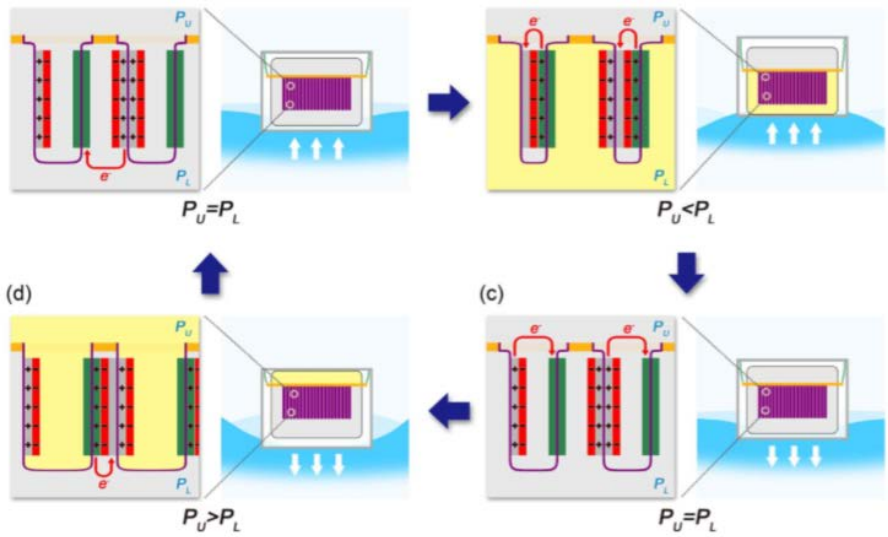

Figure 12. Air Driven TENG in Ocean Waves. Source: [10].

A group of 38 of these individual TENGs were assembled to form one large energy producing unit [10]. The device has a top row of 20 TENGs, connected in parallel through each of the two electrodes, and a bottom row of 18 units, also connected in parallel. A rectifier combines the electricity produced by each row. Table 1 shows various output values for one TENG vs a network of 38 TENGs [10].

Table 1. Individual vs Network of Air Driven Oscillator TENGs. Source: [10].

	Voltage, Open Circuit	Current, Peak Rectified Short Circuit/Cycle	Transferred Charge, Q/cycle
Air Driven Oscillator TENG (1 Unit)	600V	12.5 μA	0.22 μC
Air Driven Oscillator Network (38 Units)	600V	187 μA	15 μC

Several resistors of different magnitudes were tested to determine the optimum resistive load that maximizes the output power. This TENG had an optimal resistive load of 8 MΩ, a maximum power of 10mW and peak power density of 13.23W/m^3 [10].

The internal oscillator fluctuates at the frequency of the ocean waves in which it floats [10]. There exists a resonance frequency, f, for the exact parameters of this TENG, at which the output power is maximized. Although the output decreases above the resonance frequency, one impact can induce several cycles and can harvest more energy off one wave. The oscillation of this TENG proved to be an efficient way to absorb and store mechanical energy in the ocean environment where wave frequency is haphazard and random [10]. The number of individual TENG units could be adjusted to form the single power device which could be attached to land through cables [10].

b. Spring-Assisted TENG

To harvest the most energy out of the reliable but low frequency mechanical motion of waves, a team of scientists designed a TENG with a spring, Figure 13 [5]. The internal spring stores the mechanical energy of a wave impact and converts it to elastic potential energy. This energy then produces continuous, higher frequency oscillations, abet smaller than in magnitude compared to the single wave impact, for a longer time period. This consistent output of energy not only made the TENG more efficient, but it also increased the accumulated charge of each wave interaction [5].

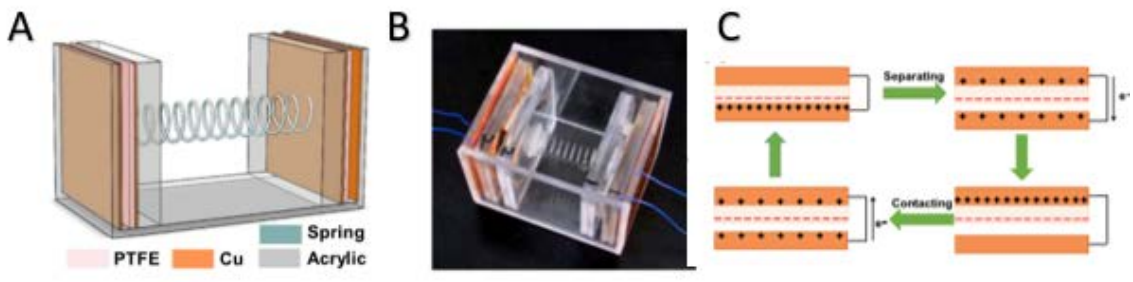

(a)-(c) components, design and working mode of spring-assisted TENG

Figure 13. Spring Assisted TENG. Source: [5].

The box design of the spring-assisted, contact-separation mode TENG has a spring connected to two copper-PTFE covered acrylic blocks [5]. Behind each block is a copper electrode anchored to opposite internal walls. Electrons travel from copper electrode on the wall to the PTFE film increasing the negative charge of the PTFE until it reaches its maximum distance from the wall. This dipole moment and cyclic separation between the PTFE films, on the moving, spring-connected blocks, and the copper electrodes on the stationary wall create induce a flow of electrons, AC current and electrical output. The stored elastic potential energy in the spring oscillates the internal acrylic blocks after the initial wave impact has concluded. However, if the frequency of the block oscillations becomes too great, the transferred charge rate decreases due to the reduced collision time between the two electrodes [5].

Parameters of the cubic TENG and the spring were tested to optimize the energy output [5]. Rigid, moderate and flexible springs with compression rates of 1 kg/cm, 0.2 kg/cm and 0.1 kg/cm, respectively, and various spring lengths were assessed with respect to output voltage, current and charge transfer, Figure 14 [5].

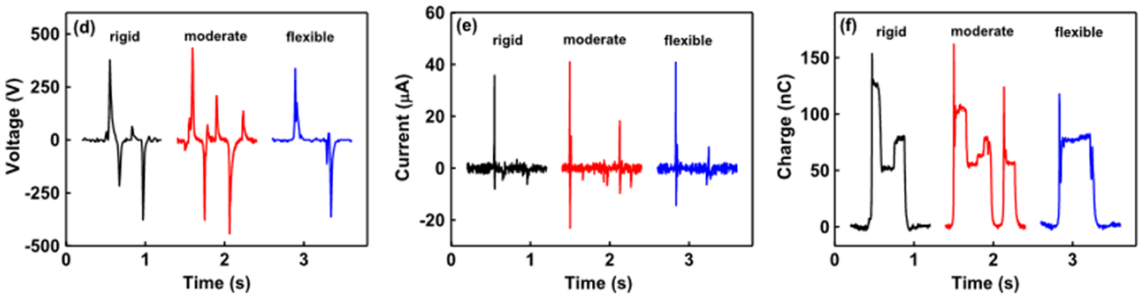

Spring Rigidity vs. (left) output voltage (middle) output current (right) transferred charge.

Figure 14. Effects of Spring Rigidity on Spring Assisted TENG
Source: [5].

The rigid spring has two strong cycles, but high damping prevents it from producing adequate small cycles [5]. The flexible spring has only one strong cycle because it did not have enough energy to continue oscillating the acrylic blocks. The moderate spring, with a length of 4.5 centimeter, demonstrates the best efficiency and produces relatively substantial cycles consistently. This yields a higher output performance with more electric energy. The spring length must facilitate both contact and separation between the box walls and the acrylic blocks. Lengths too short inhibit wall contact while lengths too long inhibit wall separation [5].

By replacing the spring with a rigid acrylic strip, the scientists were able to show that the spring TENG increased voltage by 22.8%, current by 29.6%, accumulated charge by 113%, electrical energy output by 150.3% and efficiency by 150.3%, Figure 15 [5].

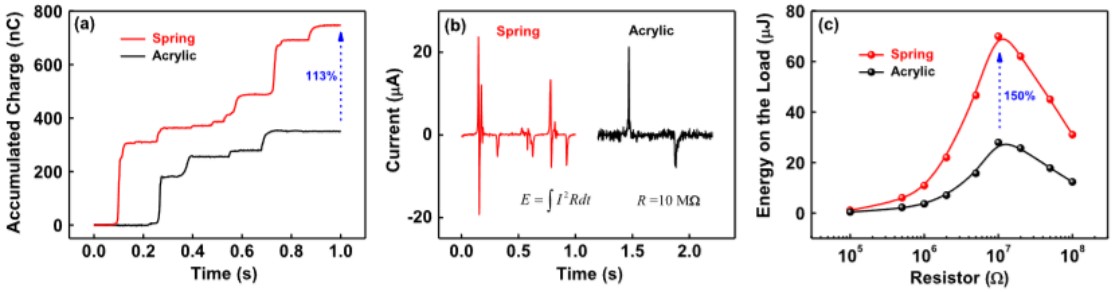

Figure 15. TENG Using Springs. Source: [5].

Four of the optimized TENG units were connected in parallel for testing in water waves [5]. Since each TENG unit box has 2 TENGs, the overall system had 8 TENGs creating electricity in a waterproof acrylic box. A rectifier bridge connected the TENGs and the generated electricity can either power a series of LED lights or charge a capacitor. As the number of TENG units increases, the average voltage peak amplitudes remain relatively constant while the peak voltage density and current amplitude increases. Maximum power density is 726.48 mW/m^3 [5].

For this TENG design to successfully harvest ocean wave energy on a large scale, the anticorrosive properties of the system's outer shell must be further developed to prevent seawater from destroying the mechanism of electricity generation. Moreover, the ability to store energy in a capacitor or battery or transfer it ashore must be further researched [5].

c. Energy Storage

TENGS generally produce high voltage and low current [3, 11]. Depending on the mode and operating environment, the electricity generated could be unstable and unpredictable. For example, if a TENG model generates power by wind or ocean waves, it would generally produce more electricity when wind and waves are larger. If an impact TENG produces electricity based on a series of high-intensity impacts followed by periods of no activity, there is not a consistent flow of current and voltage.

Therefore, for this electricity to be efficiently used by a load, the power must be consistent and regulated [3,11]. Several TENG models currently incorporate use of springs to have a more consistent power output from elastic potential energy. Capacitors and batteries are being developed in various TENG models to harvest and then transfer the captured energy [3,11].

A study of a wavy-structured, direct water-wave-impact TENG and an enclosed ball collision TENG, investigates how structural parameters and operating environment affected the charging of a capacitor, Figure 16 [11,13].

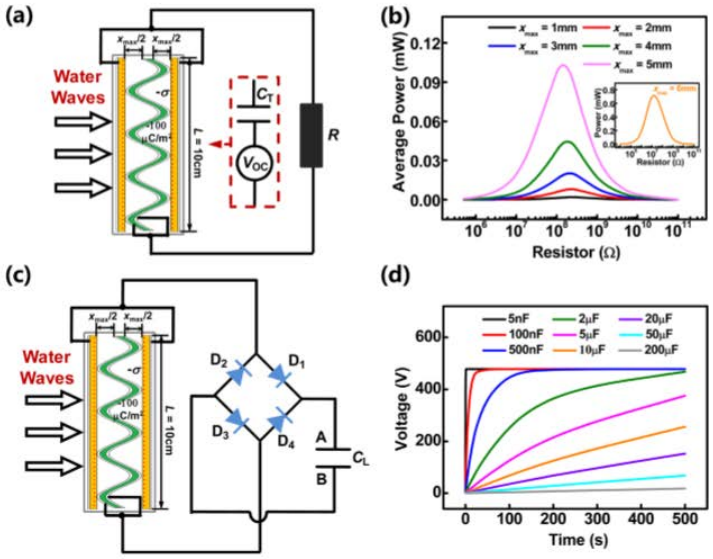

(a) Circuit model of TENG under direct water wave impact with (a) resistor and (c) capacitor; (b) average output power for load resistance with various deformation depths, xmax; (d) voltage-time relationships at different load capacitances, CL when xmax = 6mm.

Figure 16. Wavy-Structured, Direct Water-Wave-Impact TENG. Source: [13].

Scientists observe the correlation of load capacitance, charging cycle number and deformation depth, the separation between the filmed plates [13]. A simple circuit consisting of a TENG, the capacitor and a full bridge diode rectifier was constructed for this purpose, Figure 17.

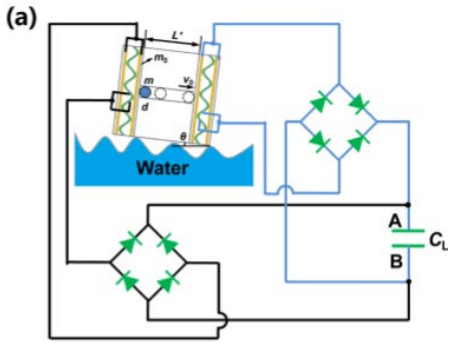

Figure 17. Circuit Diagram of TENG Charging Capacitor. Source: [13].

The rectifier prevents the AC current from leaking back from the capacitor to the TENG when the direction of current switches [11]. While keeping deformation depth constant, smaller capacitance allows voltage to reach its saturation point quickly while the stored current in the capacitor remains close to zero. When capacitance is larger, the voltage is negligible, and the stored current is maximized. Maximum stored energy and the magnitude of optimum capacitance increase as cycle number increases. Stored energy and the maximum energy storage efficiency improves with increasing deformation depth and with stronger impact forces [11].

In the same study, the charging characteristics of a TENG powered by the collision between an enclosed ball and the TENG walls was evaluated [11]. As ocean waves cause the TENG structure to slope, a steel ball rolls and creates friction against the walls in the enclosed TENG. Slope angle, maximum length of ball movement, ball diameter and capacitor charge were tested at various dimensions. The engineers discovered that there exists an optimum capacitance and optimum ball diameter to store the most power effectively. When investigating ball mass, researchers concluded that the amount of stored energy increases with increasing ball mass because more mass causes faster compression and greater deformation depth. Higher slope angles from larger wave heights also produces more stored energy [11].

3. Challenges

a. Harvesting Energy from Low Frequency, Varying Waves

Most generators such as EMGs use high frequency, high power rotation to produce electricity [4]. In order to produce energy from the surface of the ocean, the new generation of generators must be able to harness energy from low frequency and low power oscillations. Several design factors must maximize that low frequency movement created by a wave [4].

The spacing between dissimilar materials and electrodes, is incredibly important for TENGs [1]. There must substantial contact time with each electrode, but the friction must also traverse both electrodes at a sufficient rate. Various studies have investigated

how structural parameters such as size, mass, number of electrode strips, nanostructure of material surface, etc., can most efficiently produce electricity [1–10, 14, 15].

The size and design of a TENG must be optimized for the specific frequency and magnitude of waves in an environment. When an oscillating or lateral TENG moves at its resonance frequency, its voltage and current output is most efficient. Since nature rarely produces a perfectly consistent environment, designs should use the mean wave height and period to achieve its resonance frequency as much as possible. NOAA's wave data from buoys around the world can provide this data for most locations along the U.S. coastline [16].

b. Storing Energy

TENGS generally produce high voltage and low current. Depending on the mode and operating environment, the electricity generated could be unstable and unpredictable. For example, if a TENG model generates power by wind or ocean waves, it would generally produce more electricity when these forces of nature are larger. If an impact TENG produces electricity based on a series of high-intensity impacts followed by periods of no activity, there is not a consistent flow of current and voltage.

Therefore, for this electricity to be efficiently used by a load, the power must be consistent and regulated [3,5]. Several TENG models currently incorporate use of springs to output a more consistent power from elastic potential energy. Capacitors and batteries are also being developed in various TENG models such as the spring-assisted TENG, to harvest and then transfer the captured energy [3,5,11].

Research for the efficient storage of electricity in capacitators or batteries as well as the transfer of generated electricity to land through cables must be explored.

c. Protection from Water

Although a liquid-solid interface can transfer charges in certain TENG designs, the use of these TENGs in the ocean environment is not practical [15,13,12]. One study investigated a solid-liquid electrification TENG's performance in deionized water, tap water and deionized water with a concentration of NaCl comparable to sea water. The tap

water and NaCl water produced 30% and 76%, respectively, of the current produced in deionized water. Even though the TENG was covered in the hydrophobic polymers PDMS and PTFE, the PDMS film could not eliminate water drops from its surface after separation from the water. The electrolytes in both tap water and especially saltwater inhibit the efficient flow of electrons. The electrolytes in the water remain on the film and partially screen the tribo-charge transfer. A much smaller electrical output is produced with the electrolyte-loaded tap and saltwater samples [15,12].

This conclusion makes water-solid triboelectrification use in the ocean environment quite undesirable and inefficient due to the water's high level of electrolytes. Unless scientist can develop more hydrophobic materials to repel the electrolytes found in NaCl concentrated water, other modes of TENGs are more attractive [15,12].

d. Protection from Ambient Humidity

Several studies, such as the floating oscillator-embedded TENG and the magnetic-assisted noncontact TENG, have tested charge transfer efficiencies in humidity [1,14]. It is crucial for the TENG device to be isolated from environmental factors for proper and efficient power generation. In humid environments, water molecules surround and reside on the surface of each friction material. Like it does with the solid-liquid interface TENGs, water inhibits the easy transfer of electrons from on material to another [1,14].

The FO-TENG study showed that voltage decreased by 64% when humidity was increased from 10%-90%, Figure 18 [14]. Therefore, encapsulation and isolation from the environment is key [14].

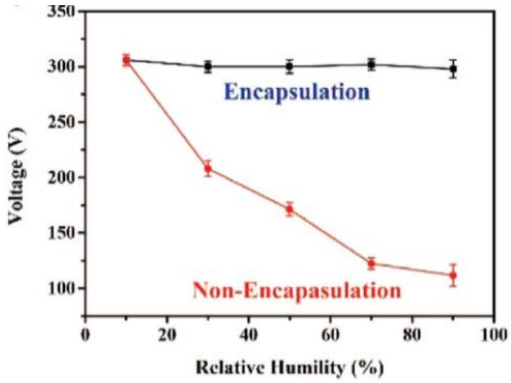

Figure 18. Voltage vs Relative Humidity for FO-TENG. Source: [14].

e. Material Abrasion and Degradation

Future studies must investigate how charge density changes with surface roughness and dielectric properties. Since contact friction and material abrasion is a major concern with system longevity, these materials must be tested over a long period. The possibility that materials become less efficient at transferring charges the more they interact or does the effectiveness sustain itself should be investigated over a long period of time.

f. Low Current and Low Power Density

TENGs are, by nature, small in scale. Thus, the current produced by each individual unit is relatively small as well. Typical current values are in the microamps or nanoamp range. Therefore, unless a TENG is powering a simple LED light bulb or microelectronic device, a network of TENGs is necessary to produce a reasonable amount of electricity that would be stored or sent to a power grid. The power density of current TENG models can range from less than 10 W/m^2 to 500 W/m^2 [4,17]. Research efforts that alter various design factors such as springs, dimensions of electrodes, internal resistance, and movement modes, continue to improve so that individual TENGs can maximize the current output [1,5,9,10,17–19].

4. Potential of Blue Energy TENGs

TENGs have significant potential in the ocean environment with the seemingly ceaseless movement of ocean waves and current [20–25]. At any given location in the

ocean, several naturally produced “energy sources” are present including water waves, wind, and flowing currents. One TENG design has been shown to capture all three of those energy sources, Figure 19 [26].

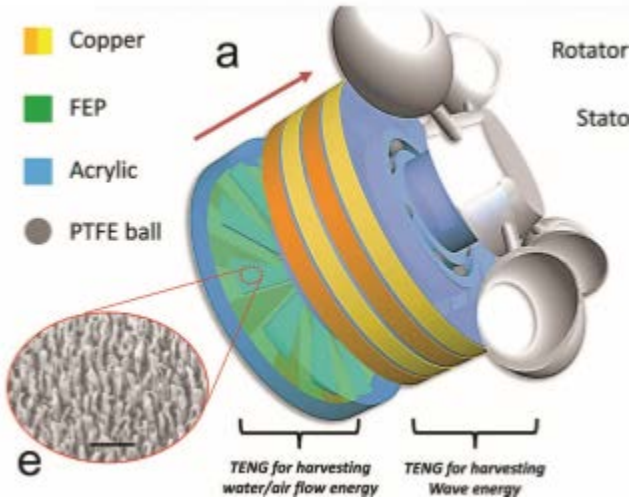

Figure 19. TENG Powered by Blue Energy. Source:[26].

TENGs have already shown promise as offshore or remote self-powered sensors [9,13] One study used a TENG electricity to light a distress signal while another desalinated water [14,13]. As shown from the research involving TENG networks, offshore TENG farms have the potential to produce significant energy that could be stored or sent back to a land power grid [5,10].

THIS PAGE INTENTIONALLY LEFT BLANK

II. EXPERIMENTATION PROCESS

A. DEVELOPMENT OF NPS TENG MODEL

The design for the TENG fabricated at the Naval Postgraduate School (NPS) in Monterey, California was adapted from a TENG produced and tested at the NASA Ames Research Center's Center for Nanotechnology in Moffett Field, California [28]. The TENG produced is completely fabricated using 3D or 2D printers. This showcases how 3D printing technology is incredibly applicable to the simple, inexpensive, easily designed and fabricated, versatile nature of TENGs. The size and material needed for TENGs, unlike enormous EMGs or more complicated piezoelectric generators, are within the capability of even the most standard 3D printers [28].

1. NASA Ames Model

The NASA Ames TENG model consists of a 3D printed outer casing, oscillator and spring and a 2D printed interdigitative electrode, Figure 20 [28].

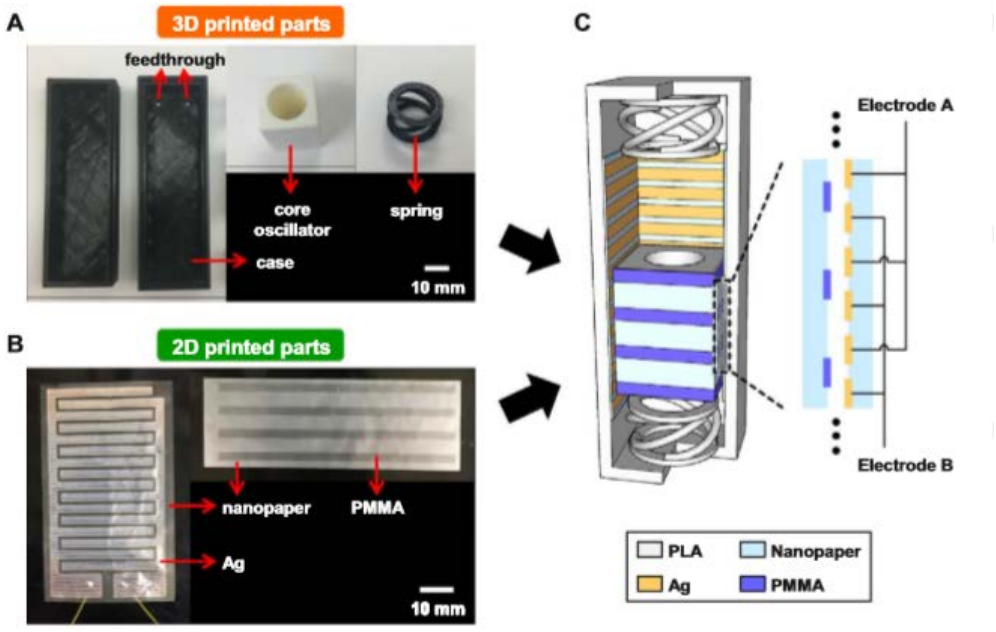

(a) Components of TENG; (b) 2D printed Ag electrode and triboelectric layer nanopaper; (c) working mechanism of TENG when constructed.

Figure 20. NASA Ames 3D Printed TENG. Source: [28]

The 3D printed exterior, oscillator and spring are PLA, the 2D printed interdigitative electrode is silver nanoparticle ink, and the 2D printed triboelectric layer is polymethyl methacrylate (PMMA). Both 2D printed materials use nanopaper. The silver interdigitated electrodes have lines that are 3 millimeters wide with 1.5 millimeter spacing. The electrodes are attached to the wall of the box in order to facilitate the sliding of the inner oscillatory block and its triboelectric layer over the electrode. The PMMA pattern has lines that are 3 millimeters in width and a gap of 6 millimeters. The grating pattern amplifies charge transfer from the sliding motion of the contacted materials. Because the width of the PMMA lines are twice that of the electrode lines, the triboelectric layer completely overlaps with the right and left electrode. Electrons transfer from the negatively charged PMMA to the positively charged silver electrode, Figure 21 [28].

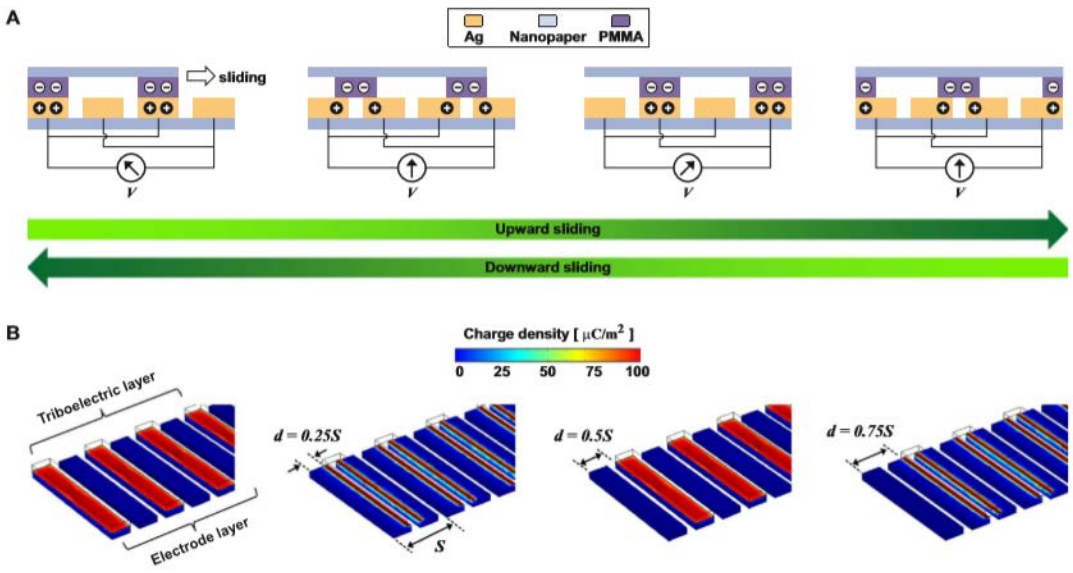

(a) charge distribution as triboelectric layer (purple) slides over electrode layer (yellow); (b) profiles of charge distribution as the electrode slides over triboelectric layer.

Figure 21. Charge Transfer across NASA Ames TENG Interdigitative Electrode. Source: [28].

Researchers produced electricity with this sliding-mode TENG using a vibration generator. Electrical current and voltage was quantified using a Keithley 6514 electrometer. The open circuit voltage had a load resistance of 200 TΩ while the short

circuit current had a load resistance of 2Ω. Abrasion damage was observed on the vulnerable 2D printed layers from the friction of the contact vibrations [28].

Through experimentation at various scan velocities, both current and voltage were shown to increase as the scanning velocity increased. However, the faster scans had shorter generation times. As the amplitude of the distance traveled by the oscillator increased, the output energy increased. Further, the correlation of current production and the frequency of vibration was tested at various amplitudes, Figure 22 and Figure 23. All amplitudes showed a bell-shaped relationship showing an optimal range of 30–60 Hz that corresponds to the natural frequency range of a typical mechanical system. Of note, the average current, I_{avg}, was used in this test instead of instantaneous current, I_{inst}, because produced energy is overestimated at higher sliding velocities. The TENG exemplified the produced power by illuminating light-emitting diode (LED) lightbulbs and by charging a capacitor using a full-bridge rectifier [28].

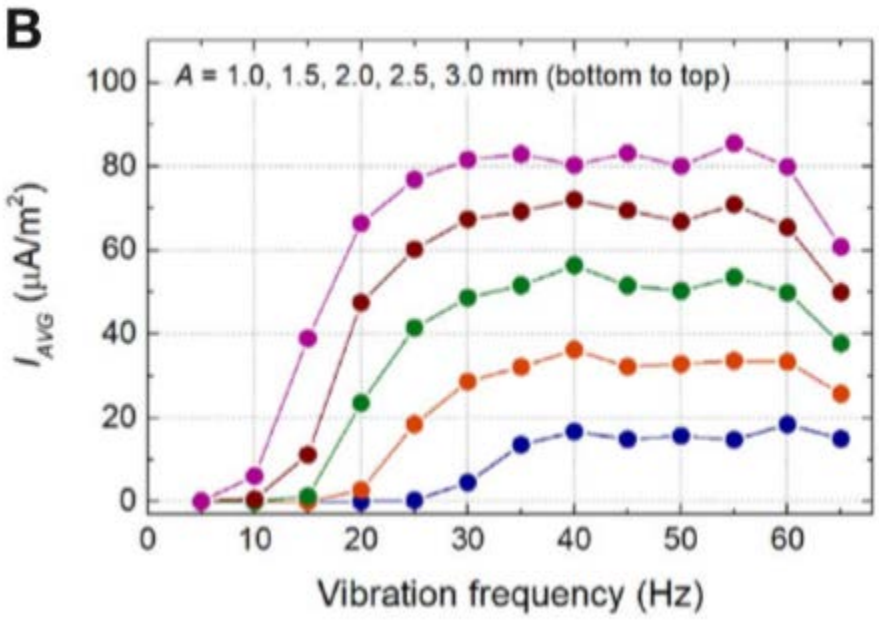

Figure 22. NASA Ames TENG: Vibration Frequency vs. Average Current Output at Various Amplitudes. Source: [28].

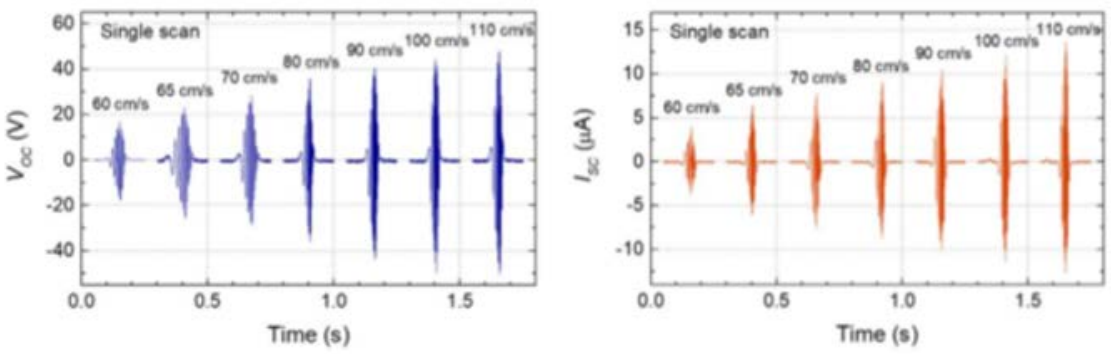

Figure 23. NASA Ames TENG: Voltage and Current vs. Time at Various Frequencies

Since the research showed that the amplitude of voltage and current corresponded to the sliding distance and not direction, this TENG operated well with linear, oscillating motion. The interdigitative electrode and grating pattern proved very effective for random, unpredictable input movements. Therefore, the simplicity of the design and fabrication along with this versatility makes this TENG ideal for the varying oscillation of ocean waves [28].

2. NPS TENG Model

A sliding-mode TENG was designed and fabricated at the Naval Postgraduate School in Monterey, California, to ultimately generate electricity from the oscillating, vertical, linear motion of waves. An interdigitative electrode with 3 millimeter finger widths and 1.5 millimeter spacing, like the 2D printed silver ink electrode, was machined out of a 0.5 millimeter depth copper plate. An electrical wire was soldered to the end of each electrode, Figure 24, to facilitate voltage and current measurements [29]. The surface area of both interdigitative electrodes is 2.118 cm^2.

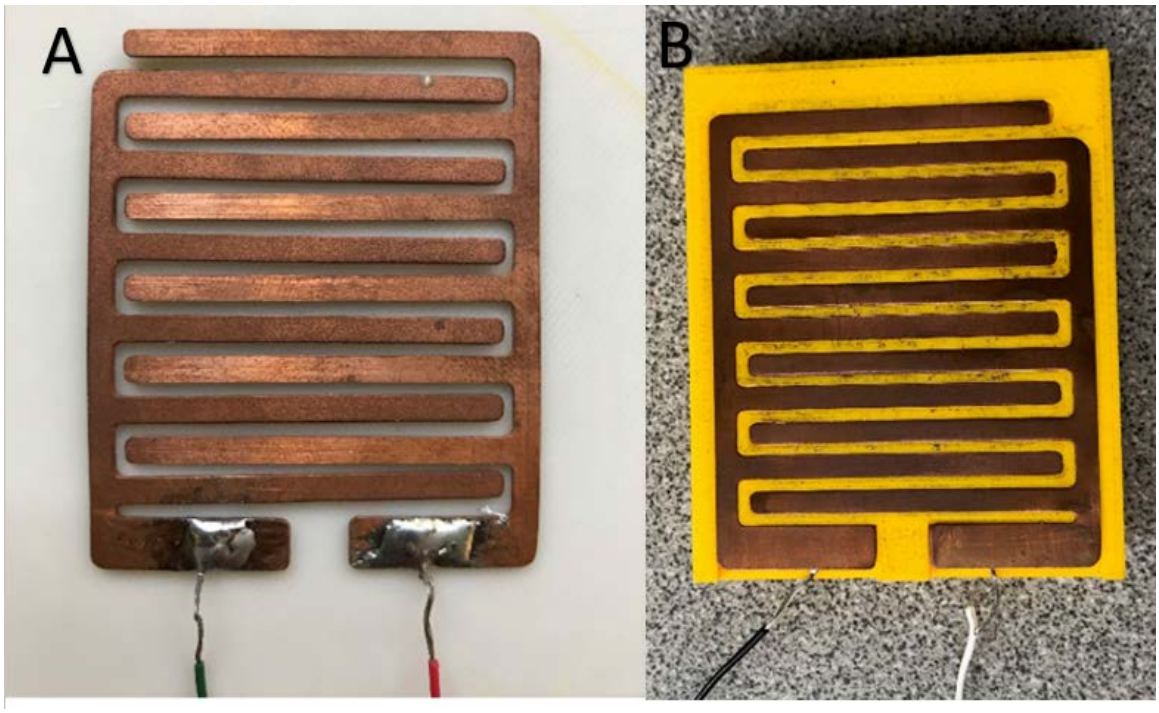

(a) soldered electrical wire on each electrode; (b) 3D printed electrode cradle.

Figure 24. Machined Copper Electrode

The triboelectric material used is a PTFE adhesive tape. Since the electrode cradle component has a width of 56 millimeter, the track has an inner width of 65 millimeters to reduce excessive friction on the side rails. The length of the track is 155 millimeters, but it could easily be extended based on the application.

The cradle for the thin, copper electrode and the track with the PTFE tape were both 3D printed using PLA. Both 3D printed parts were designed in Solidworks and printed using a Ultimaker 3 Extended at the RoboDojo on NPS's campus, Figure 25.

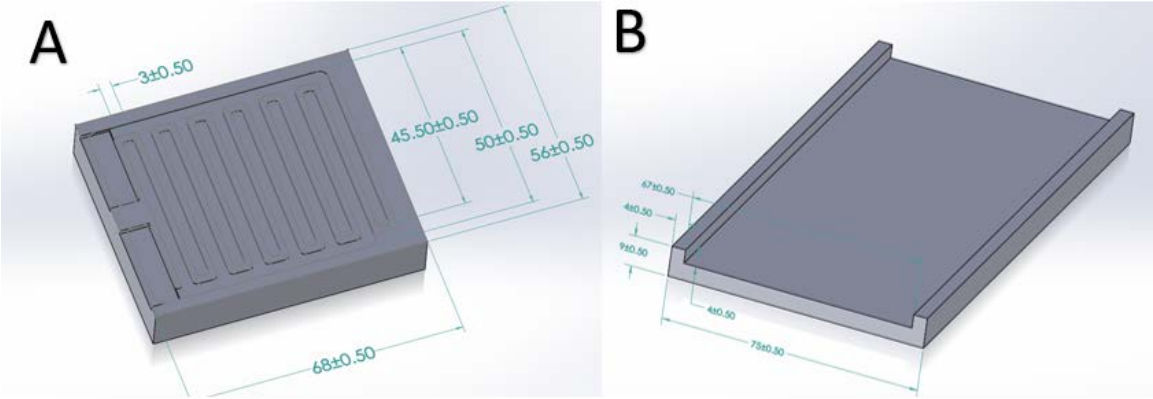

Figure 25. Solidworks Designs For 3D Printed Electrode Cradle (a) and Track (b). Source: [29].

In the first experiments conducted by ENS Sarah Reilly, two PTFE tape widths were tested. Track A had PTFE tape that was 12.5 millimeter thick with a gap width of 12.5 millimeters while Track A2 had a 6.25 millimeter tape thickness and a 6.25 millimeter gap width, Figure 26.

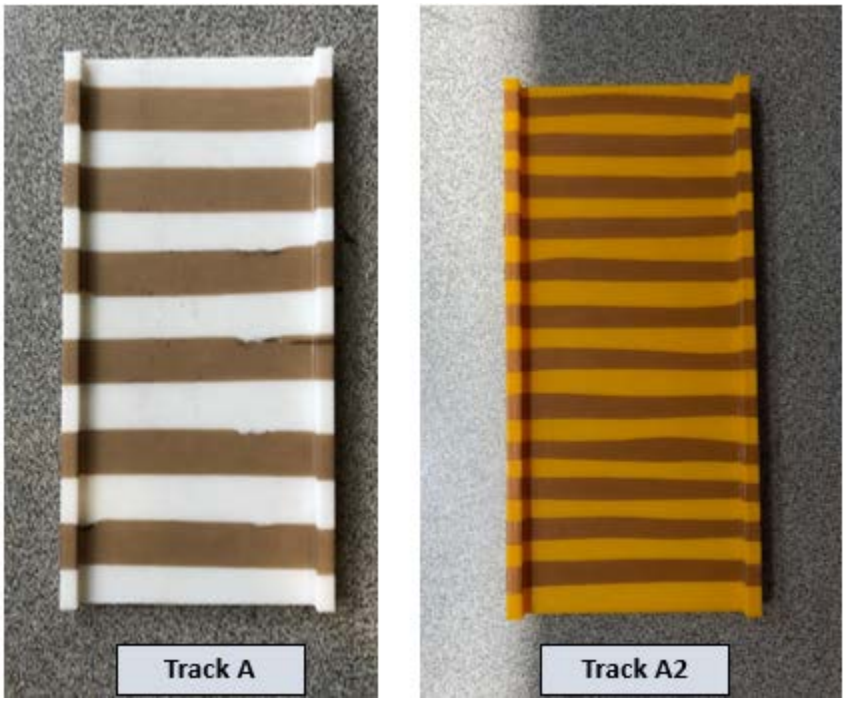

Figure 26. Tracks Used by ENS Sarah Reilly [29]

Using an adjustable-speed Bemonoc DIY Design DC 24V Linear Actuator Reciprocating Motor with a stroke of 70 millimeters, the NPS TENG was tested at two different speeds, 2.083 hertz and 4.167 hertz, under three different weight conditions. The linear reciprocating motor experiment showed that there was no noticeable trend with additional weight on the TENG. However, it demonstrated that the amount of alternating current (AC) voltage produced increased as the frequency of the TENG movement increased [29]. Results concluded that the thicker, 12.5 millimeter tape width, produced more AC voltage [29].

A mathematical model was produced from the experimental results of the TENG with no additional weight in order to predict the upper half of the AC voltage signals, V, at a given time, t, at a certain frequency, f, Equations 4 and 5.

$$\boldsymbol{V(t) = V_{peak} * sin(\omega * t)} \quad (4)$$

$$\boldsymbol{\omega = 2 * \pi * f} \quad (5)$$

Experimental data from the linear reciprocating motor testing determined the peak voltage, V_{peak}.

a. New PTFE Track Variations

For the latest round of experiments, three tape widths were used during experimentation, Figure 27. Track A was the same as ENS Reilly's and had PTFE tape that was 12.5 millimeter thick with a gap width of 12.5 millimeters. Track B had PTFE tape that was 5 millimeter thick with a gap width of 7 millimeters. Finally, Track C had PTFE tape that was 3 millimeter thick with a gap width of 6 millimeters. Track C's spacing aligns with the 3 millimeter width of the copper electrode to maximize electrical output.

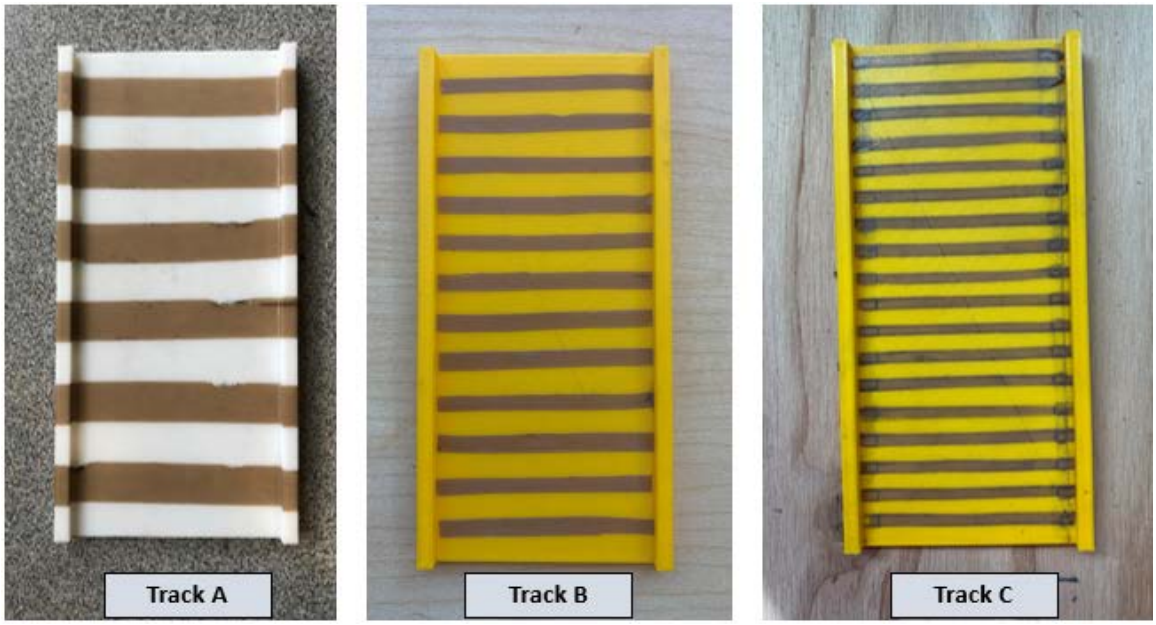

Track A: Tape width of 12.5 millimeter with 12.5 millimeter gap; Track B: Tape width of 5 millimeter with 7 millimeter gap; Track C: Tape width of 3 millimeter with 5 millimeter gap.

Figure 27. Track for Triboelectric Material

b. Wave Actuated, Oscillating Column TENG

Now that voltage could be produced and measured, the NPS TENG was attached to a device that could extract the cyclic motion of the ocean waves. A fixed, oscillating column (OC), a type of point absorber that rises and falls with each wave, replicated the same linear reciprocating motion of the tabletop motor in the ocean environment. If the OC is restricted to just vertical motion, its vertical displacement corresponded to wave height [29].

An acrylic column apparatus with diameter of 25.4 centimeters and a height of 24.5 centimeters was designed in Solidworks and then 3D printed using a Fortus 400mc in Bullard Hall at NPS. The OC's 3D printed cap was attached to polyvinyl chloride (PVC) pipe that was closed on one side. This end of the structure would ultimately float at the wave surface and facilitate the OC for moving only in the heave direction. The TENG was glued to the side of the OC on a specially designed, 3D cap that was flat on the glued side and curved on the OC side, Figure 28 and Figure 29.

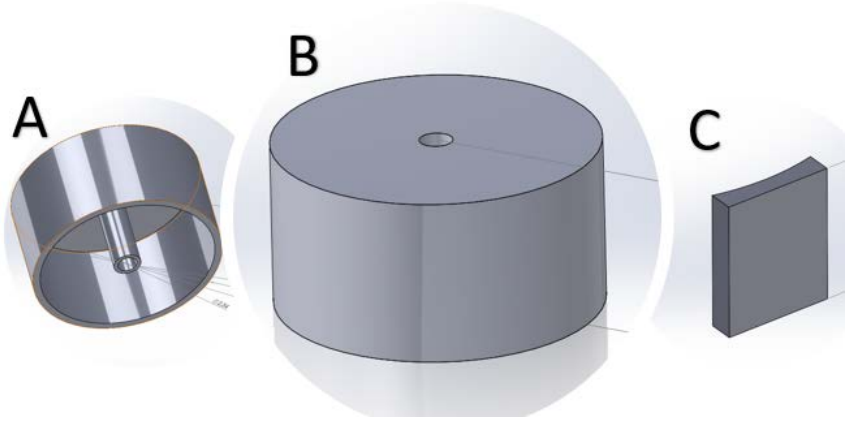

Figure 28. Components of Oscillating Column as Designed in Solidworks. Source: [29].

Figure 29. Complete Oscillating Column with Attached Electrode Side of NPS TENG. Source: [29].

PVC pipe was used to restrict the yaw and pitch motion of the OC. The PVC pipe along with another piece of wood that supported the triboelectric surface track were attached to a suspended wooden beam above the wave tank in Halligan Hall at NPS.

Therefore, the electrode side of the TENG, attached to the OC, aligned and contacted the triboelectric surface track, Figure 30 [29].

Figure 30. The OC in the NPS Wave Tank as Positioned Before Data Collection. Source: [29].

Seven frequencies of incident waves, 1.716, 1.475, 1.315, 1.2, 1.002, 0.903 and 0.816 hertz, were tested at the same wave amplitude of 2.54 centimeters, or wave height of 5.08 centimeters. The frequency of the TENG is twice that of the incident waves because for every wave, the TENG experiences both an up and down motion [29].

In contrast to the testing conducted with a horizontal linear reciprocating motor, the maximum peak-to-peak AC voltage produced in the wave tank did not increase as frequency increased. It is suspected that the challenge of having the TENG move in a vertical motion vice a more stable horizontal motion, affected the consisted contact force necessary for successful electricity generation, Figure 31 and Table 2 [29].

Table 2. Summary of OC and TENG Testing. Source: [29].

Wave Frequency	TENG Frequency	Average Max Peak to Peak AC Voltage
1.716	3.4	14.2
1.475	3.0	18.2
1.315	2.6	8.1
1.2	2.4	17.2
1.002	2.0	17.9
0.903	1.8	15.1
0.816	1.6	15

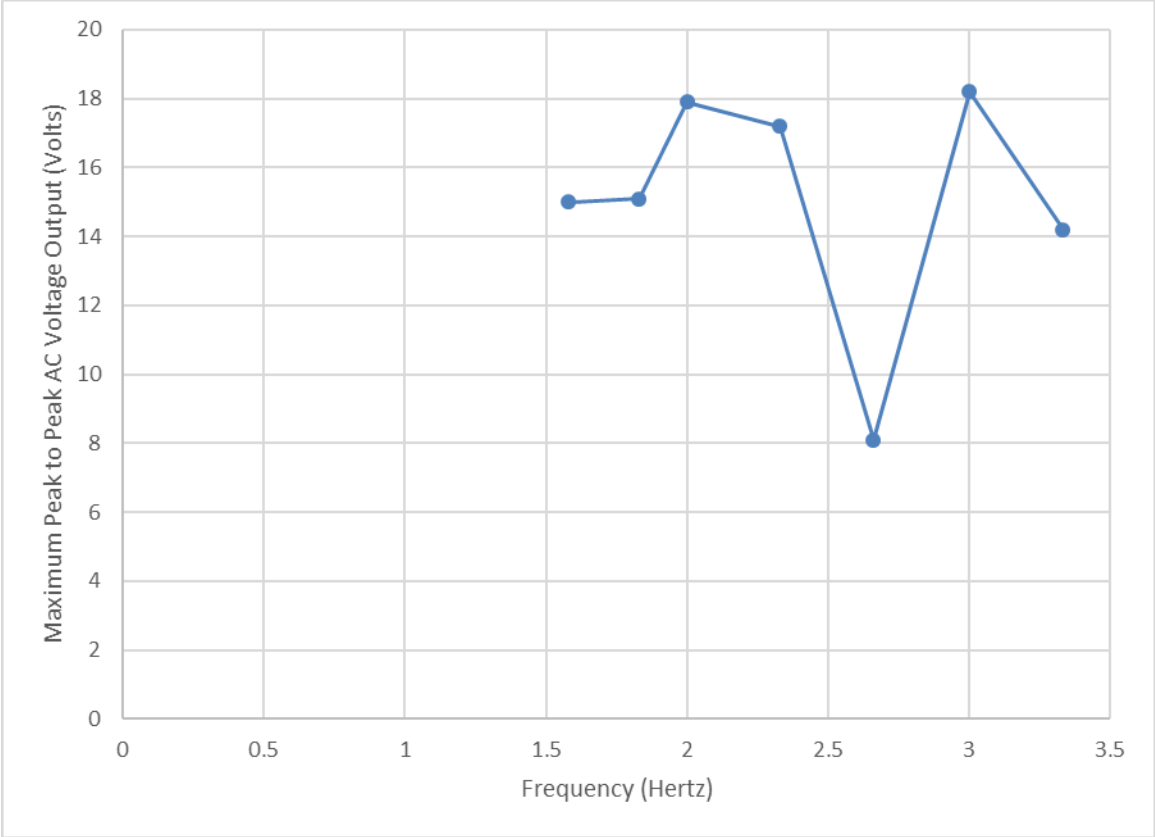

Figure 31. Frequency vs Maximum Peak-to-Peak AC Voltage Output for TENG in Wave Tank. Source: [29].

The model developed from the reciprocating motor experiment, Equation 4, was applied to the TENG's performance in the wave tank. This model was less accurate in predicting the voltage at a given time and frequency compared to the linear motor experiment, but it represented the overall trend of the data successfully [29].

B. USING GEAR BOX FOR FURTHER FREQUENCY ANALYSIS

The previous TENG research conducted at NPS suggested that the AC voltage of the NPS TENG would continue to increase as the frequency of the TENG motion increased [29]. The NASA Ames TENG, however, showed that the trend between electrical output and increased frequency did not continue indefinitely. Rather, a designated frequency range existed where current and voltage were optimized [29]. The spring driven TENG discussed early showed similar results; that is, that if the frequency of the TENG exceeded a certain

range, the transfer of charges would decrease and the TENG's effectiveness would decrease [5]. Therefore, it is desirable to find out the ideal frequency range for this TENG model so that energy production is maximized.

As discussed, the ocean environment has many challenges in relation to TENG application. Wave heights and period change constantly and create TENG frequencies that are relatively low. If the most efficient frequency range for a specific TENG model can be identified, it would be desirous to obtain that frequency of TENG movement despite the relatively low frequency of the wave providing the energy. The use of a gear box has the potential to be incredibly effective in taking the slow heave motion of waves and converting it to a higher frequency linear motion at the TENG. If the average wave period of a designated environment is known, then an appropriate gear box could be configured onto the TENG to reach this frequency range.

1. Development of Gear Box

A gear box was designed, using LEGO Mindstorm gears and other pieces from NPS's RoboDojo Laboratory, to investigate a range of frequencies in order to that maximize current and voltage output of the NPS TENG. Further, this gear box was attached to another gear assembly that would take the linear motion of the motor or ocean waves, translate it to circular motion, and enable its frequency to be adjusted using gears.

For the gear box to increase the frequency of motion, one-direction circular motion is necessary. A LEGO Mindstorm EV3 medium servo motor, Figure 32, was used to provide circular motion. The maximum rotations per minute (rpm) of the circular motor is 250 rpm, its running torque is 8 N/cm and its stalled torque is 12 N/cm. The motor is controlled using a LEGO Mindstorm EV3 Intelligent Brick, Figure 32, that is then connected to LEGO Mindstorm EV3 Programing software installed on a nearby laptop.

Figure 32. LEGO Mindstorm EV3 Intelligent Brick (left) and Medium Servo Motor (right)

Because the NPS TENG needs reciprocating linear motion in order to operate, a mechanism that translates one-direction circular motion to the two-direction reciprocating motion is required, Figure 33. For every 360° rotation that is inputted into this motion conversion mechanism (MCM), the TENG experiences one "lap" of 3.175 centimeter displacement. Therefore, the overall gear ratio is 2:1 at the MCM. The track with the PTFE tape is affixed to the same plane as the whole gear box apparatus and the TENG is attached to this MCM.

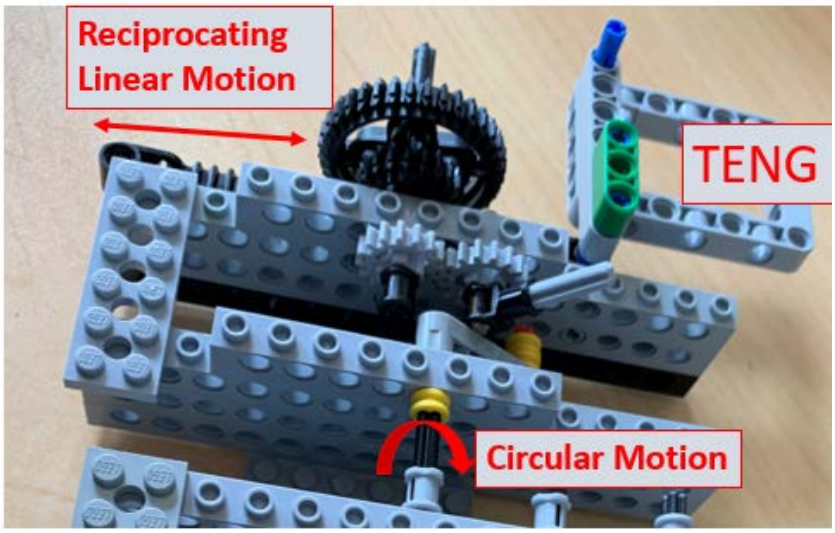

Figure 33. MCM Working Mechanism

Two different types of gears were used in the gearbox. The larger driving gears had 24 teeth while the smaller gears had 8 teeth, Figure 34. Therefore, the intertwined gears produced a gear ratio of 1:3.

Figure 34. Driving Gear and Driven Gear for MCM

The gear box contained three shafts, 2 of which were used to increase the rpms of the input shaft, Figure 35. The motor could be moved to connect to each shaft in order to obtain a desired "step" ratio. Shaft 1 did not incorporate any gears, so it translated the circular motion of the motor directly to the input of the MCM at a 1:1 ratio. If the motor was attached to Shaft 2 where the gear ratio was 1:3, the rpms at the MCM would be 3 times greater than that at the circular motor. Finally, if the motor was attached to Shaft 3, the rpms at the MCM would be 9 times greater than the circular motor's output rpm because it would experience two sets of gears before connecting to the MCM on Shaft 1.

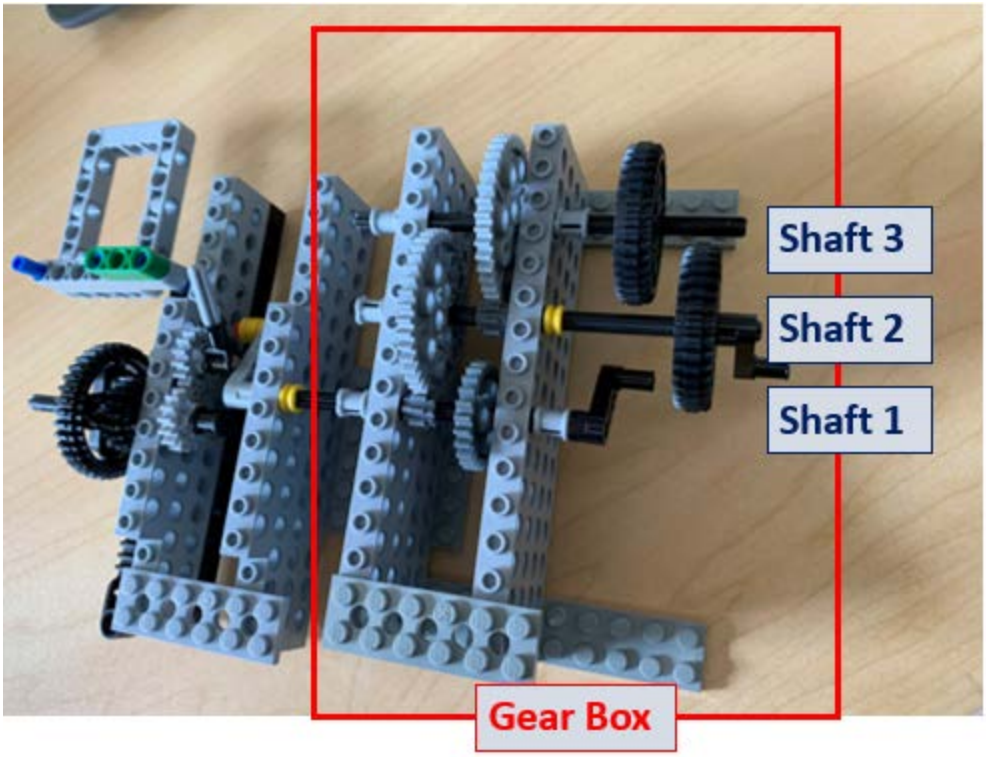

Figure 35. MCM Depicting Shafts 1, 2, and 3

As gears in a gear box experience greater "step ups," the torque of the shafts increased. Therefore, the toque needed to rotate shaft 1 is less than shaft 2 and much less than shaft 3. Due to the torque limitations of the circular motor and the 1:9 gear ratio between shaft 1 and shaft 3, the circular motor was not able to properly rotate shaft 3. However, its operation was demonstrated by a hand crank. If this design was constructed with stronger, more robust building material that could handle the appropriate amount of torque, the gear step-up could seemingly continue to increase. The data obtained by this frequency experiment focused on the range of frequencies produced on shaft 1 and shaft 2 at various motor speeds, Figure 36.

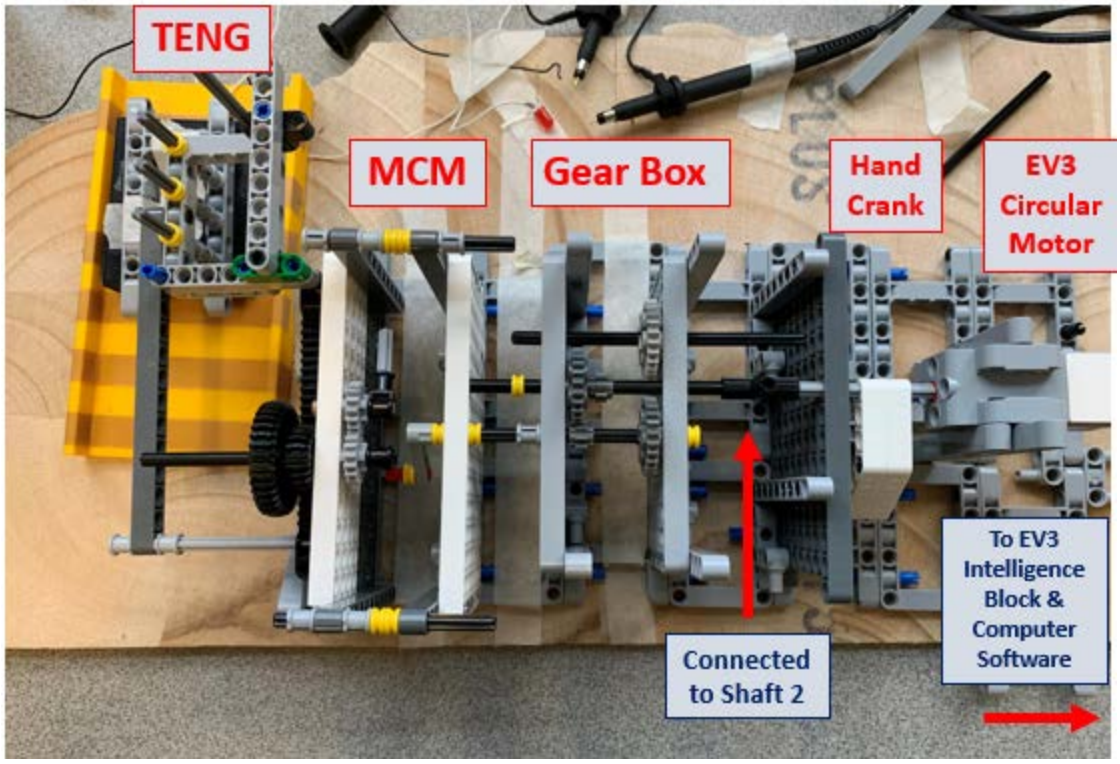

(from left) Input circular motion from EV3 circular motor, the gear box with three shafts, the MCM and sliding TENG.

Figure 36. Experimental Setup of MCM

2. Converting Reciprocating Linear Wave Motion to One Direction Circular Motion

In order for this gear box and associated MCM to be applicable to the oscillating column in an ocean wave environment, it must be able to take reciprocating, two-directional motion as its input. A second motion conversion system (MCS) was constructed using LEGO Mindstorm material to prove that the two directional motion, provided by the linear reciprocating motor used in the previous experiment, could be translated through this worm gear-driven MCS, Figure 37.

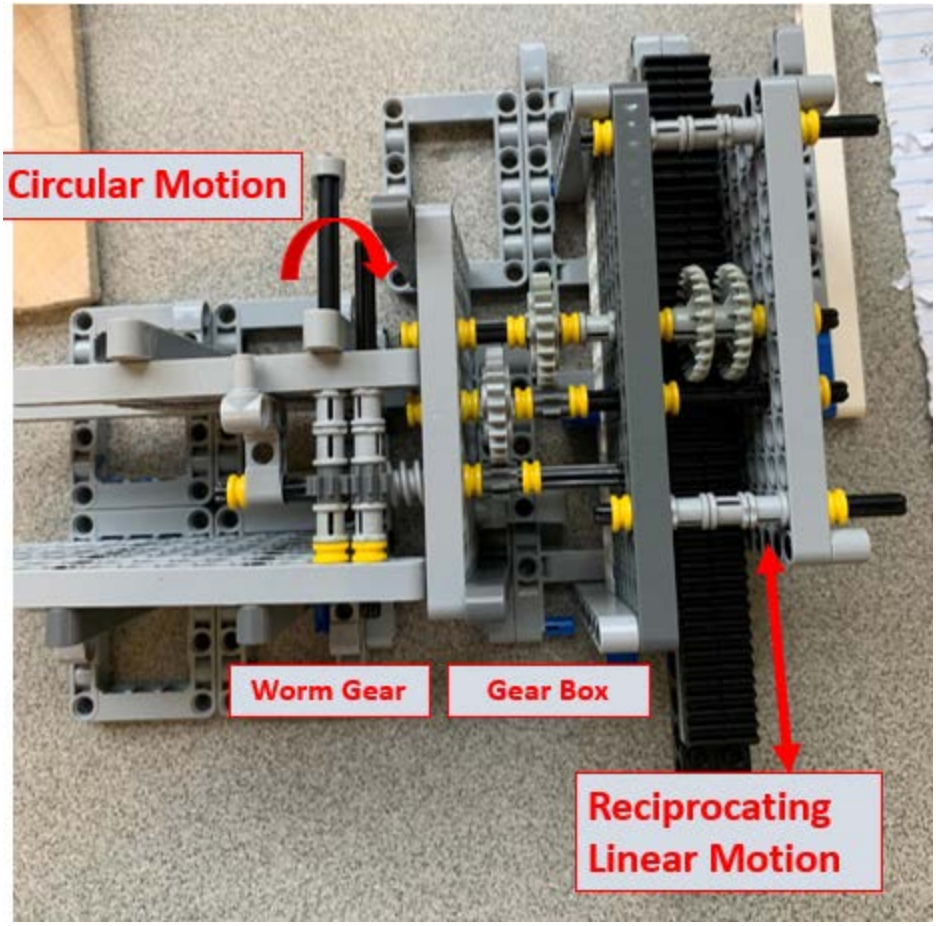

Figure 37. MCS System

This MCS consists of an input wheel housing structure that rotates through the reciprocating motion of the linear motion source. The linear motion source must have a track attached to it in order to turn this wheel. Next, a set of gears steps up the circular motion provided by the input wheel by a ratio of 1:9. The output shaft of this gear set, moving 9 times faster than the input shaft, then connects to a worm gear apparatus. The worm gear, which as 5 teeth, moves back and forth between two gears rotating inward with 8 teeth. However, once the worm gear moves 6 rotations by both small gears, it is "released" and continues to rotate only in the counter-clockwise direction. If the direction of the input wheel is reversed, the worm gear will move back through the two smaller gears but again, continue to rotate in the same counter-clockwise direction. It is important to note that 6 rotations of the worm gear are needed in order to completely transfer it from one side

of the small inward turning gears to the other. Therefore, with each change of direction, 6 revolutions of the shaft connected to the worm gear are loss. In addition, once the worm gear is rotating the output shaft, it has an 8:1 gear reduction. The shaft with the worm gear is the "output" shaft of the MCS. Ultimately, for a linear reciprocating input frequency of 6 hertz, the output shaft, with this current gear configuration, has a frequency of 6.75 hertz.

Based on the input frequency of the linear reciprocating motion source and the desired output, the gear ratio of the MCS gear box can be adjusted. Additionally, the length of the worm gear could be altered to increase the efficiency of the system and reduce the number of revolutions per minute. Based on the nature of the gears used, the system must be constructed with strong enough material to keep the shafts and gears aligned in order to handle the operating torques.

If the output shaft of the MCS, which has one direction circular motion, is connected to any of the shafts of the gear box, the rpms of the circular motion are increased to obtain the desired range of reciprocating motion frequency at the TENG, Figure 38. This entire mechanical system proves the concept that a variable amplitude and frequency two-directional reciprocating motion, provided by energy sources such as waves, can be translated to one direction circular motion where its speed can be adjusted to facilitate a desired two-directional reciprocating linear motion at the TENG side.

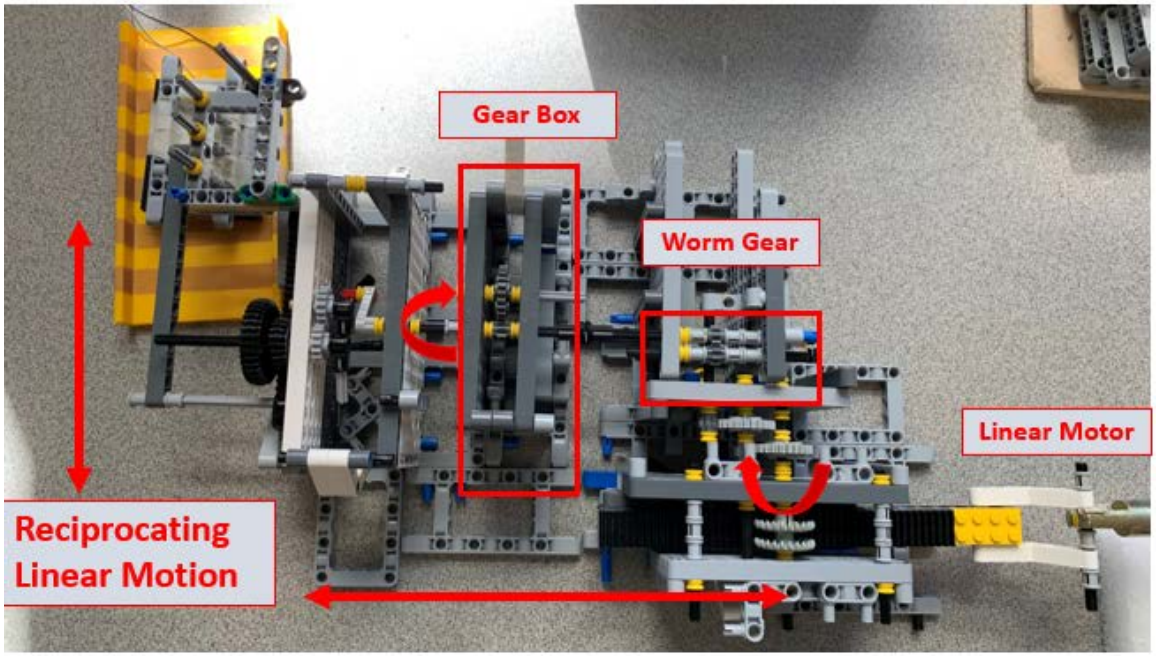

This system depicts how linear reciprocating motion can be converted to one-directional circular motion, amplified by a gear box, and translated again to linear reciprocating motion.

Figure 38. Complete MCM and MCS System

The current model's biggest obstacle is its strength and durability. The LEGO Mindstorm connections and pieces were not designed to handle the torques and forces associated with the gears, motion-type conversions, axial stresses and torsional stresses. However, if this system were constructed with a metal housing structure, shafts, gears, etc., with the ability to withstand the magnitude of forces and torques, the system would be able to handle both a vast range of input frequencies and amplitudes and output TENG frequencies.

C. PULLEY SYSTEM TO FACILITATE HORIZONTAL MOTION AND WATER PROTECTION

The NPS TENG has already been successfully tested in a laboratory-created ocean environment while attached on the OC apparatus [29]. However, the smaller AC voltage values produced by the OC compared to the table-top linear motor testing suggests that the vertical sliding motion of the wave tank apparatus decreased the friction and subsequent transfer of charges [29]. ENS Sarah Reilly recommended that future testing should attempt

to improve the reliable, consistent contact between the TENG and the PTFE-taped track. Additionally, she suggested that both pre-wave tank testing and any experiment in the wave tank should be conducted on the same axis plane [29]. Because of this and the requirement that TENGs be enclosed and isolated them from any exposure to water, a system was designed to improve the consistency and overall performance of the NPS TENG [15,13,12].

This new system connects the linear reciprocating motion of either the table-top linear motor or the floating OC to the horizontally-sliding NPS TENG via a cable, Figure 39. Since a 90° translation is necessary to convert the vertical motion of the OC to horizontal motion, a fixed, free-rotational pulley will provide the necessary 90° axis change. A spring will ensure that the NPS TENG returns to its original position on the track after each positive displacement stroke. This system will not only keep the axis of operation of the Watkins laboratory table-top testing identical to the Halligan Hall wave tank testing, but it will also make efforts to isolate the TENG system from crippling exposure to water much easier. Figure 39 shows the conceptual design of the system.

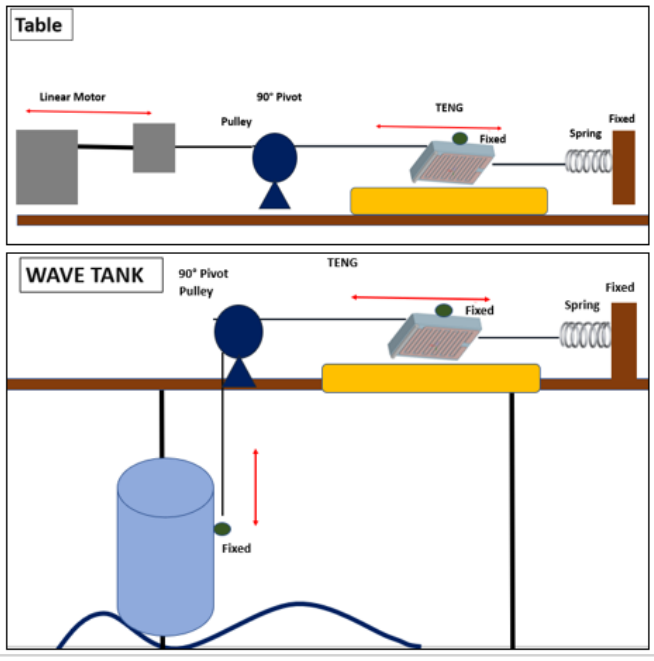

Figure 39. Conceptual Design of Tabletop and Wave Tank System

In theory, the cables connecting the OC to the horizontal-moving TENG could have various lengths based on the application. For example, if an OC were placed on the water surface underneath a dock at a U.S. Navy base, a TENG could sit at a much less vulnerable location on top of the dock. By connecting the TENG and OC with a cable, the TENG would not be as susceptible to ocean spray, storm waves, emersion from large tidal variations and even curious ocean life. Rather, the TENG could be enclosed in a structure that would provide protection and allow for normal operations throughout the pier. This same design also has the potential to produce electricity from the free-surface-effect waves in a U.S. Navy ship's ballast and oil-water-compensation tanks. An internal OC could heave continuously in the tanks and transfer that movement to a TENG sliding outside the enclosed, humid and aqueous environment of the tank.

1. Linear Motor, Tabletop System

A tabletop model of the pulley-spring system was constructed to a 60.96 centimeter by 60.96 centimeter wooden support in the NPS Watkins Hall Laboratory. The reciprocating linear motor was fastened to the wooden support 12.7 centimeter from a fixed, 2.5 centimeter steel ball bearing pulley, when fully extended. The pulley's track is 4.92 centimeter from the base of the wooden board to align with the 4.92 centimeter height of the linear motor's arm. A twisted mason line cable is then attached to the "eye" at the end of the linear motor's arm, run through the pulley and attached to the NPS TENG via a fixed support piece. The pulley facilitates a 90° translation in the cable direction. The support piece is a Mindstorms LEGO rectangular support and it is attached to the 3D printed electrode cradle using Velcro strips. This cable then continues through the support piece and is ultimately attached to a spring. This helical spring is attached to another wooden block at the same height as the pulley and linear motor, 4.92 centimeter. The spring's maximum working load is 1.1 kilograms, its length is 4.8 centimeters, its spring diameter is 8.7 millimeters and the diameter of the wire itself is 0.6 millimeters. This spring allows the TENG to retrack to its original position, when the linear motor is fully extended. Upon each stroke of the linear motor, the motor displaces the NPS TENG 70 millimeters towards the pulley and the spring provides counter pressure to bring the NPS TENG back to the original position as the linear motor extends again. A 3D housing structure made

from PLA contains the track which is held steady by metal brackets. Figure 40 shows the components of the tabletop system while Figure 41 shows the entire assembly.

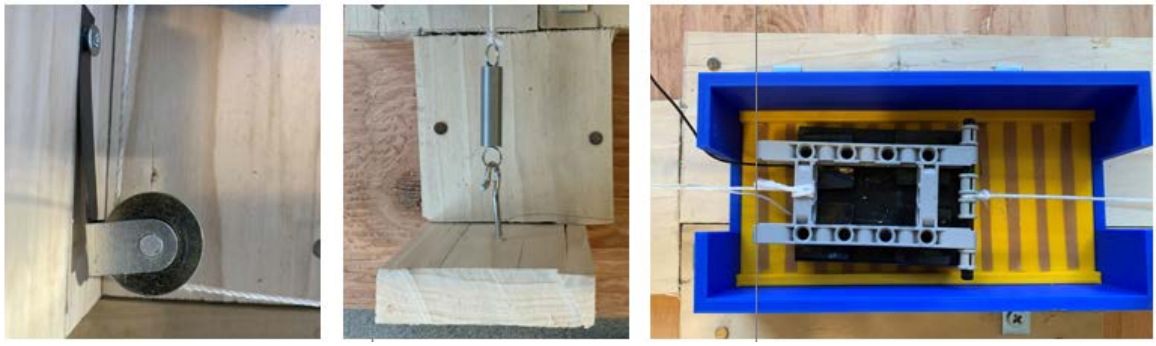

Figure 40. Components of Tabletop and Wave Tank Systems

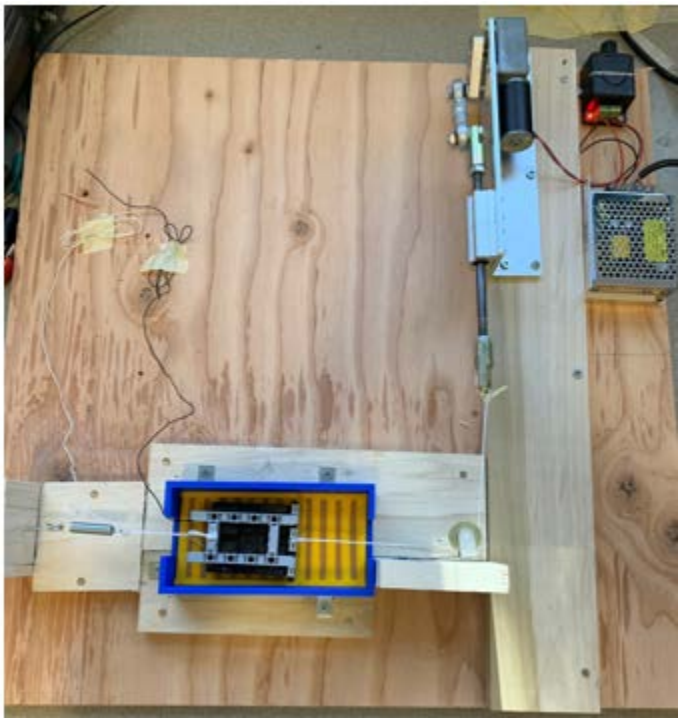

Figure 41. Linear Motor Tabletop Assembly

2. Oscillating Column, Wave Tank System

The system constructed for use with the oscillating column in the Halligan Hall wave tank is almost identical in operation to the one constructed for tabletop testing with

the linear reciprocating motor. However, the pulley facilitates a 90°, perpendicular change from the horizontal plane to the vertical plane. All the components including the spring, pulley, cable, TENG and track are the same.

The spring, TENG track and pulley are all affixed to a wooden beam that supports the PVC pipe through which the OC heaves. The PTFE-taped track is fixed 7.5 centimeter away from the spring and 17.5 from the center of the pulley. The cable then connects the spring, the rectangular support glued to the TENG, the pulley track and then the top of the oscillating column. It is important to attach the cable to the spring and TENG so that the original position represents the estimated maximum wave height or crest. Therefore, as a wave falls into a trough, the OC will drop and the force of the OC dropping will displace the TENG. Figure 42 depicts the system installed across the wooden beam in the wave tank. Figure 43 shows a close-up view of how the cable is attached to the OC.

Figure 42. Oscillating Column with TENG Pulley-Spring System

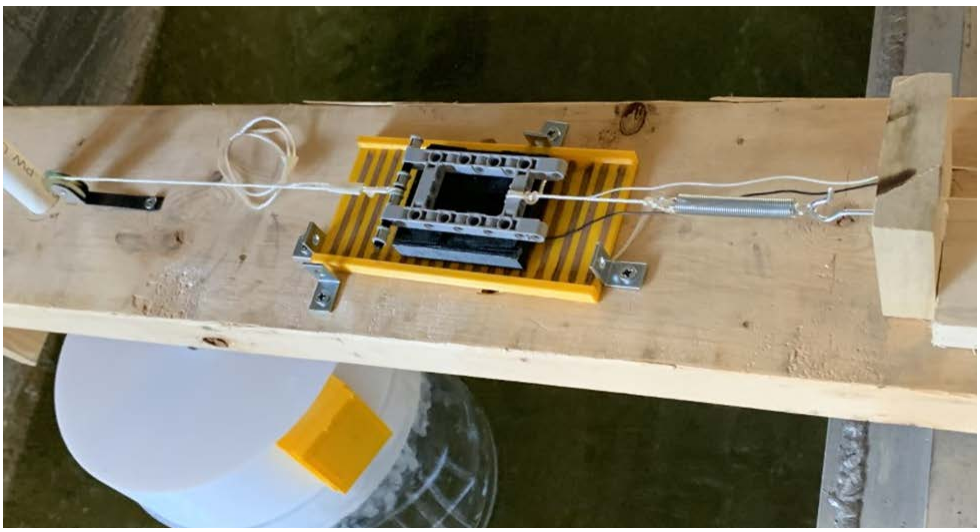

Figure 43. Pulley-Spring System for Wave Tank Assembly

For the spring-pulley system to work properly, the spring must be at its natural state when the maximum anticipated wave height is reached. Once the maximum anticipated wave height is defined, the appropriate length of cable between the OC and TENG can be adjusted.

D. MEASUREMENT SYSTEM

The previous experimentation on the NPS TENG quantified only AC voltage using a Keysight DSO1052B digital oscilloscope [29]. This analysis measured not only AC voltage but also the closed-circuit current produced by the NPS TENG. The same copper interdigitative electrodes, 3D printed electrode cradle and 3D printed track that were used by ENS Sarah Reilly were used for this analysis, with the addition of two more tracks [29]. New PTFE tape was placed on Track A and the wires connected to each copper electrode were cut, restriped and re-soldered to bolster the connection used for electrical measurement.

A newer oscilloscope, the Teledyne Lecroy WaveJet Touch 334, was used with a standard passive probe to measure open circuit AC voltage, Figure 44. The Keysight DSO1052B digital oscilloscope was used to capture some images of voltage generation.

Since the current produced by TENGs in general and this model particularly, are so small, standard current measurement devices such as the Tektronix TCPA300 Amplifier, AC/DC Current Probe and Fluke 87 True RMS Multimeter did not accurately collect current readings. However, the Keithley 617 Programmable Electrometer, which measures current to the picoamp range (10e-9 A), captured the closed-circuit current produced by the TENG. The developers of the NASA Ames model also used a Keithley (Model 6514) Electrometer to measure closed-circuit current [28].

Figure 44. MCM Voltage Testing with Teledyne Lecroy Oscilloscope

The LEGO EV3 medium servo motor produced the circular motion necessary to test various frequencies using the MCM. The turning rate of the motor was adjusted via the EV3 Intelligence block which was then connected to and controlled through the EV3 Programing Software on a laptop computer.

Finally, the Bemonoc DIY Design DC 24V Linear Actuator Reciprocating Motor with a stroke of 70 millimeters, the same motor used for ENS Sarah Reilly's research was used to simulate the heave of ocean waves prior to wave tank testing, Figure 45 [29].

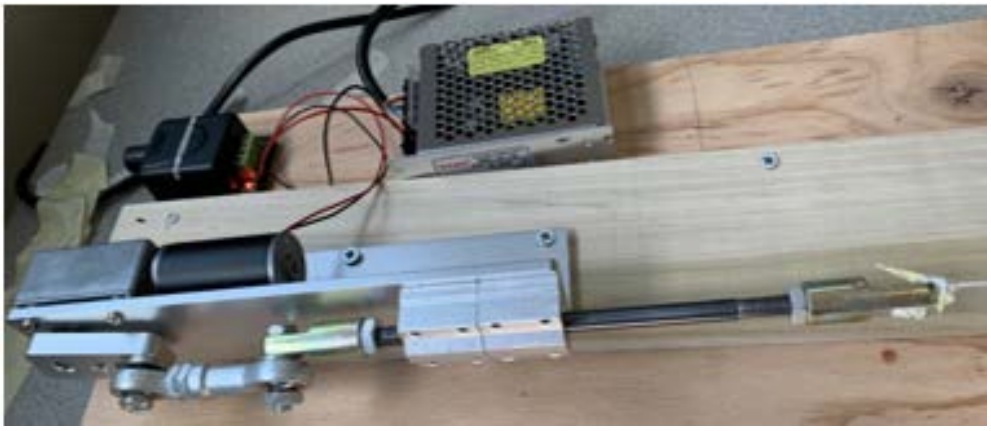

Figure 45. Bemonoc DIY Design DC 24V Linear Actuator Reciprocating Motor with a 70-Millimeter Stroke

III. RESULTS FROM EXPERIMENTATION

Three separate series of experiments were conducted on the NPS TENG. First, the correlation of TENG frequency to AC voltage and closed-circuit current was tested at various speeds using the MCM, gear box and EV3 medium servo circular motor using Track A. Next, AC voltage and closed-circuit current was measured at three speeds using the table-top apparatus consisting of the Bemonoc linear reciprocating motor, a pulley with a 90° change and the NPS TENG. Data was collected for Track A, Track B and Track C in the tabletop testing. Finally, AC voltage and closed-circuit current data was collected using the modified OC with the 90° change pulley that facilitates the TENG sliding on the horizontal plane using Track C. Seven different wave frequencies, all at a fixed wave height, were tested in NPS's Halligan Hall wave tank. Every different testing parameter was tested three times to ensure consistency.

A. EXPERIMENTAL RESULTS OF TENG FREQUENCY ANALYSIS WITH ATTACHED GEAR BOX AND CIRCULAR MOTION

The following are the results of the NPS TENG frequency analysis using a circular motor, attached gear box and Track A. AC output voltages and closed-circuit current readings from the NPS TENG at two gear ratios and 12 total frequencies. The MCM was configured on shaft 1 with a gear ratio of 1:1 at 5%, 10%, 15%, 25%, 50%, 75% and 100% of the speed of the LEGO EV3 motor. Next, shaft 2 with a gear ratio of 1:3, was engaged by the EV3 motor at 5%, 10%, 15%, 25%, 50%, 75% and 100% of the motor speed as well. Table 3 shows the conversion from EV3 motor speed percentage to frequencies, in hertz. Two runs were conducted at each gear ratio and frequency for redundancy. Of note, 15% and 75% at a gear ratio of 1:1 had the same frequency as the 5% and 25% runs, respectively, at a gear ratio 1:3.

Table 3. Frequencies Tested with MCM for Frequency Analysis

Speed (%)		RPM at Motor	RPM at TENG	Hertz
1:1 Gear Ratio				
5%	0.05	12.25	12.25	0.204
10%	0.10	24.5	24.5	0.408
15%	0.15	36.75	36.75	0.613
25%	0.25	61.25	61.25	1.021
50%	0.50	122.5	122.5	2.042
75%	0.75	183.75	183.75	3.063
100%	1.00	245	245	4.083
1:3 Gear Ratio				
5%	0.05	12.25	36.75	0.613
10%	0.10	24.5	73.5	1.225
15%	0.15	36.75	110.25	1.838
25%	0.25	61.25	183.75	3.063
50%	0.50	122.5	367.5	6.125
75%	0.75	183.75	551.25	9.188
100%	1.00	245	735	12.250

Two frequencies tested were redundant (highlighted in yellow) at the 1:1 gear ratio and at the 1:3 gear ratio.

1. Voltage Data

AC voltage data was collected by the Keysight DSO1052B digital oscilloscope at 1 sample/100 microseconds or 10 samples/second for 40 seconds. Therefore, each sample period consisted of 400 data points.

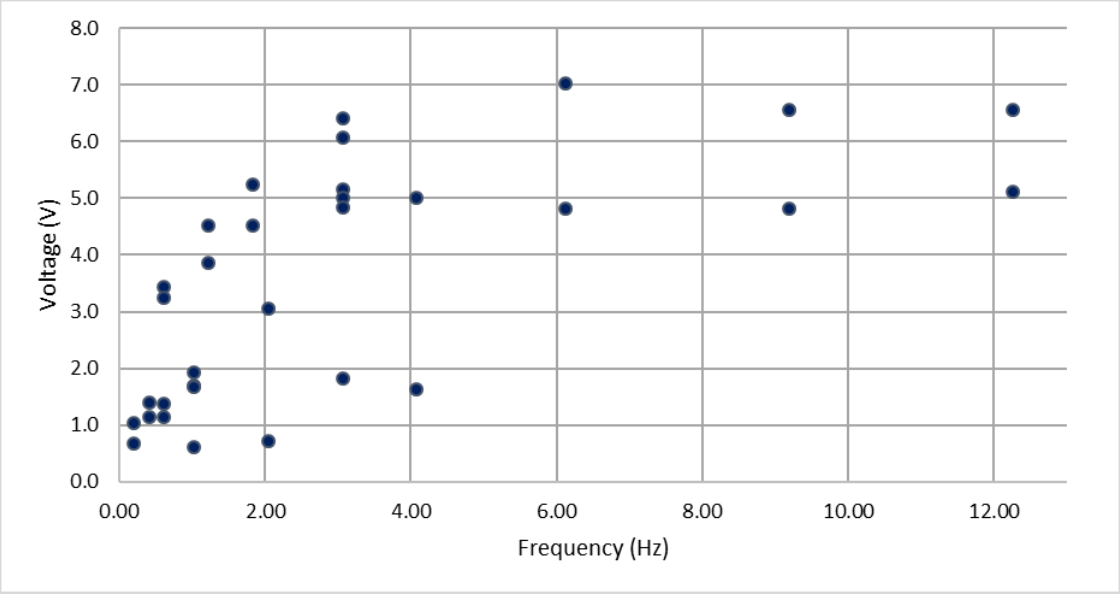

Figure 46. Maximum Peak-Peak AC Voltage for Each Frequency Tested

Just as ENS Sarah Reilly concluded in previous testing of the NPS TENG, AC voltage increased as frequency increased [29]. Although the highest voltage reading occurred at a frequency of 6.125 hertz, the follow-on voltages were still relatively high. Figure 46 suggests that voltage will increase as frequency increases but will eventually hit a frequency when it will plateau. More data results from each series of test runs at each of the two gear box ratios can be found in Appendix A.

2. Current Data

Closed circuit current data was collected by the Keithley 617 Programmable Electrometer at the instrument's maximum sampling rate of 1 sample/360 microsecond which is the equivalent of 2.78 samples/ second. Since the instrument can only save up to 100 data points, a maximum of 100 data points could be collected in 37 seconds.

Figure 47 depicts an example of a slow frequency run, 0.408 hertz, at the lower 1:1 gear ratio.

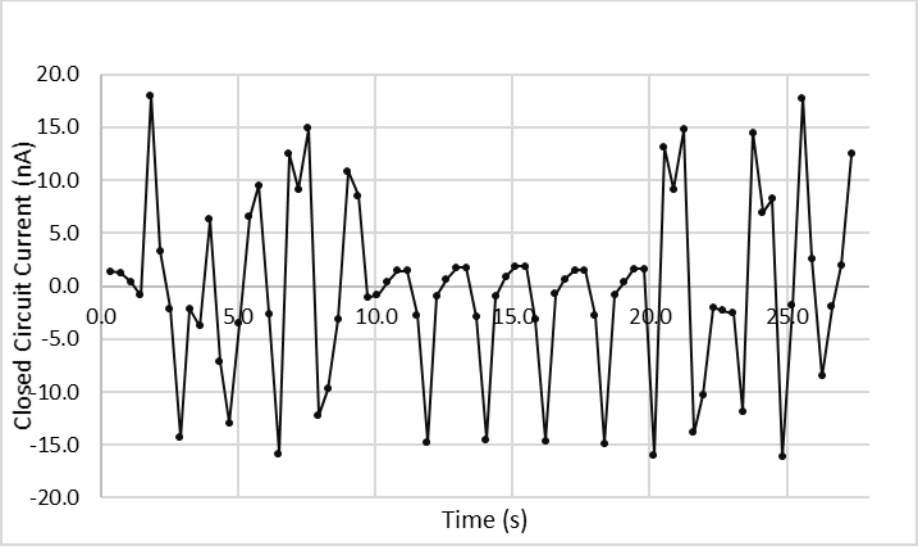

Figure 47. Closed Circuit Current at 1:1 Gear Ratio and 0.408 Hertz

This low frequency test run produced some of the largest values of current of any of the test runs, approximately 19 nA and -16nA. The pulses of current were relatively consistent throughout the testing period.

Figure 48 represents a high frequency, 6.125 hertz, run at the higher 1:3 gear ratio.

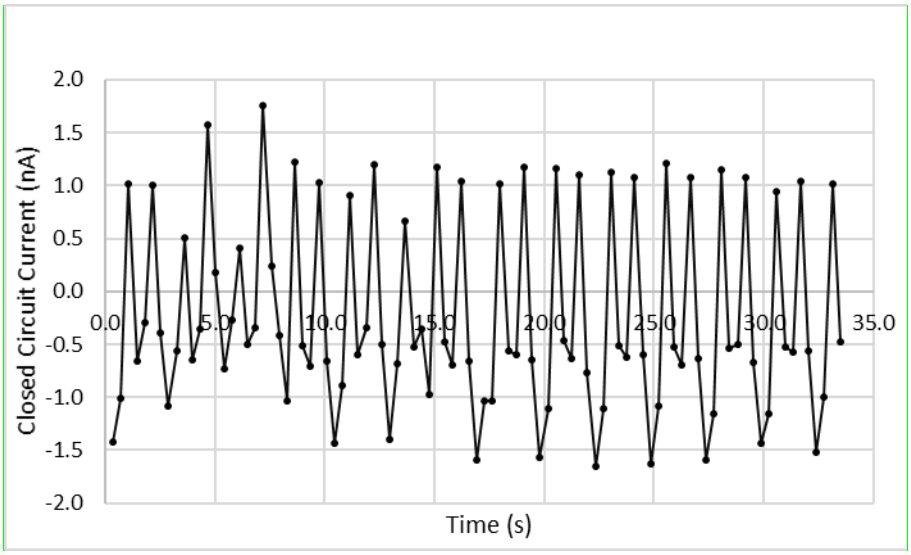

Figure 48. Closed Circuit Current at 1:3 Gear Ratio and 6.125 Hertz

This relatively high frequency test run produced consistent pulses of current, but the amps measured, approximately 1.8 nA, were much lower than the values produced in the low frequency test run, Figure 47. The positive and negative peaks correspond to the reciprocating, sliding motion of the NPS TENG.

Finally, Figure 49 shows the rectified maximum values versus frequency for every test run in the frequency analysis experiment.

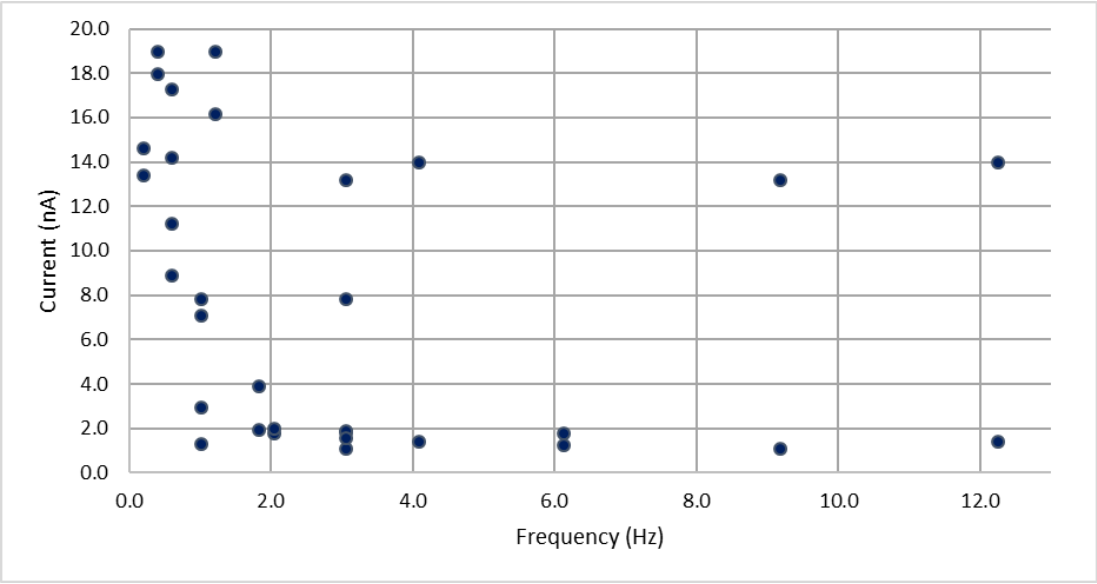

Figure 49. Maximum Closed-Circuit Current during Frequency Analysis Testing

Figure 49 depicts the unanticipated findings that the lower frequency test runs produced higher maximum values than the higher frequency test runs. Also, results from one of the two test runs at higher frequencies produced much smaller current values than the previous test run.

More data results from each series of test runs at each of the two gear box ratios can be found in Appendix A.

3. Summary of Frequency Analysis Results

The frequency analysis testing led to some trends between the frequency of the NPS TENG and the maximum AC voltage and closed-circuit current. The maximum AC voltage increased with an increase of frequency until approximately 6 hertz where it then plateaued at approximately 6 V. Further, current measurements were greatest at slower frequencies, in contrast to what was expected. However, once the frequency of the NPS TENG reached 9 hertz, the current stayed above 7 nA. Table 4 summarizes the averaged maximum voltage and current results while Figures 50 and Figure 51 depict the trends. If there were more than one measurement for a certain frequency, the value shown was the average of the data collected at that frequency.

Table 4. Summary of Maximum, Averaged Peak-Peak AC Voltage and Closed-Circuit Current for Frequency Analysis Testing

Frequency (Hz)	AC Voltage Max (V)	Closed-Circuit Current Max (nA)
0.204	0.859	13.999
0.408	1.270	18.464
0.613	2.298	12.894
1.021	1.476	4.781
1.225	4.200	17.554
1.838	4.890	2.906
2.042	1.889	1.879
3.063	4.878	4.561
4.083	3.319	7.682
6.125	5.920	1.496
9.188	5.685	7.122
12.250	5.840	7.684

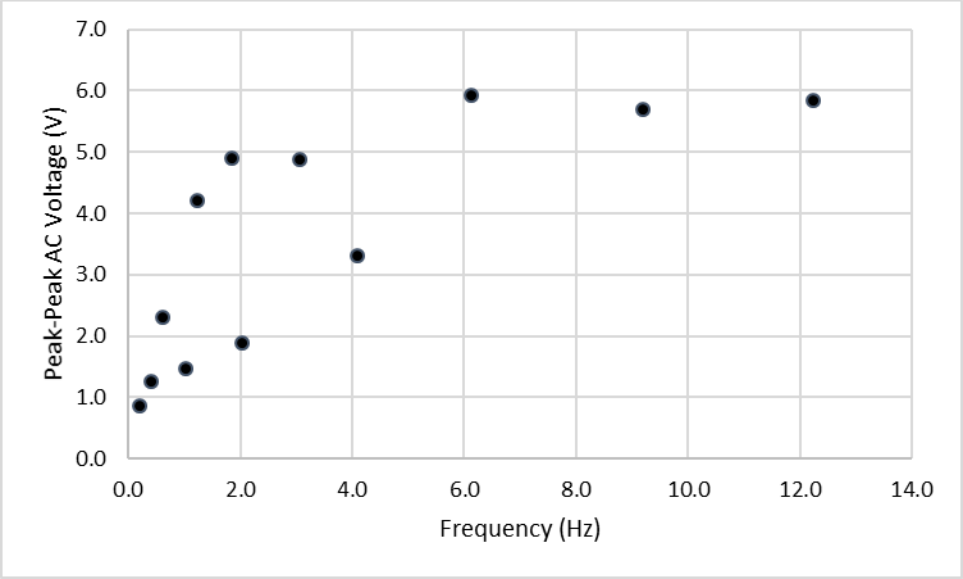

Figure 50. Averaged Maximum Peak-Peak AC Voltage vs. Frequency for NPS TENG

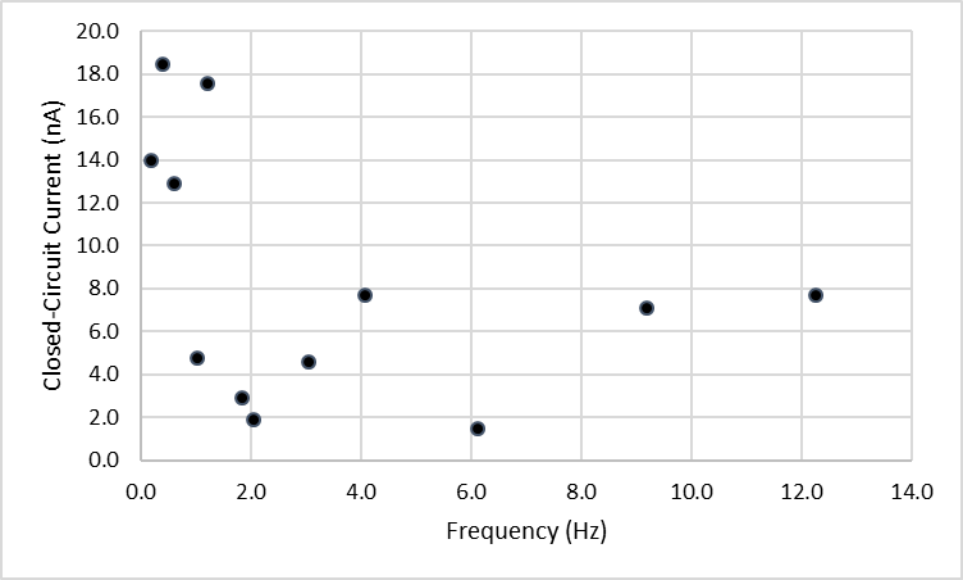

Figure 51. Averaged Maximum Closed-Circuit Current vs. Frequency for NPS TENG

Based on the current and voltage testing conducted on the NPS TENG, potential power and power density, using the surface area of the copper electrode, were calculated, Table 5. The surface area of the two copper electrodes, 24.188 cm^2, is used to calculate

power density. Figure 52 depicts the potential power produced at each frequency while Figure 53 displays the power density at each frequency.

Table 5. Summary of Maximum, Averaged Potential Power and Power Density for Frequency Analysis Testing

Frequency (Hz)	Potential Power (nW)	Power Density (nW/cm^2)
0.204	12.018	0.497
0.408	23.449	0.969
0.613	29.417	1.216
1.021	6.857	0.283
1.225	73.725	3.048
1.838	14.210	0.587
2.042	3.549	0.147
3.063	20.316	0.840
4.083	25.498	1.054
6.125	8.858	0.366
9.188	40.488	1.674
12.250	44.875	1.855

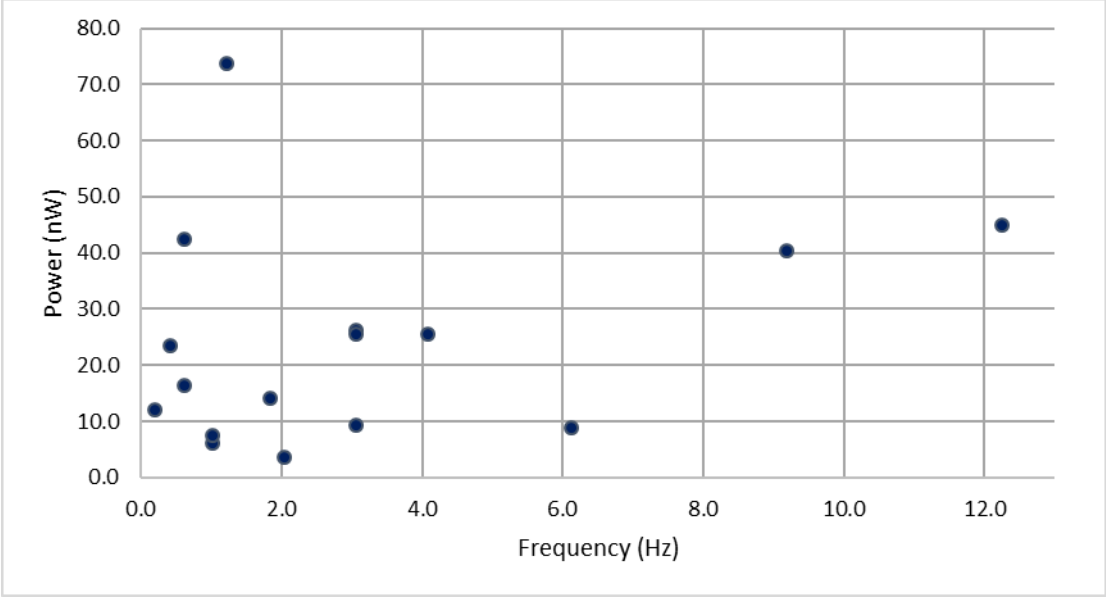

Figure 52. The Potential Power Generated vs. Frequency

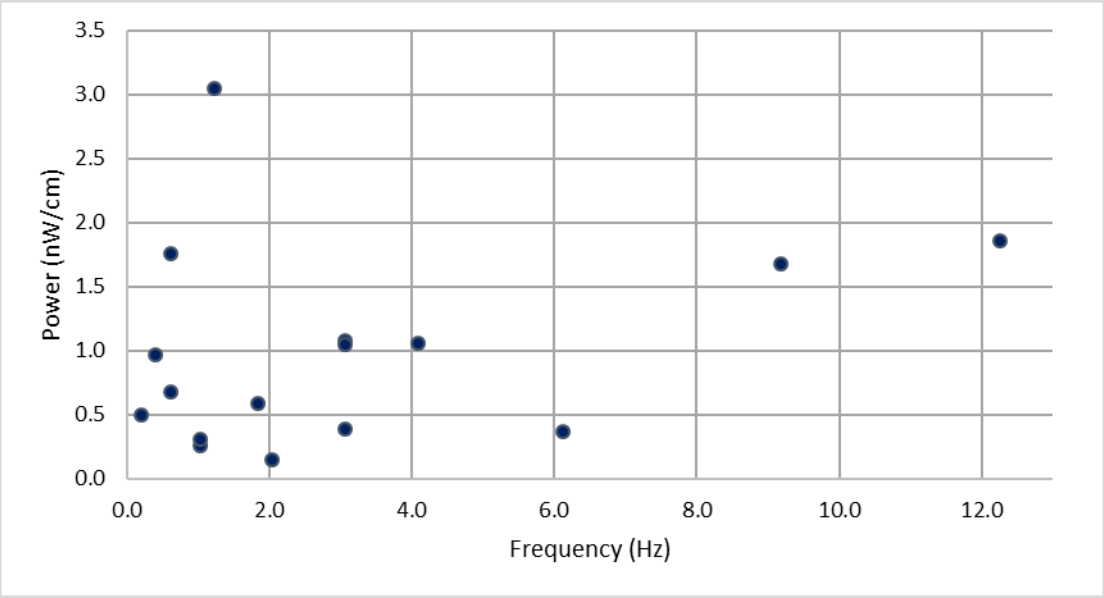

Figure 53. The Potential Power Density vs. Frequency

Even though current measurements decreased as frequency increased, Figure 52 and Figure 53 suggest that the power generated will continue to increase as frequency increases.

B. EXPERIMENTAL RESULTS OF PULLEY SYSTEM TENG USING LINEAR MOTOR

The following are the results of the NPS TENG frequency analysis using the tabletop mechanical system in NPS's Watkins Hall Laboratory. This system uses a spring, pulley and linear reciprocating motor to translate motion direction by 90° and then slide the NPS TENG horizontally over the fixed PTFE track. The AC voltage and closed-circuit current of the NPS TENG were collected at three speeds: 1/3, 2/3, and full. Table 6 shows the conversion from the linear motor speed to frequency, in hertz, and period, in seconds. Three runs were conducted at each motor speed for redundancy. All three tracks, Track A, Track B and Track C, were tested with the NPS TENG.

Table 6. Linear Motor Speed in Hertz

Speed	Ave Time/ 10 rotations (s)	Hertz (Hz)	Period (s)
1/3	14.37	0.696	1.437
2/3	7.57	1.320	0.757
Full	4.61	2.168	0.461

1. Voltage Data

AC voltage data was collected by the Teledyne Lecroy WaveJet Touch 334 digital oscilloscope at 1 sample/100 microseconds or 10 samples/second for 40 seconds. Each sample period consisted of 400 data points. Figure 54 and Table 7 show the maximum peak-peak AC voltage of the three tracks at each motor speed.

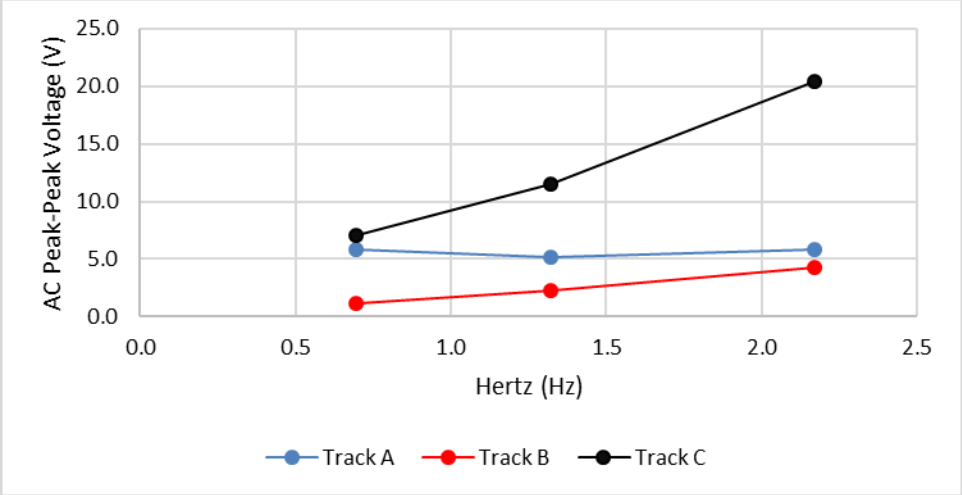

Figure 54. TENG Frequency and AC Peak-Peak Voltage for Tabletop Test

Table 7. Summary of AC Peak-Peak Voltage for Tabletop Test

	Track A (V)	Track B (V)	Track C (V)
0.696 Hz	5.81	1.1808	7.03
1.320 Hz	5.12	2.2782	11.5600
2.168 Hz	5.87	4.219	20.4600

Track C produced the greatest magnitude of AC voltage. The dramatic, positive-sloped projection suggests that the maximum voltage for Track C would continue to increase as frequency increases. Track A and Track B produced less voltage than Track C and their respective positive-sloped trajectories are much shallower than that of Track C. More data results can be found in Appendix A.

The Keysight DSO1052B digital oscilloscope captured the characteristics of the magnitude of AC voltage as the TENG completed a complete oscillation against each track. Figures 55–57show the amount and magnitude of pulses during a 3 second timeframe on Track C at each frequency.

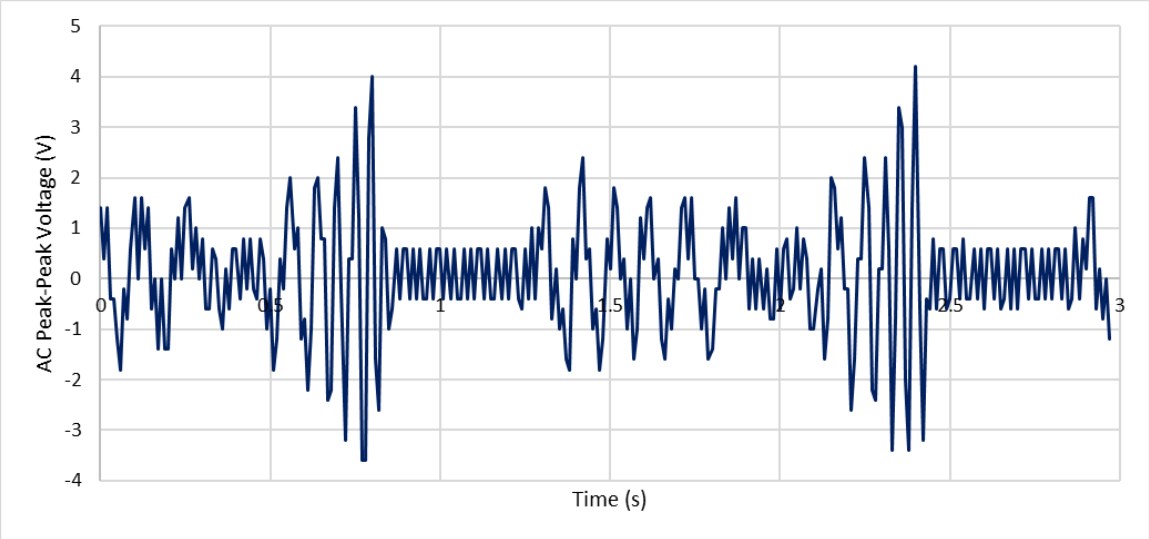

Figure 55. Track C: Peak-Peak AC Voltage at 0.696 Hertz

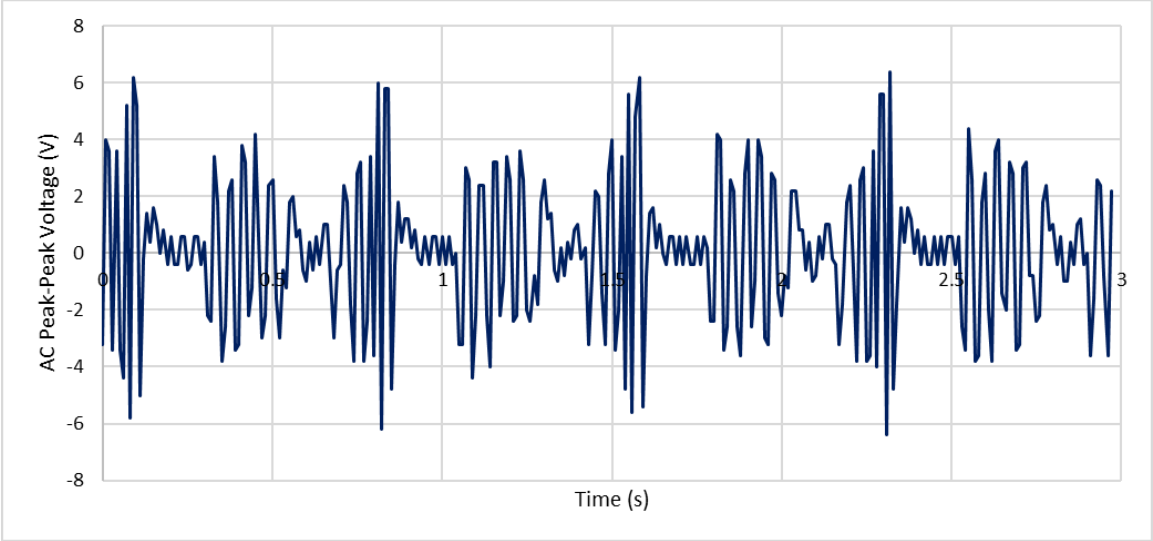

Figure 56. Track C: Peak-Peak AC Voltage at 1.320 Hertz

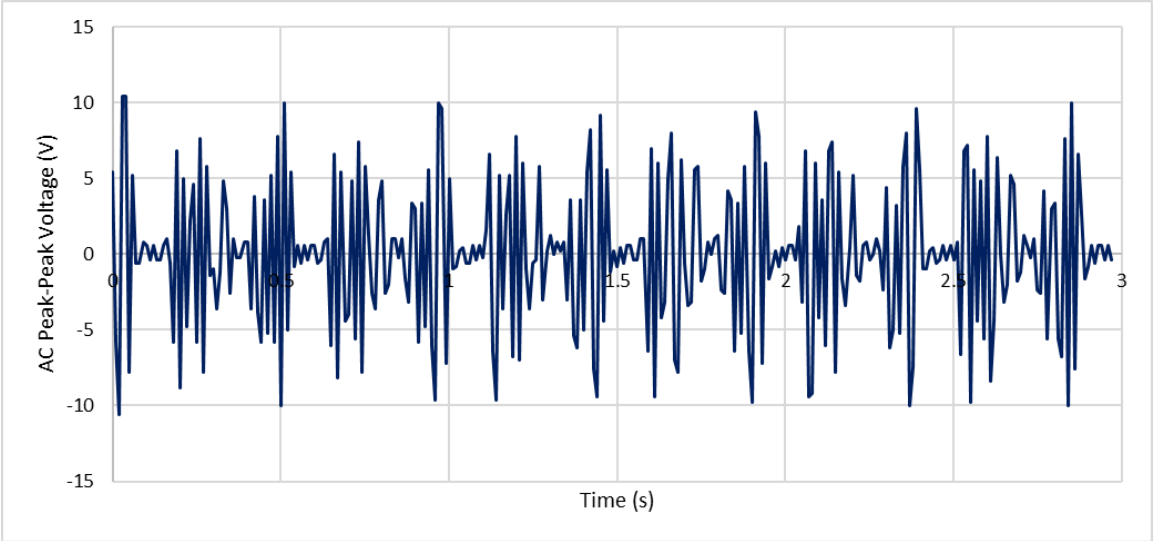

Figure 57. Track C: Peak-Peak AC Voltage at 2.168 Hertz

It is important to note that the TENG produces voltage on both directions of travel. However, the amount of "stagnant" time, or time when the voltage is below 1 V, decreases as the motor speed increases. In addition, the peak-peak voltage magnitude increases as the frequency increases.

2. Current Data

Closed circuit current data was collected by the Keithley 617 Programmable Electrometer at the instrument's maximum sampling rate of 1 sample/360 microsecond which is the equivalent of 2.78 samples/ second. Since the instrument can only save up to 100 data points, a maximum of 100 data points could be collected in 37 seconds. Figure 58 and Table 8 show the maximum closed circuit current of the three tracks at each motor speed.

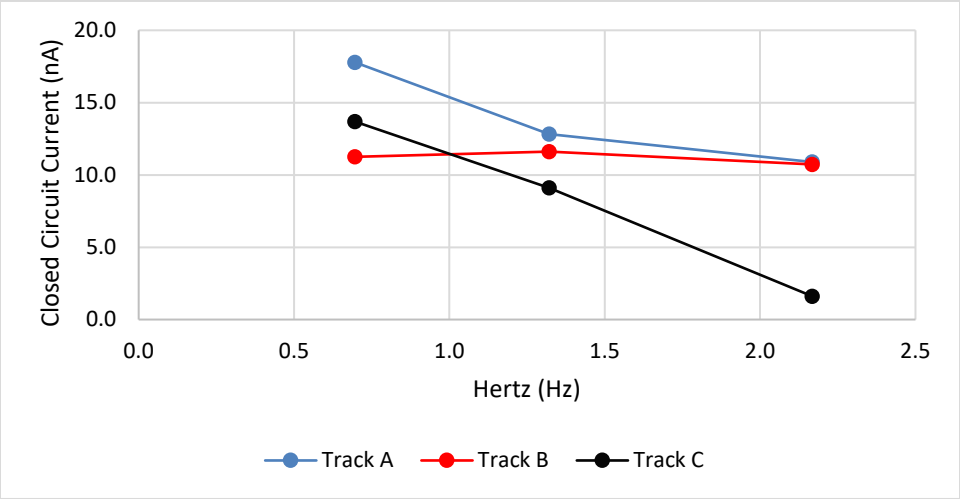

Figure 58. TENG Frequency and Closed Circuit for Tabletop Test

Table 8. Summary of Closed Circuit Current for Tabletop Test

	Track A (nA)	Track B (nA)	Track C (nA)
0.696 Hz	17.786	11.245	13.688
1.320 Hz	12.827	11.612	9.111
2.168 Hz	10.893	10.727	1.6134

In contrast to the voltage results, the magnitude of the current measured at Track C is less than the current measured at Track A and Track B for each frequency. Each track shows a downward trend of current as frequency increases but the slope for Track C is significantly steeper. More data results can be found in Appendix A.

3. Summary of Tabletop Pulley

The tabletop testing successfully translated the reciprocating motion of the linear motor 90° in preparation for the TENG to operate on a plane that is 90° from that of a floating oscillating column. The spring and pulley system ensured the frequency at the TENG matched the frequency and displacement of the motor.

Track C had the highest voltage readings but the lowest overall current readings. For each track, voltage increased as frequency increased. In addition, the current readings were greatest at the slower frequencies and least at the highest frequency.

Based on the current and voltage testing conducted on the NPS TENG, potential power and power density, using the surface area of the copper electrode, were calculated. The surface area of the two copper electrodes, 24.188 cm^2, is used to calculate power density. Figure 59 and Figure 60 depict the potential power and power density, respectively, produced at each frequency. Table 9 and Table 10 also summarize this power data.

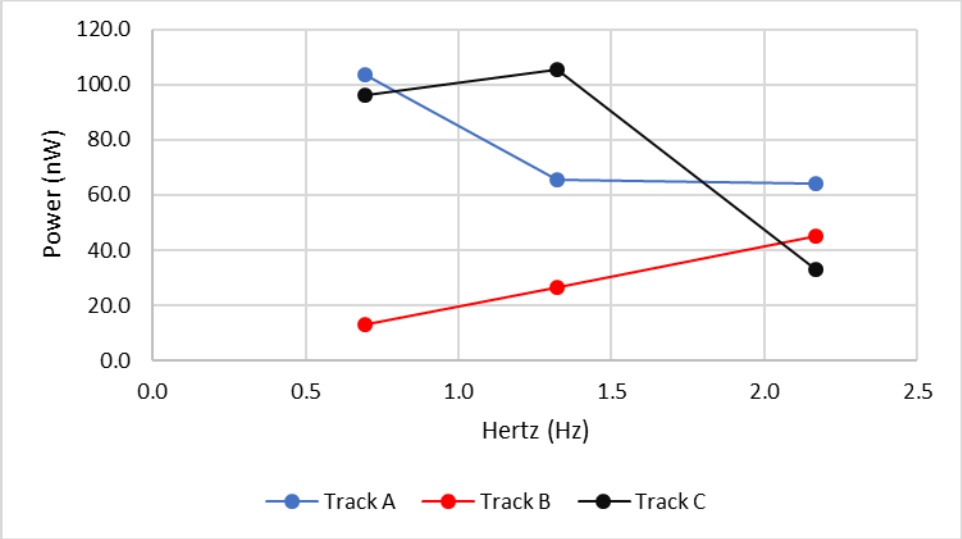

Figure 59. TENG Frequency and Potential Power Generated during Tabletop Test

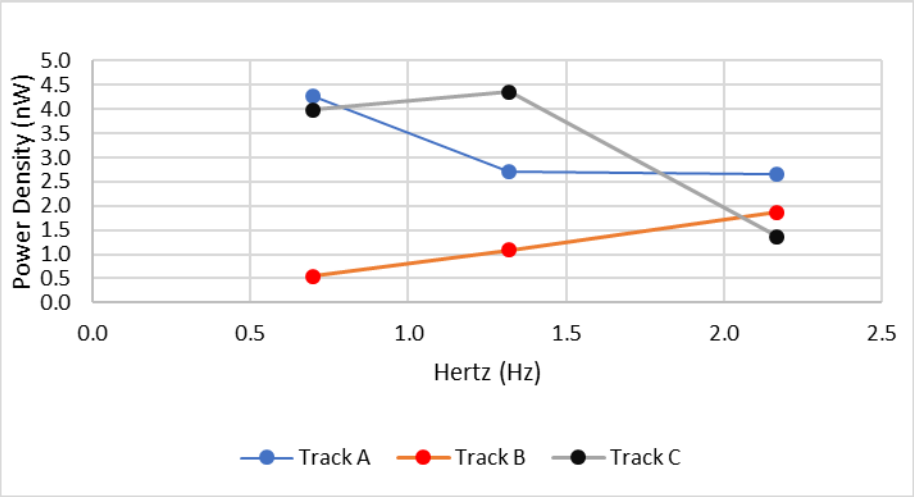

Figure 60. TENG Frequency and Potential Power Density during Tabletop Test

Table 9. Summary of Potential Power for Tabletop Test

	Track A (nW)	Track B (nW)	Track C (nW)
0.696 Hz	103.337	13.278	96.227
1.320 Hz	65.674	26.454	105.323
2.168 Hz	63.942	45.257	33.010

Table 10. Summary of Potential Power Density for Tabletop Test

	Track A (nW/cm2)	Track B (nW/cm2)	Track C (nW/cm2)
0.696 Hz	4.272	0.549	3.978
1.320 Hz	2.715	1.094	4.354
2.168 Hz	2.644	1.871	1.365

Each track has its highest potential power at a different frequency. Maximum power and power density occur at 0.696 hertz for Track A, 2.168 hertz for Track B, and 1.320 hertz for Track C. Track A has a negative, polynomial trend and Track B has a positive, linear trend. Track C has a rather parabolic trend that suggests that the highest possible power would occur at a frequency of 1.320 hertz.

It is promising that voltage data has a consistent, upward trend for each track. However, the sporadic nature of the current data suggests that the Keithley 617 is not

accurately capturing the current magnitude and waveform. As shown in Figure 22 and Figure 23, the NASA Ames TENG produced more current and voltage as both the frequency and amplitude of its motion increased [28]. Since the NPS TENG is modeled from the NASA TENG, it is anticipated that they should have similar trends. Therefore, further investigation into the NPS TENG's current measurement is desirable.

C. EXPERIMENTAL RESULTS OF PULLEY SYSTEM WAVETANK TENG USING WAVE TANK

The following are the results of the NPS TENG frequency analysis using the similar mechanical system in NPS's Halligan Hall wave tank. This system harnesses the heaving, vertical motion of the OC and then translates the linear, reciprocating motion 90° to slide on a horizonal plane. The AC voltage and closed-circuit current of the NPS TENG were collected at five frequencies of incident waves: 0.815, 0.905, 1.000, 1.197, 1.478 hertz. Since each wave provides two-directional back and forth motion at the TENG, the frequency experienced at the TENG is twice that of the incident waves. Therefore, the frequencies of the TENG are 1.630, 1.810, 2.000, 2.394, 2.956 hertz.

To ensure the NPS TENG stayed within the confines of the 155 millimeter long, 3D printed track, the wave height for each test run remained at 5.08 centimeters with a wave amplitude of 2.54 centimeters. Therefore, each wave period displaced the TENG approximately 5.08 centimeters. Five runs were conducted at each wave frequency for redundancy.

Despite the low current readings in the tabletop frequency analysis, Track C is the most promising track for the NPS TENG because of the complimentary tape dimensions to the copper electrode. Therefore, Track C will be used for the OC testing in the wave tank.

1. Voltage Data

AC voltage data was collected by the Keysight DSO1052B digital oscilloscope at 100 samples/second for 6 seconds. Each sample period consisted of 600 data points. The oscilloscope was position right next to the wave tank and connected to the TENG's

electrode wires. Figure 61 and Table 11 show the maximum peak-peak AC voltage of the TENG during the five wave conditions tested.

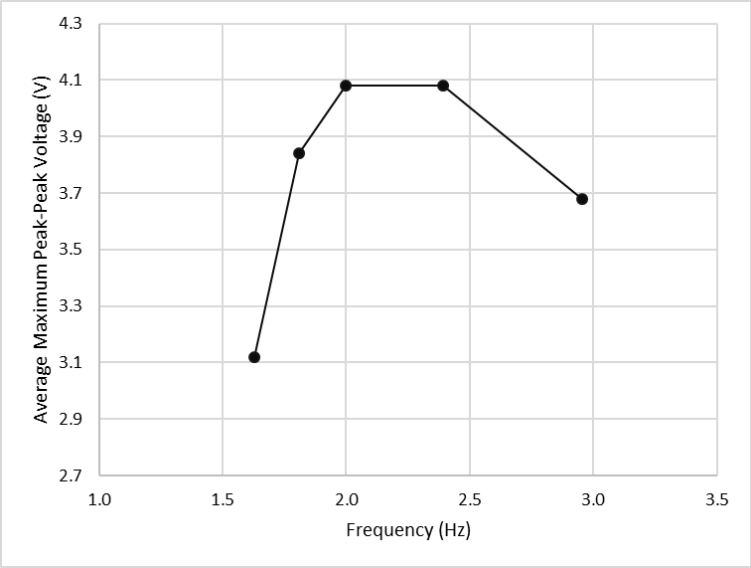

Figure 61. TENG Frequency and AC Peak-Peak Voltage for Wave Tank Test

Table 11. Summary of AC Peak-Peak Voltage for Wave Tank Test

Wave Frequency (Hz)	Frequency at TENG (Hz)	Average Maximum Peak-Peak AC Voltage (V)
0.815	1.630	3.120
0.905	1.810	3.840
1.000	2.000	4.080
1.197	2.394	4.080
1.478	2.956	3.680

Average maximum peak-peak AC voltage had a positive trend as the wave frequency increased, as it did in the tabletop testing. At the jump in wave frequency from 1.197 hertz to 1.478 hertz, the voltage did go down. The magnitude of this voltage was approximately half of the peak-peak AC voltage produced at a similar frequency in the tabletop testing. More data results can be found in Appendix C.

The TENG produced consistent peaks in voltage during both directions of motion in the wave tank that corresponded to the frequency of motion. Figure 62 shows the characteristics and magnitude of pulses during a 6 second timeframe at a wave frequency of 1.147 hertz.

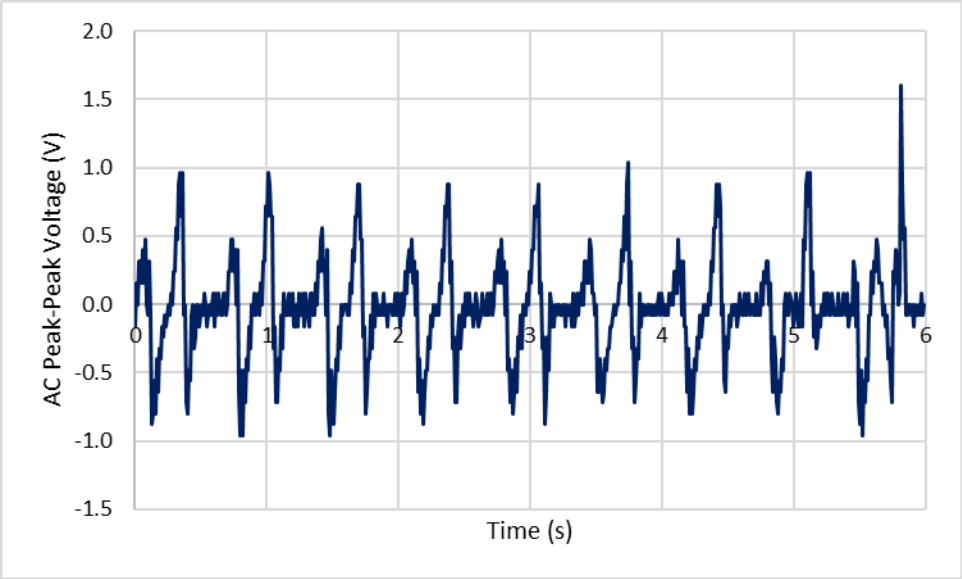

Figure 62. Peak-Peak AC Voltage at 1.147 Hertz in Wave Tank

Just as the TENG did in the tabletop testing a frequency analysis, it produces voltage in both directions of travel. Although the magnitude of the voltage created in the wave tank is considerably less than that by the linear motor, the fact that wave energy can be produced by the OC is promising. The slight variation in each wave pulse, Figure 62, suggests that the TENG would respond well to varying input wave conditions.

2. Current Data

Closed circuit current data was collected by the Keithley 617 Programmable Electrometer at the instrument's maximum sampling rate of 1 sample/360 microsecond which is the equivalent of 2.78 samples/ second. The electrometer was placed next to the wave tank and connected to the TENG's electrode wires. Figure 58 and Table 8 show the maximum closed circuit current at each of the five wave conditions tested.

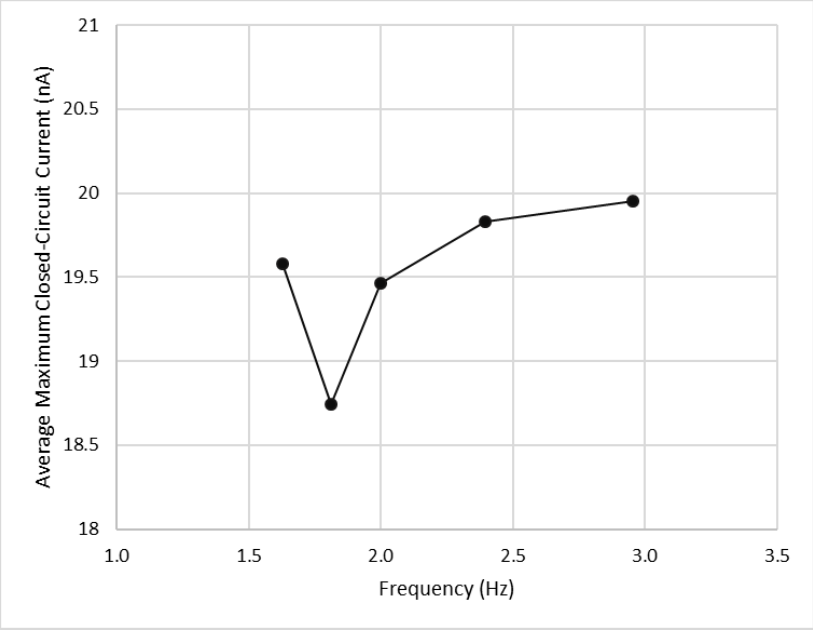

Figure 63. TENG Frequency and Closed Circuit for Wave Tank Test

Table 12. Summary of Closed Circuit Current for Wave Tank Test

Wave Frequency (Hz)	Frequency at TENG (Hz)	Average Maximum Peak-Peak Closed Circuit Current (nA)
0.815	1.630	19.579
0.905	1.810	18.741
1.000	2.000	19.461
1.197	2.394	19.83
1.478	2.956	19.951

In contrast to the results found in the tabletop testing, the maximum peak-peak closed circuit current had a positive trend as TENG frequency increased. There was a dip in current output at a wave frequency of 0.905 hertz but overall, the current reading was highest at the fastest frequency. The magnitude of current measured for Track C during the wave tank testing was approximately twice that of similar frequency testing in the tabletop apparatus. More data results can be found in Appendix C.

3. Summary of WT Pulley

The wave tank testing successfully translated the vertical, oscillating motion of the floating OC 90° to horizontal motion along the adjacent beam. The spring and pulley system ensured the frequency at the TENG matched the frequency and displacement of the waves. The scale, stiffness and characteristics of the pulley and spring system worked very well in the wave tank environment, just as it did with the tabletop experiment.

Generally, both voltage and current increased as the wave frequency increased. The five test runs per wave frequency increased the confidence factor of these trends. The voltage readings were smaller in magnitude and the current readings were greater in magnitude compared to the data collected in the linear reciprocating motor testing.

Based on the current and voltage testing conducted on the NPS TENG in the wave tank, potential power and power density, using the surface area of the copper electrode, were calculated. The surface area of the two copper electrodes, 24.188 cm^2, is used to calculate power density. Figure 64 and Figure 65 depict the potential power and power density, respectively, produced at each frequency in the wave tank. Table 13 and Table 14 also summarize this power data.

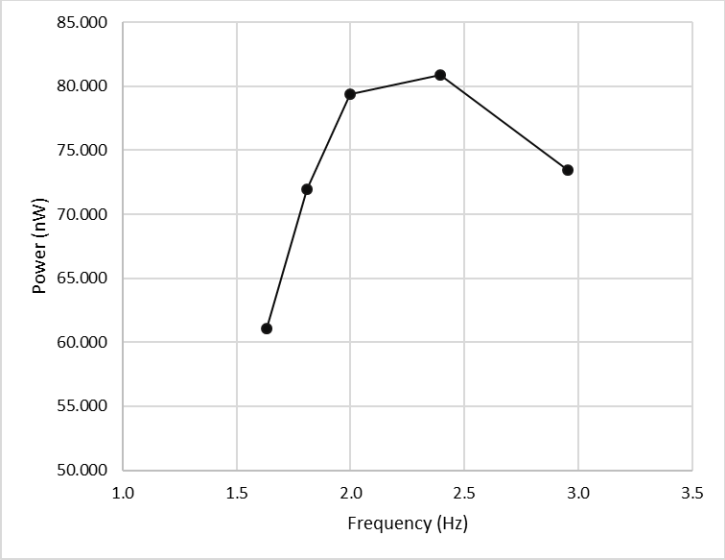

Figure 64. TENG Frequency and Potential Power Generated for Wave Tank Test

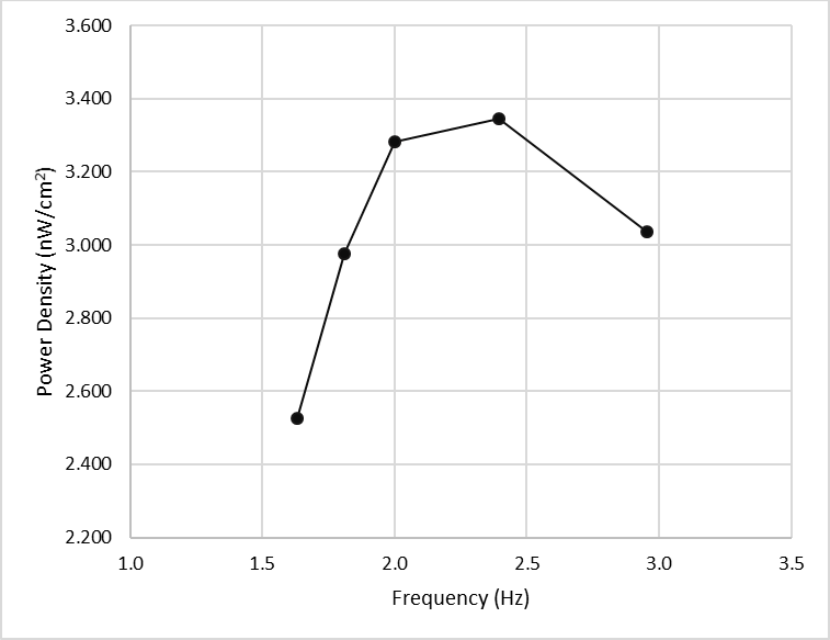

Figure 65. TENG Frequency and Potential Power Density for Wave Tank Test

Table 13. Summary of Potential Power for Wave Tank Test

Wave Frequency (Hz)	Frequency at TENG (Hz)	Power(nW)
0.815	1.630	61.086
0.905	1.810	71.965
1.000	2.000	79.401
1.197	2.394	80.906
1.478	2.956	73.420

Table 14. Summary of Potential Power Density for Wave Tank Test

Wave Frequency (Hz)	Frequency at TENG (Hz)	Power Density (nW/cm^2)
0.815	1.630	2.525
0.905	1.810	2.975
1.000	2.000	3.283
1.197	2.394	3.345
1.478	2.956	3.035

The potential power and power density trends are positive as the frequency of the TENG increases. The greatest potential power and power density were calculated at a wave frequency of. 1.197 hertz. However, the calculated power and power density values at highest frequency tested, 1.478 hertz, experienced a downward dip.

The power and power density values of the tabletop testing were like the results of the wave tank results even though the voltage readings were much lower, and the current readings were much higher in the wave tank. Further investigation is desirable in the actual wave-environment application of the NPS TENG. The TENG was shown to produce both current and voltage in both directions of motion and successfully converted the variable movement of the waves into electrical potential. The translation of the vertical oscillating motion 90° to horizontal motion was effective and would be practical in a real-world application.

IV. CONCLUSION AND FUTURE WORK

A. CONCLUSION

A linear sliding contact-mode TENG consisting of two, interdigitative copper electrodes and PTFE adhesive tape was constructed on 3D printed material. With the ultimate intent of harvesting the cyclic heaving of wave to produce electricity, several experiments were conducted in order to improve the initial testing of the TENG's operation with a floating oscillating column. A system consisting of a gear box and motion converting mechanism proved the concept that the relatively low frequencies of waves could be increased to produce more power from a sliding contact-mode TENG. The system took linear, reciprocating motion, converted it to one direction circular motion using a worm gear, increased the revolution speed using a gear box and converted the circular motion back to linear, reciprocating motion using a special motion conversion mechanism. A frequency analysis experiment was conducted on this overall system to investigate both the AC voltage and closed-circuit current of the TENG at different frequencies of motion. Despite limitations of the building material used, the concept showed that an increase in frequency of motion produced more AC voltage. However, the same experiment showed that closed circuit current values decreased as the frequency increased.

Next, a table top system which included a spring and pulley was developed to translate linear, reciprocating motion 90°. Ultimately, this concept would turn the vertical reciprocating linear motion of ocean waves to horizontal reciprocating linear motion at a safe distance from the harsh environment of the ocean surface. This series of testing used a linear, reciprocating motor and measured the AC voltage and closed circuit current produced by the NPS TENG. Three different tracks of various tape widths and space widths were tested at three frequencies in order to determine which design best maximize the electrical output of the NPS TENG. Just as the frequency analysis of the gear box showed, AC voltage increased and closed-circuit current decreased as frequency of the TENG increased. The track that had tape widths the same width of the copper electrode with tape gaps equal to the sum of the copper electrode finger width and two distances between adjacent electrodes proved to be the most efficient.

This optimized track, Track C, was tested at five wave conditions in the wave tank using the developed oscillating column. Unlike a previous experiment using the OC, the TENG sat on a horizontal plane located at a safe distance above the water level of the tank. The pulley and spring system ensured that the frequency and magnitude of the heaving wave was translated properly in the horizontal plane. In order for an OC TENG to be properly deployed for use, it must be in located in an area where water vapor or sea spray will not be detrimental to the triboelectric charge transfer. The AC voltage produced in the wave tank followed the same positive trend as in previous experiments, but the magnitude of voltage was much less. However, the calculated closed circuit current of the TENG was much larger in the wave tank than it was in previous experiments and the amount of current increased as frequency increased, the opposite trend of the previous experiments.

Even though the waves produced relatively low power and power density values, the fact that the linear reciprocating heaving motion of waves could be harnessed to produce electricity is promising. These experiments show the importance of future focus on the material, frequency, circuit components, operating environment and measuring equipment that will lead to producing a more optimized and practical TENG for ocean wave energy harvesting.

B. RECOMMENDATIONS AND ERROR ANALYSIS

Improved current measurement methods would greatly benefit future TENG testing at NPS. Electrometers are ideal for quantifying the low magnitudes of current produced by TENGs. However, it is desirable to get readings at a higher frequency than is capable of the Keithley 617 in order to capture the oscillatory nature of a TENG. A data acquisition system, such as LabView, could provide a user interface to interpret the increased data points provided by a more modern electrometer. A data acquisition system could also sync voltage and current data in order to produce more real-time power measurements and graphs. It is expected that the current found using the Keithley 617 in this series of experiments did not truly capture the proper electrical potential of this NPS TENG due to the frequency limitations of the device.

The MCM and MCS models proved a point that the frequency of linear reciprocating motion can be manipulated to achieve a desirable end-state frequency to optimize electrical output from a TENG. However, these proof-of-concept models were made of materials that could not withstand the torques and axial forces associated with gears and power transmission. If this concept is pursued further, it is recommended that the MCS and MCM systems with all associated gears, shafts, etc., are constructed using a much more robust material such as metal.

As the OC floated up and down in the series of waves, some of the vertical wave movement was loss due to the horizontal and circular movement of the outside column about the central PVC pipe. Some energy was undoubtedly loss by this interference and inefficiency in design. In order to improve the use of a oscillating column in translating motion to a horizontal plane above the water, it would be advantageous to decrease the clearance area between the PVC pipe and inner circle of the OC and make that interaction less frictional by means of a set of rollers, for example. In addition, multiple PVC supports around the OC would help decrease the stress experienced by the one central PVC pole and prohibit the OC from spinning about the central axis. .

C. FUTURE WORK

The electrical characteristics such as internal impedance and the associated resistance that, if put in series, could optimize power output of the TENG should be investigated further. This internal impedance though is specific to each TENG design. For a future NPS student to truly harvest the most amount of energy from a TENG, the electrical circuit considerations, such as this optimum series resistance, should be studied. Several TENG models including the air-driven TENG and NASA Ames TENG have investigated the optimum series resistance that would maximize power output [10,28].

The NASA Ames research found the ideal frequency range of its TENG was between 30–60 hertz [28]. The highest frequency reached during this frequency analysis was only 12 hertz. Future work could analyze the performance of this TENG at higher frequencies.

For the pulley-spring tabletop and associated OC systems to someday be practical for energy generation under a U.S. Navy pier, they should be placed in a completely watertight container and consolidated for space-efficiency concerns. It would be advantageous and seemingly simple to connect a whole series of TENGs to one OC whether in series along the same line or using multiple connections to the top of the OC. Spring stiffness, track length and a material's resistance to abrasion should be optimized based on the operating environment.

Energy storage and transport methods should be explored in order to combine and utilize the electrical energy produced by this TENG. Based on the operating environment, a series of NPS TENGs could power an attached sensor or light or perhaps store energy in a capacitor or battery for future use. This analysis explored current and voltage across several frequencies and various track dimensions. However, further development of the optimized electrical circuit and subsequent electrical storage would truly take the NPS TENG out of the laboratory and into useful, U.S. Navy applications.

APPENDIX A. TENG FREQUENCY ANALYSIS RESULTS

This appendix includes some experimental data from frequency analysis with the gear box and circular motor. The voltage data was collected by the Teledyne Lecroy WaveJet Touch 334 digital oscilloscope and exported to a Microsoft Excel file where the graphs were fabricated. Current data was collected from the data storage memory of the 617 Keithley Electrometer and then transferred to Microsoft Excel.

Despite having different gear ratios, similar current results are shown for equivalent frequencies.

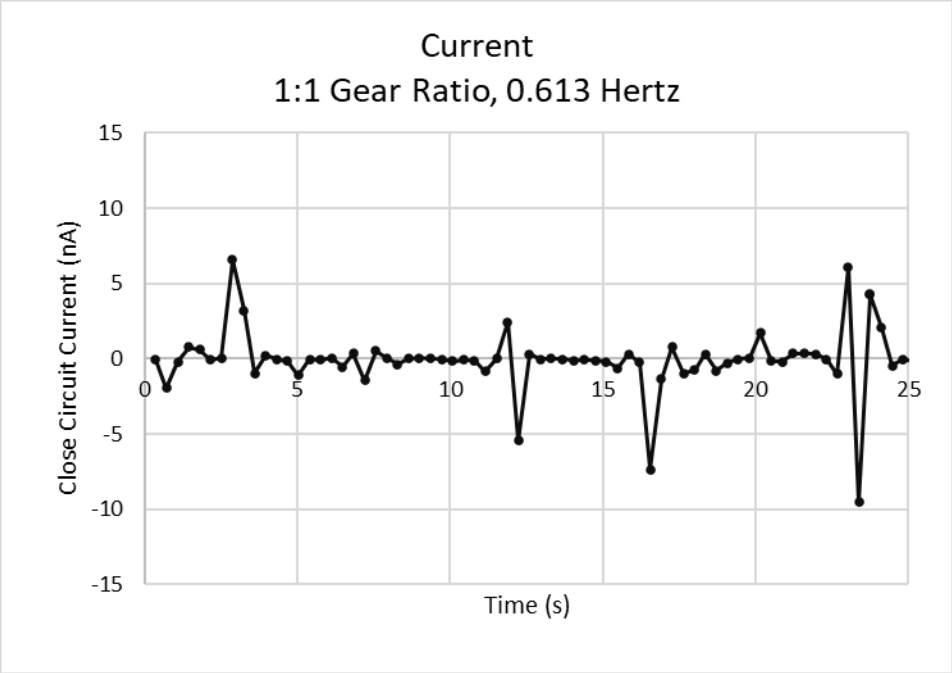

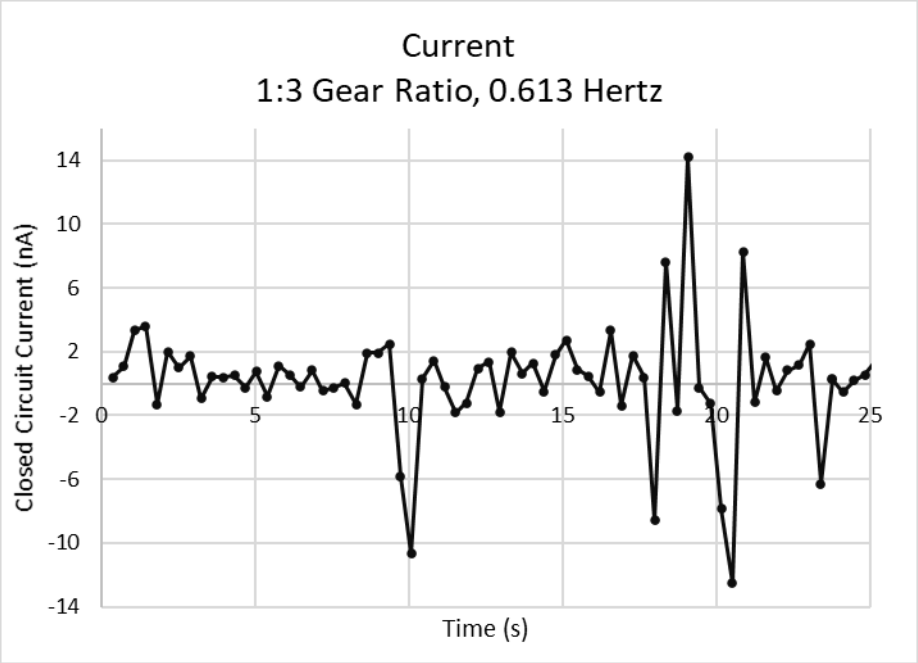

This is an example of the current data for a slow-speed run, 0.408 hertz, at a 1:1 gear ratio.

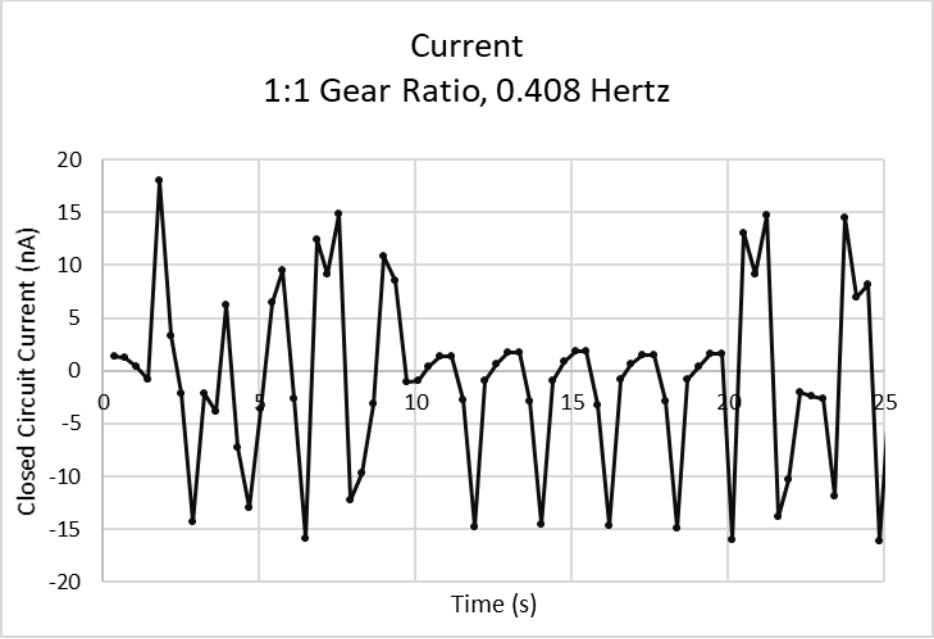

This is an example of the current data for a fast-speed run, 6.125 hertz, at a 1:3 gear ratio.

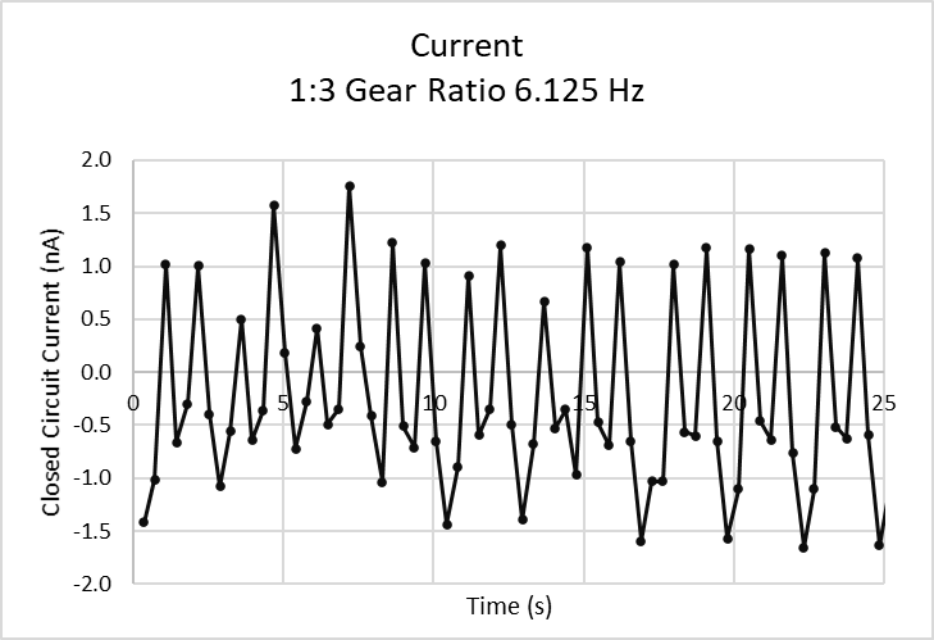

Despite having different gear ratios, similar voltage results are shown for equivalent frequencies.

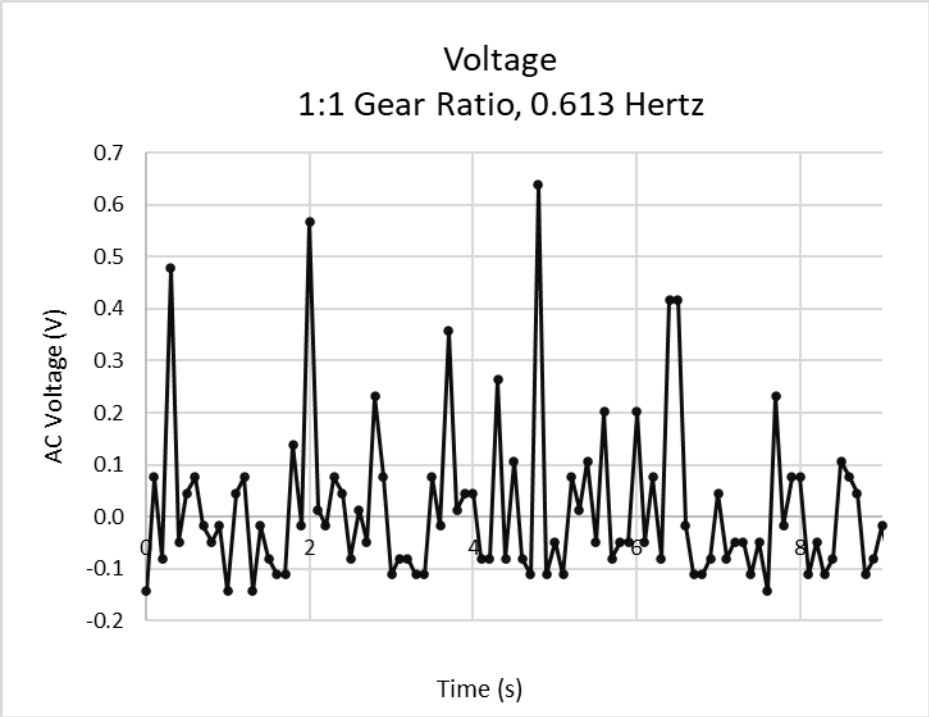

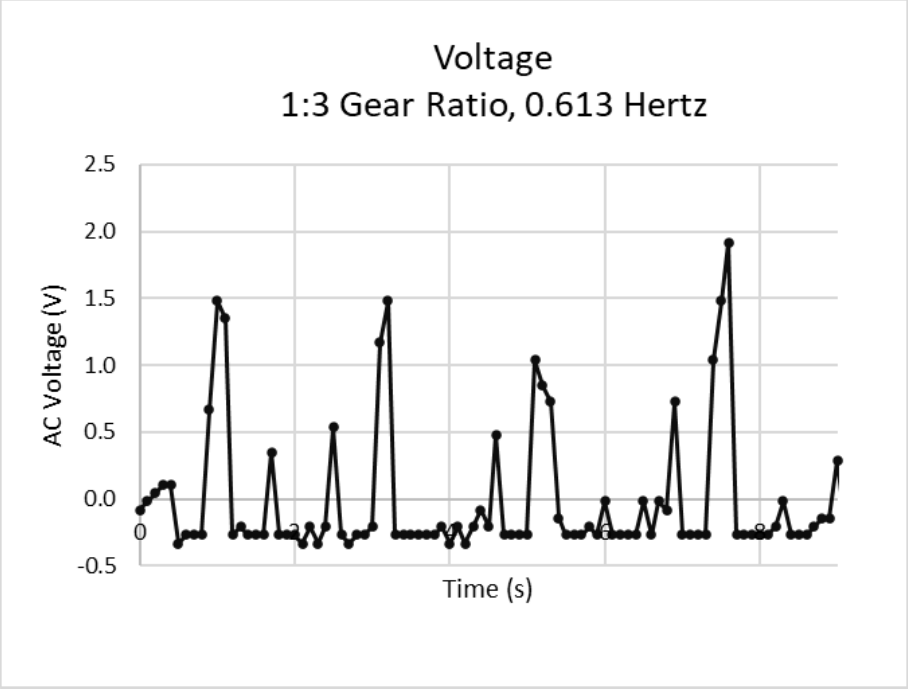

This is an example of the voltage data for a slow-speed run, 0.408 hertz, at a 1:1 gear ratio.

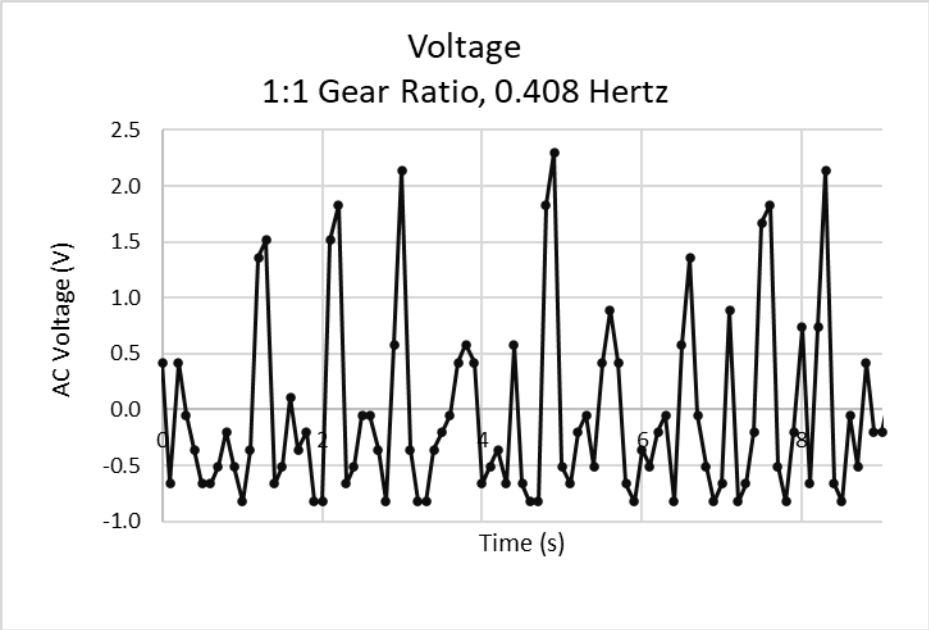

This is an example of the voltage data for a fast-speed run, 6.125 hertz, at a 1:3 gear ratio.

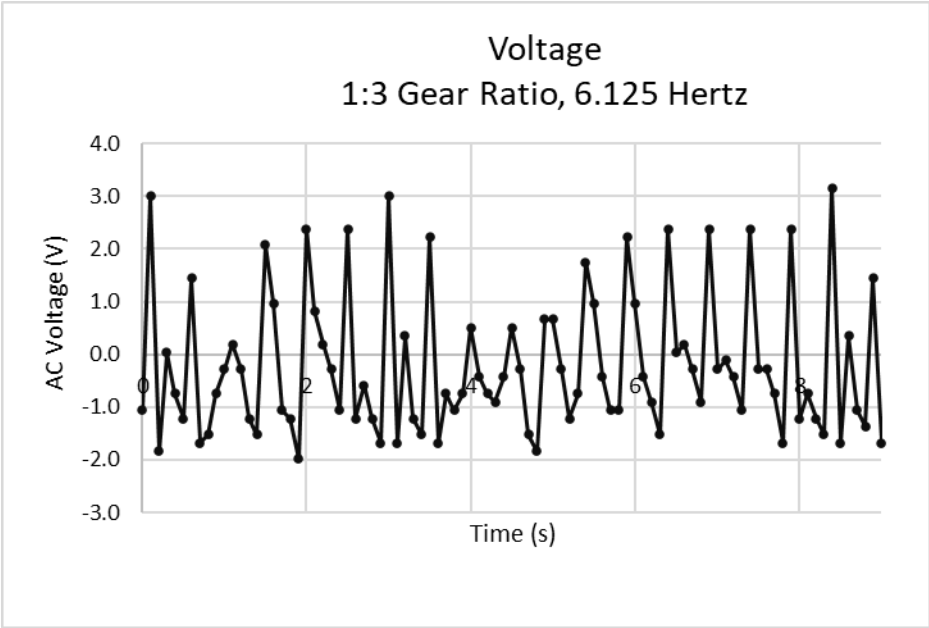

THIS PAGE INTENTIONALLY LEFT BLANK

APPENDIX B. LINEAR RECIPROCATING MOTOR RESULTS

This appendix includes some experimental data from the tabletop testing using the linear reciprocating motor. The voltage data was collected by the Teledyne Lecroy WaveJet Touch 334 digital oscilloscope and exported to a Microsoft Excel file where the graphs were produced. Current data was collected from the data storage memory of the 617 Keithley Electrometer and then transferred to Microsoft Excel. The voltage data and current data graphs depict the maximum AC voltage found for each of the three runs at each motor speed, thus the three data points at each of the motor's measured frequencies. The possible power and power density are shown as a product of the maximum current and maximum voltage. Each of the three tracks, Track A, Track B, and Track C, were each tested with the tabletop reciprocating linear motor.

(1) Track A

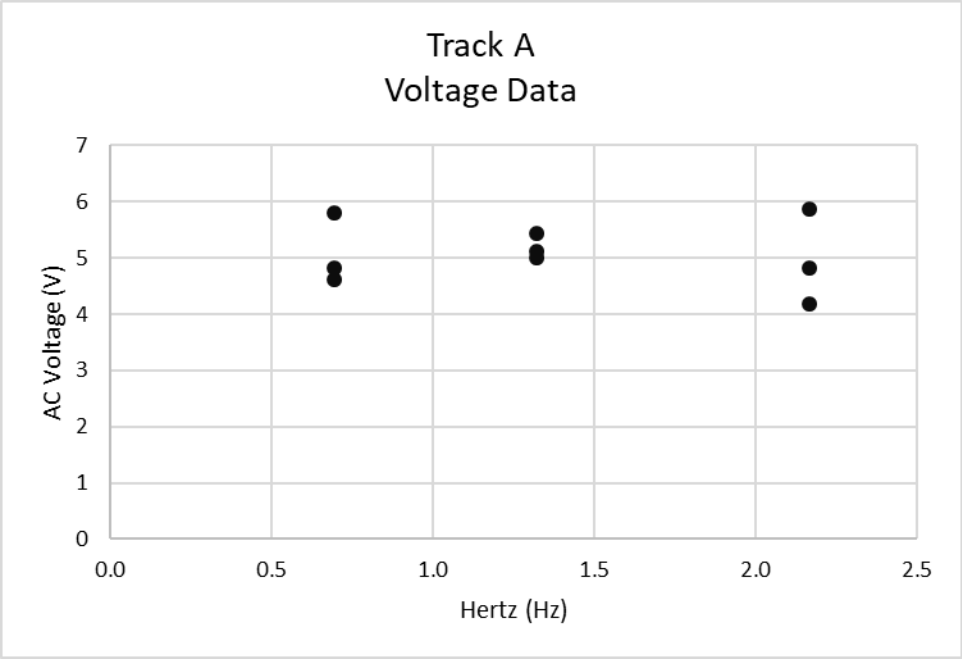

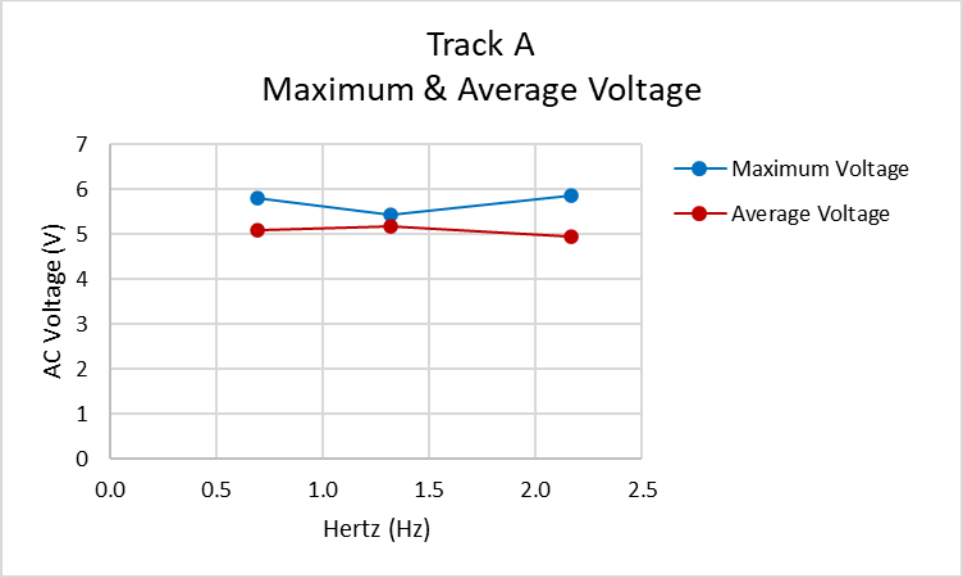
Track A
Maximum & Average Voltage
AC Voltage (V)
Hertz (Hz)
Maximum Voltage
Average Voltage
0
1
2
3
4
5
6
7
0.0
0.5
1.0
1.5
2.0
2.5

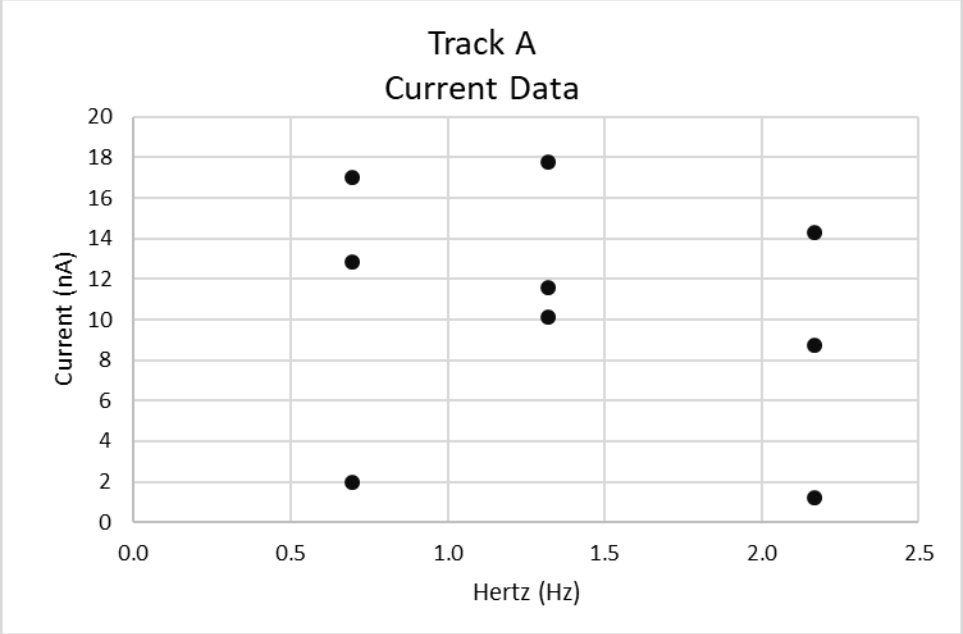
Track A
Current Data
Current (nA)
Hertz (Hz)
0
2
4
6
8
10
12
14
16
18
20
0.0
0.5
1.0
1.5
2.0
2.5

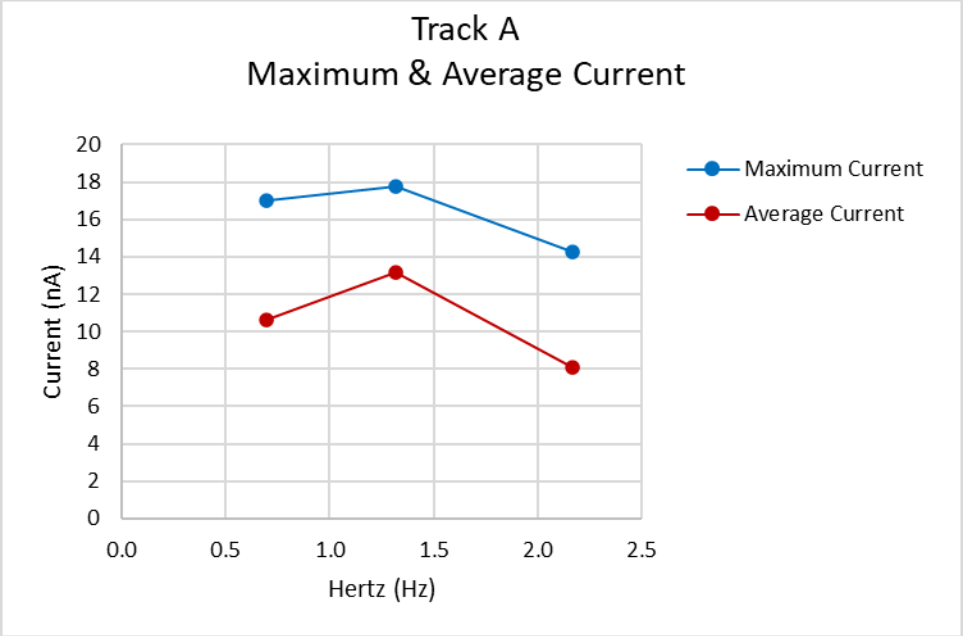
Track A
Maximum & Average Current
Current (nA)
20
18
16
14
12
10
8
6
4
2
0
0.0
0.5
1.0
1.5
2.0
2.5
Hertz (Hz)
Maximum Current
Average Current

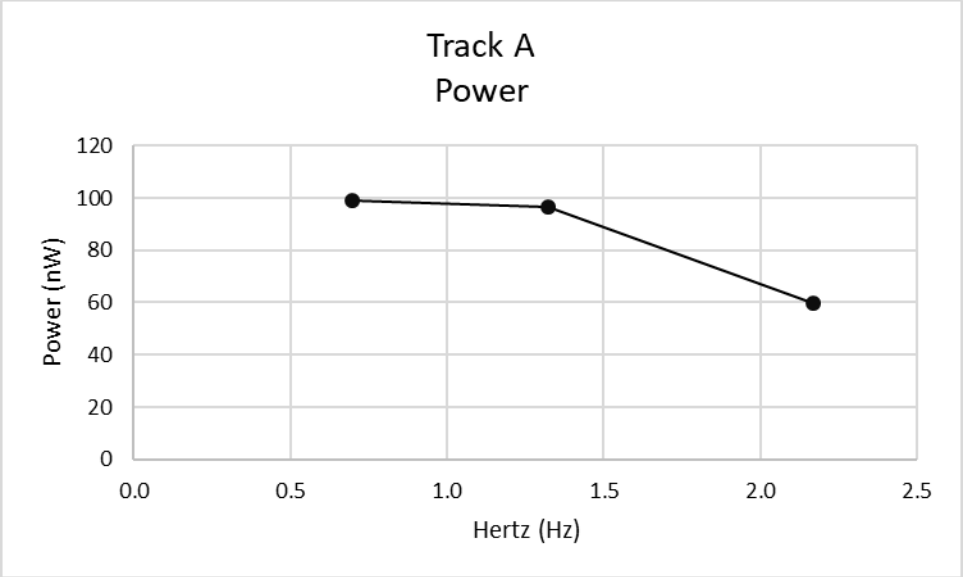
Track A
Power
Power (nW)
120
100
80
60
40
20
0
0.0
0.5
1.0
1.5
2.0
2.5
Hertz (Hz)

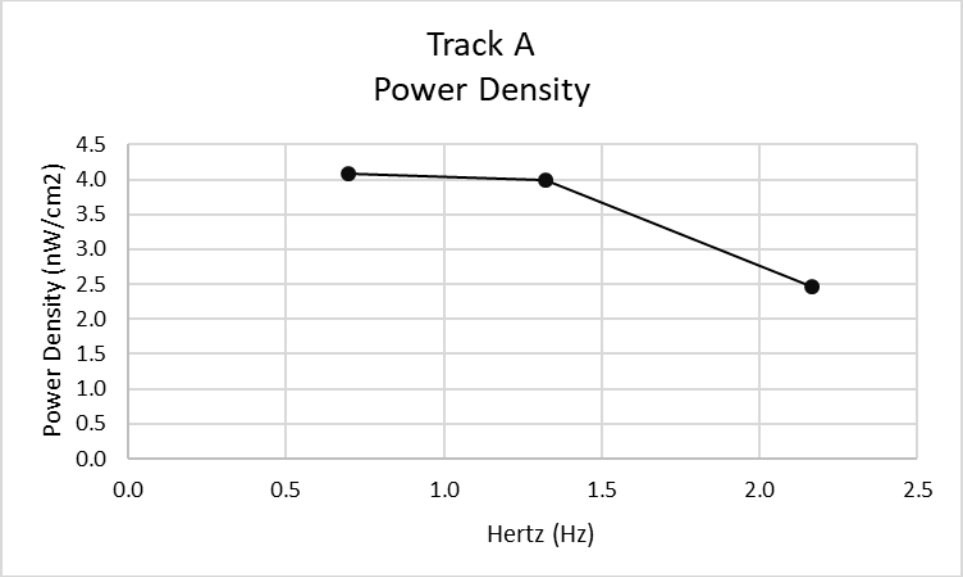
Track A
Power Density
Power Density (nW/cm2)
4.5
4.0
3.5
3.0
2.5
2.0
1.5
1.0
0.5
0.0
0.0
0.5
1.0
1.5
2.0
2.5
Hertz (Hz)

(2) Track B

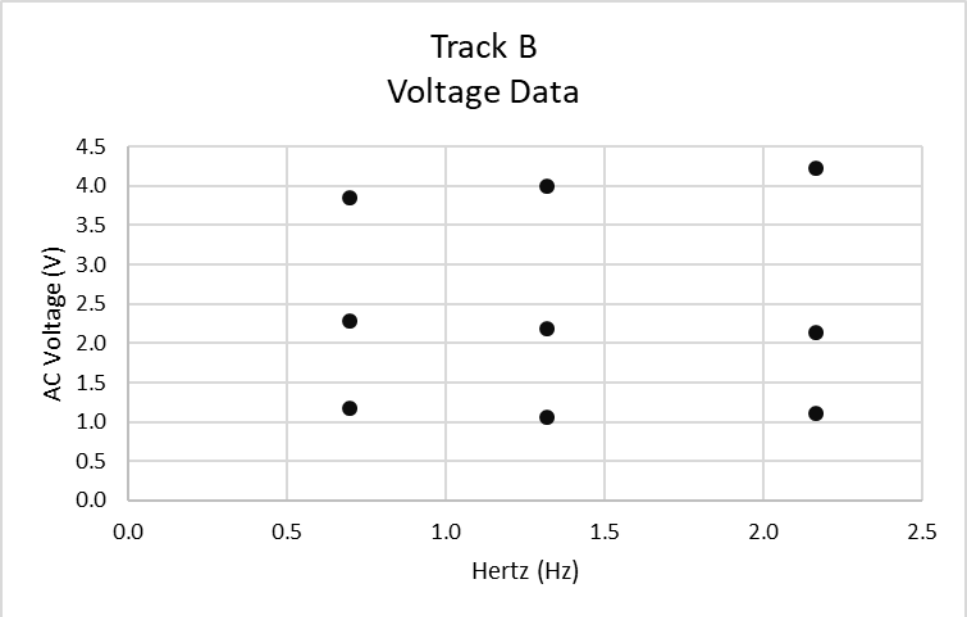
Track B
Voltage Data
AC Voltage (V)
4.5
4.0
3.5
3.0
2.5
2.0
1.5
1.0
0.5
0.0
0.0
0.5
1.0
1.5
2.0
2.5
Hertz (Hz)

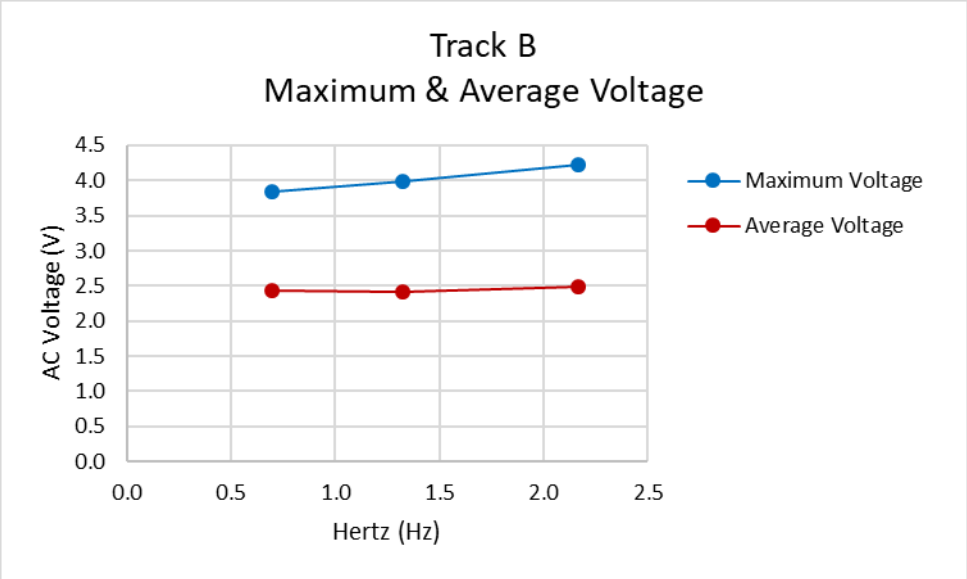
Track B
Maximum & Average Voltage
AC Voltage (V)
4.5
4.0
3.5
3.0
2.5
2.0
1.5
1.0
0.5
0.0
0.0
0.5
1.0
1.5
2.0
2.5
Hertz (Hz)
Maximum Voltage
Average Voltage

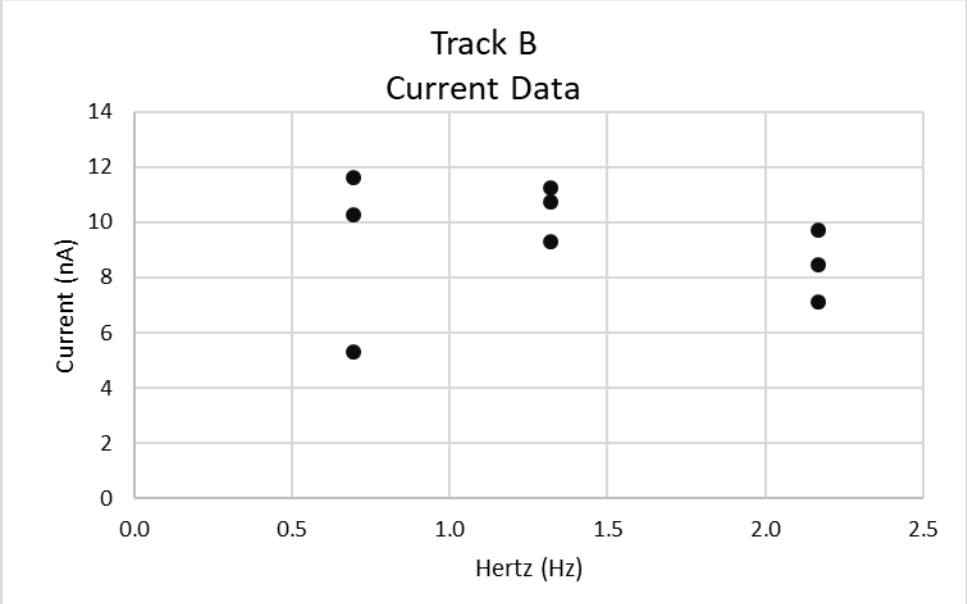
Track B
Current Data
Current (nA)
14
12
10
8
6
4
2
0
0.0
0.5
1.0
1.5
2.0
2.5
Hertz (Hz)

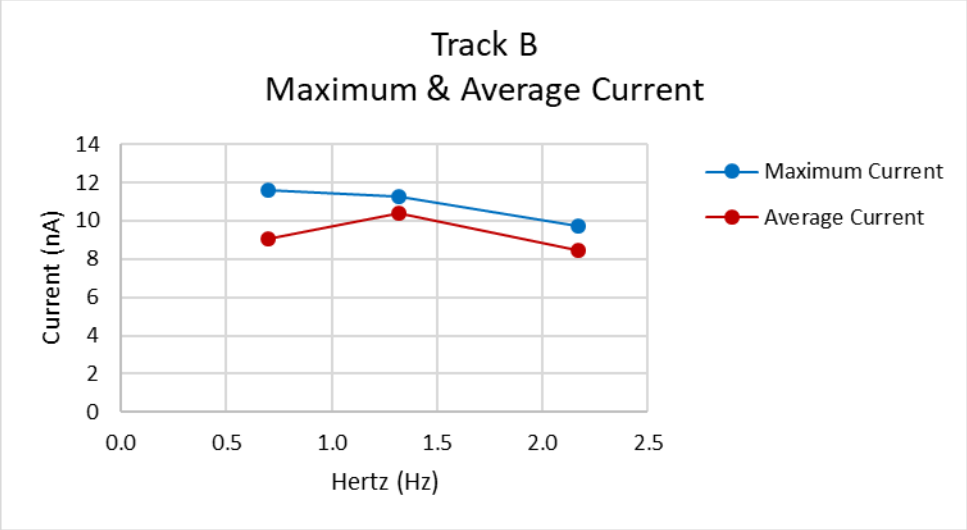
Track B
Maximum & Average Current
Current (nA)
14
12
10
8
6
4
2
0
0.0
0.5
1.0
1.5
2.0
2.5
Hertz (Hz)
Maximum Current
Average Current

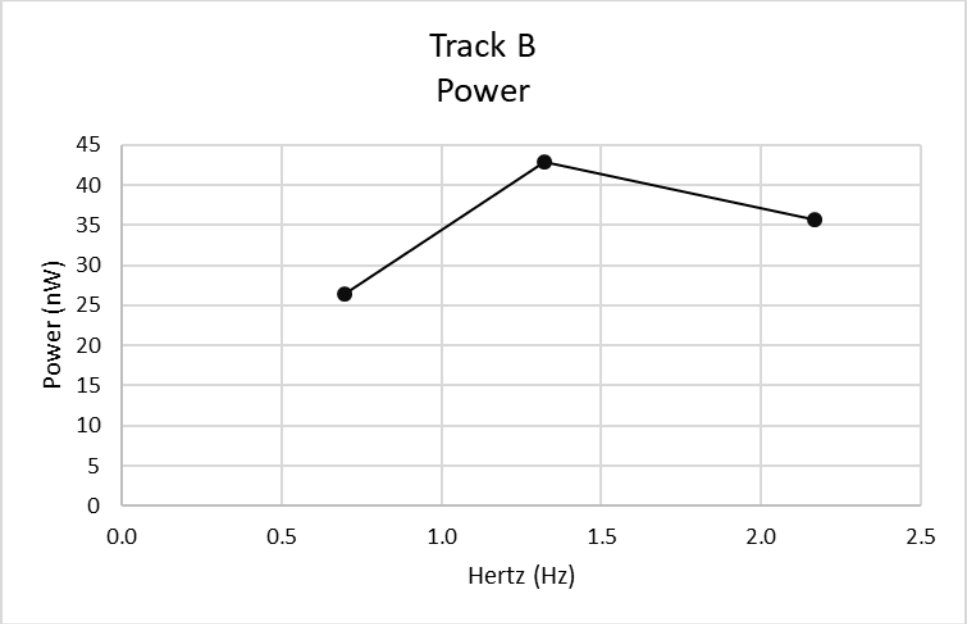
Track B
Power
Power (nW)
45
40
35
30
25
20
15
10
5
0
0.0
0.5
1.0
1.5
2.0
2.5
Hertz (Hz)

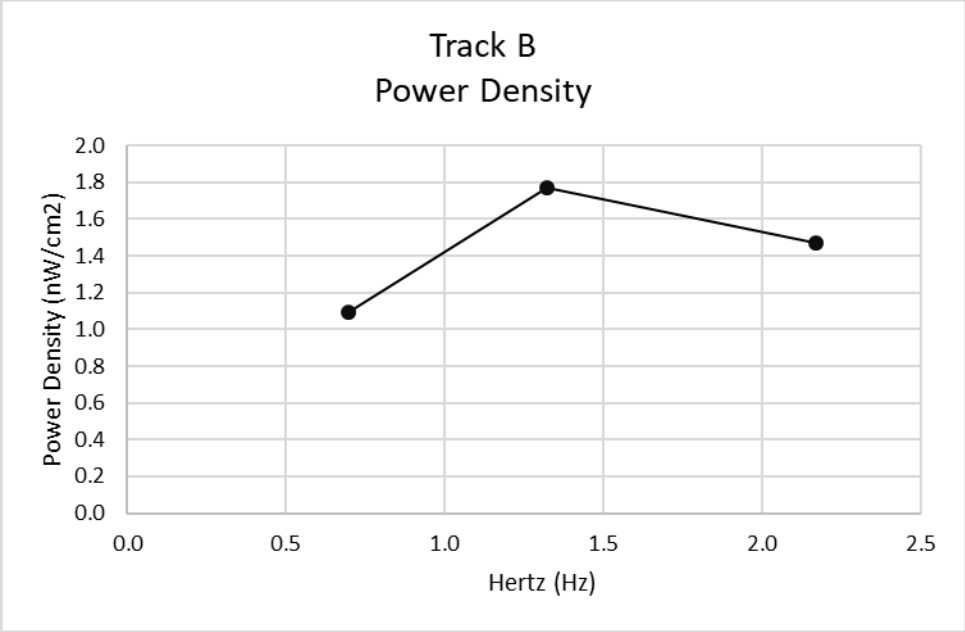
Track B
Power Density
Power Density (nW/cm2)
2.0
1.8
1.6
1.4
1.2
1.0
0.8
0.6
0.4
0.2
0.0
0.0
0.5
1.0
1.5
2.0
2.5
Hertz (Hz)

(3) Track C

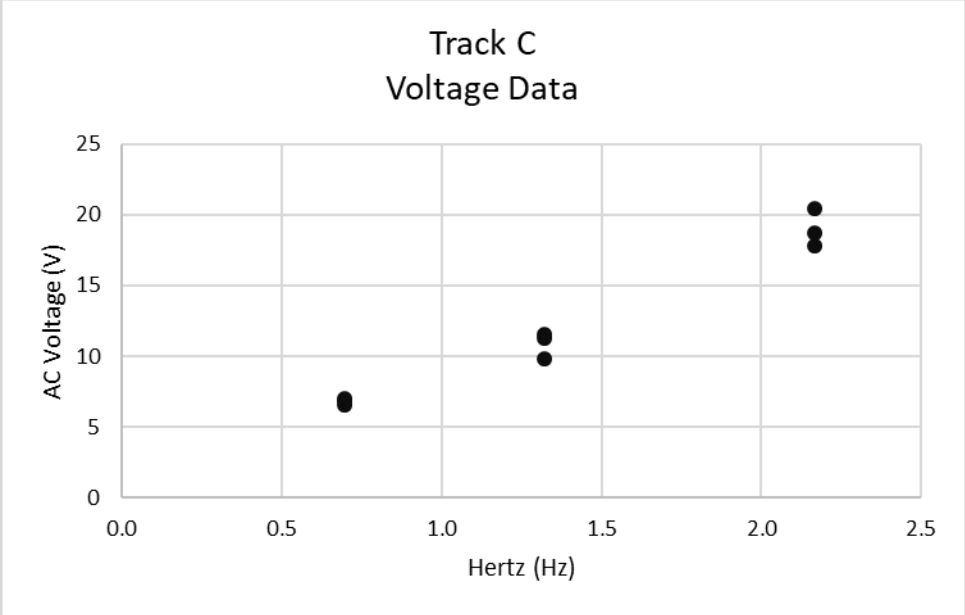
Track C
Voltage Data
AC Voltage (V)
25
20
15
10
5
0
0.0
0.5
1.0
1.5
2.0
2.5
Hertz (Hz)

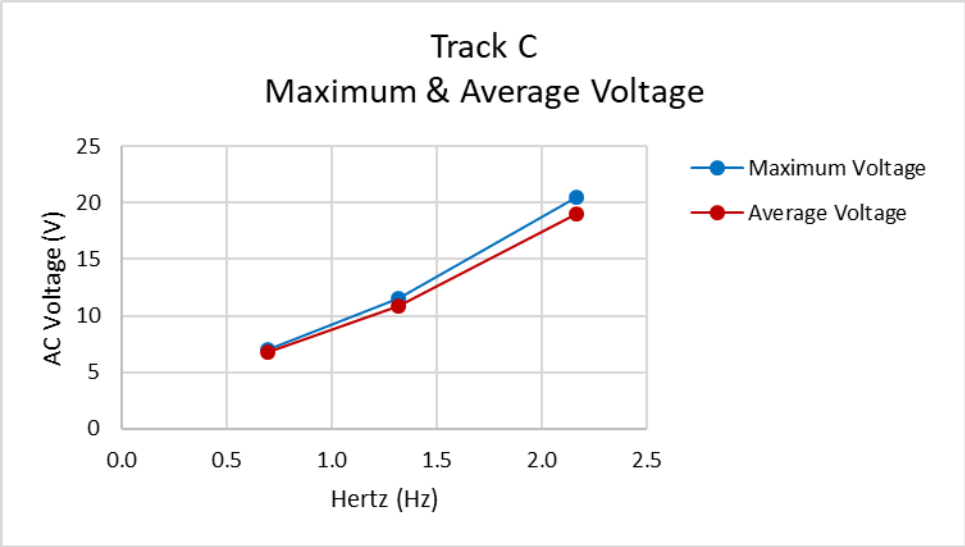
Track C
Maximum & Average Voltage
AC Voltage (V)
25
20
15
10
5
0
0.0
0.5
1.0
1.5
2.0
2.5
Hertz (Hz)
Maximum Voltage
Average Voltage

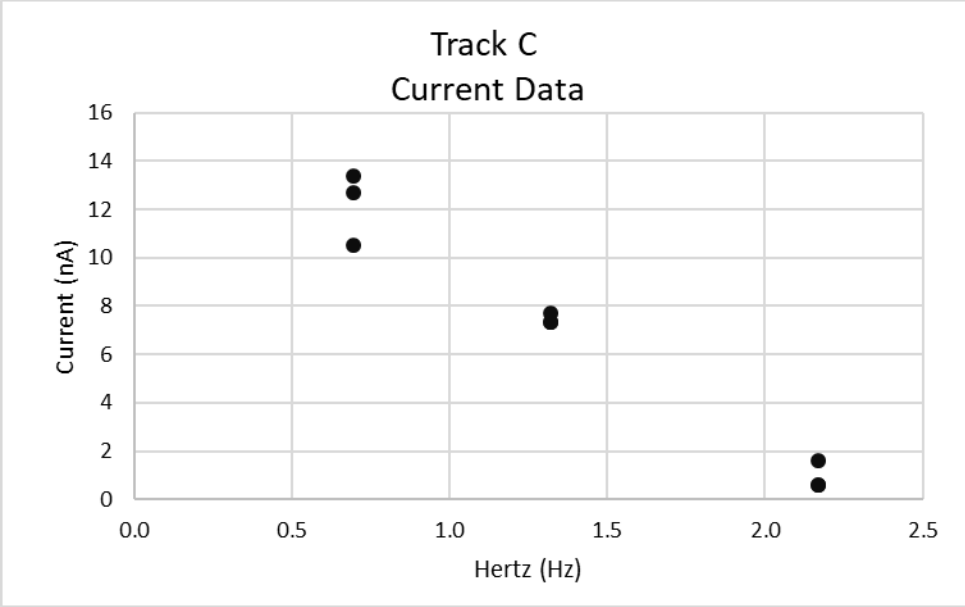
Track C
Current Data
Current (nA)
16
14
12
10
8
6
4
2
0
0.0
0.5
1.0
1.5
2.0
2.5
Hertz (Hz)

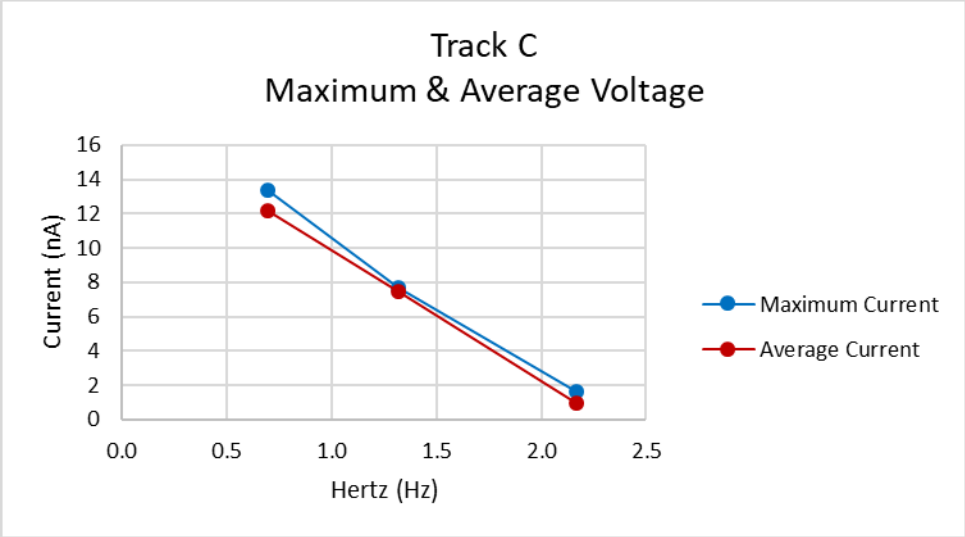
Track C
Maximum & Average Voltage
Current (nA)
16
14
12
10
8
6
4
2
0
0.0
0.5
1.0
1.5
2.0
2.5
Hertz (Hz)
Maximum Current
Average Current

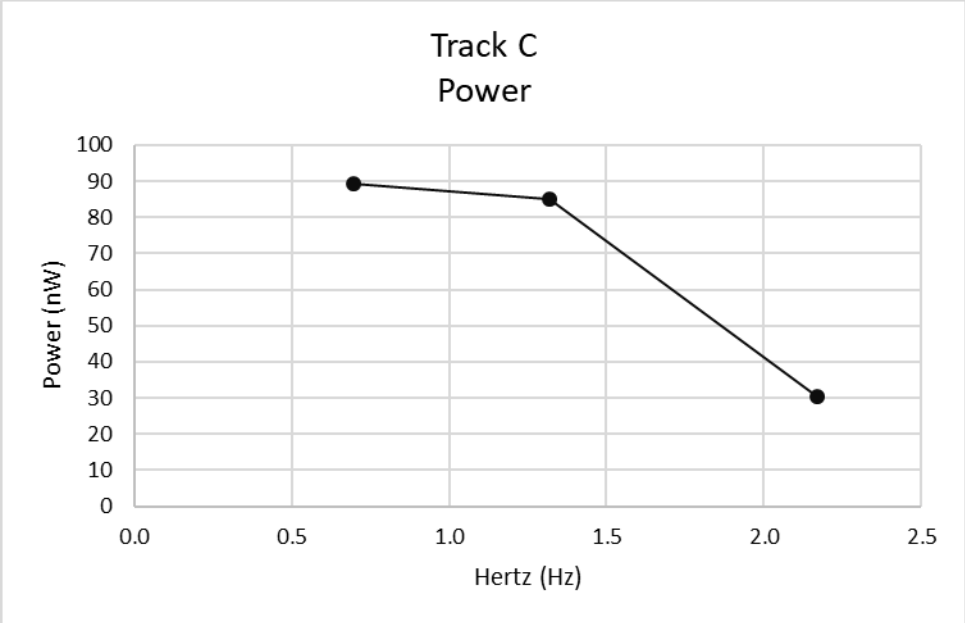
Track C
Power
Power (nW)
100
90
80
70
60
50
40
30
20
10
0
0.0
0.5
1.0
1.5
2.0
2.5
Hertz (Hz)

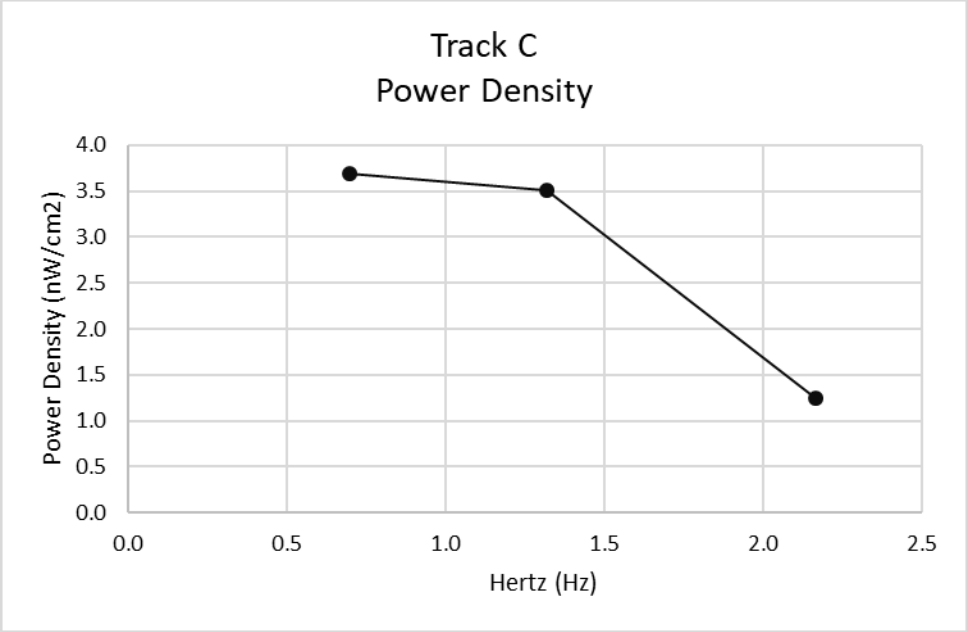
Track C
Power Density
Power Density (nW/cm2)
4.0
3.5
3.0
2.5
2.0
1.5
1.0
0.5
0.0
0.0
0.5
1.0
1.5
2.0
2.5
Hertz (Hz)

APPENDIX C. WAVE TANK RESULTS

This appendix includes some experimental data from the wave tank testing. The voltage data was collected by the Keysight DSO1052B digital oscilloscope and exported to a Microsoft Excel file where the graphs were produced. Current data was collected from the data storage memory of the Keithley 617 Electrometer and then transferred to Microsoft Excel. The minimum and maximum current values vs TENG frequency data at each of the five runs per frequency are shown. The average and maximum of the rectified maximum and minimum current values are graphed. The voltage data graphs depict the peak-peak AC voltage found twenty five runs conducted. Examples of the oscilloscope readings at each of the five frequencies are included.

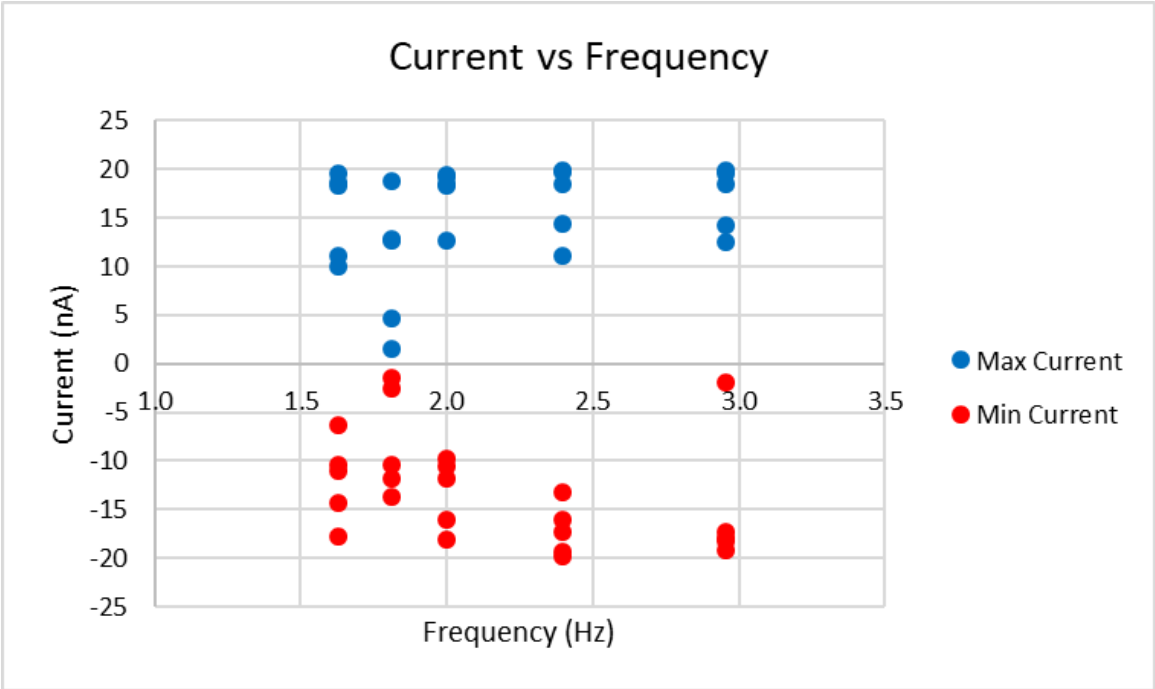
Current vs Frequency
Current (nA)
25
20
15
10
5
0
-5
-10
-15
-20
-25
1.0
1.5
2.0
2.5
3.0
3.5
Frequency (Hz)
Max Current
Min Current

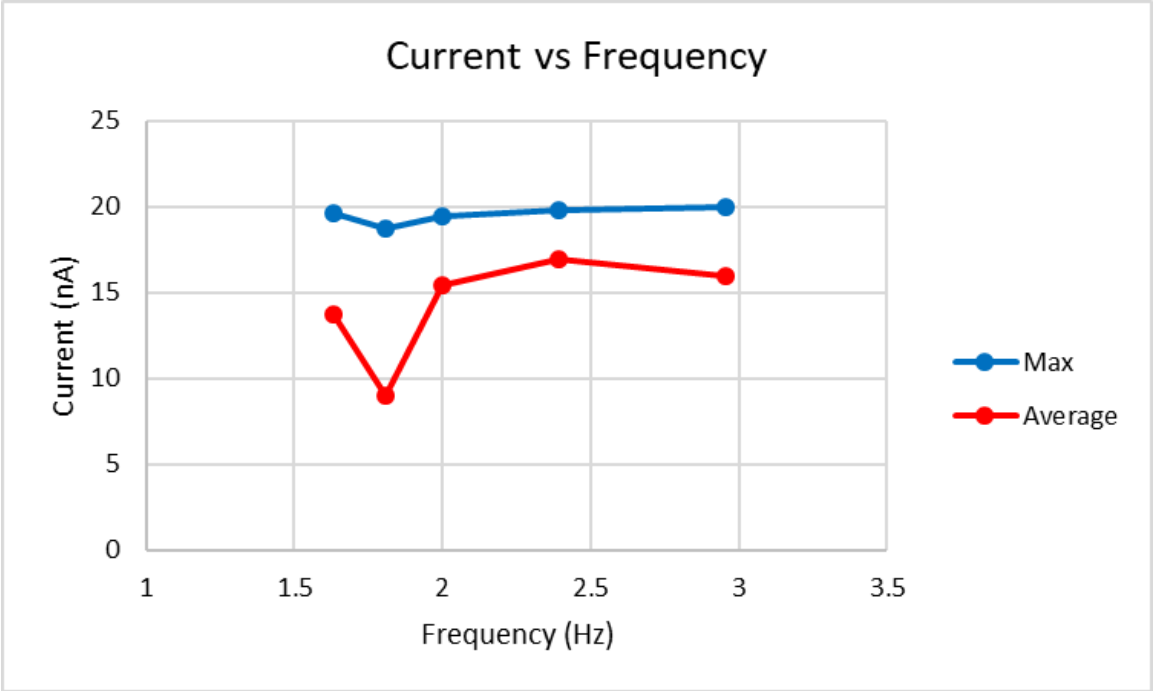
Current vs Frequency
Current (nA)
25
20
15
10
5
0
1
1.5
2
2.5
3
3.5
Frequency (Hz)
Max
Average

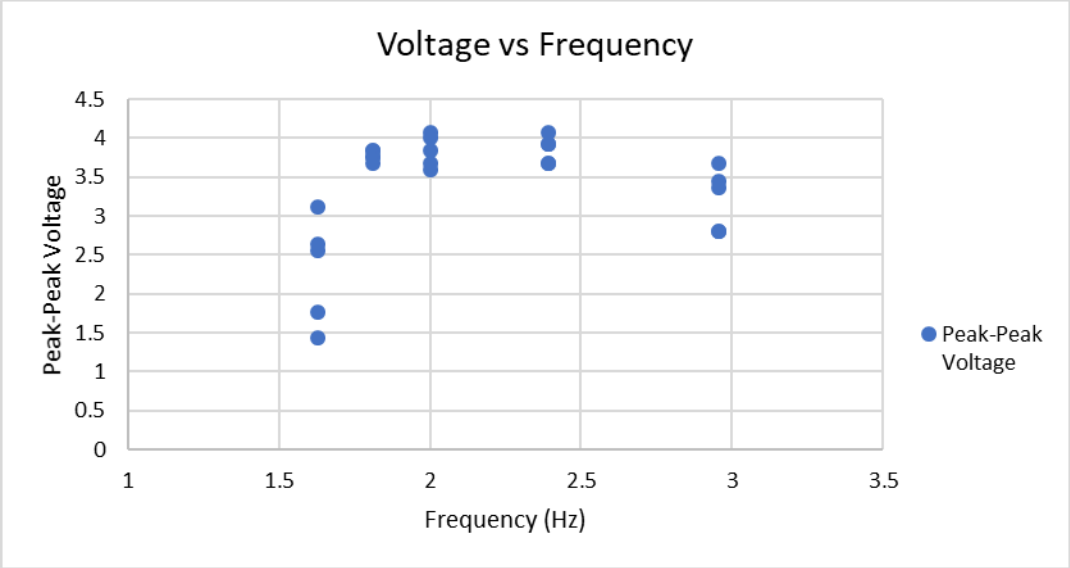
Voltage vs Frequency
Peak-Peak Voltage
4.5
4
3.5
3
2.5
2
1.5
1
0.5
0
1
1.5
2
2.5
3
3.5
Frequency (Hz)
Peak-Peak Voltage

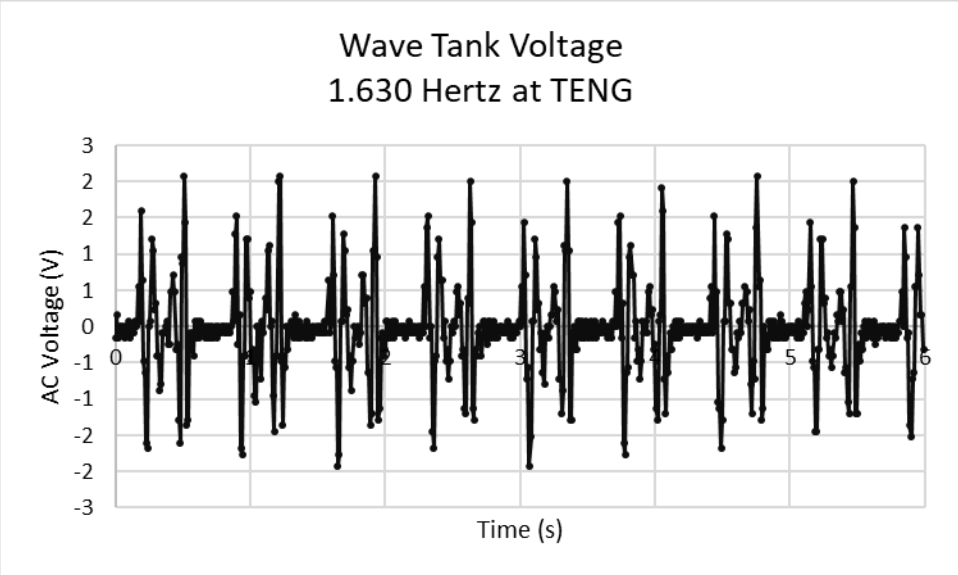
Wave Tank Voltage
1.630 Hertz at TENG
AC Voltage (V)
3
2
2
1
1
0
-1
-1
-2
-2
-3
0
3
5
6
Time (s)

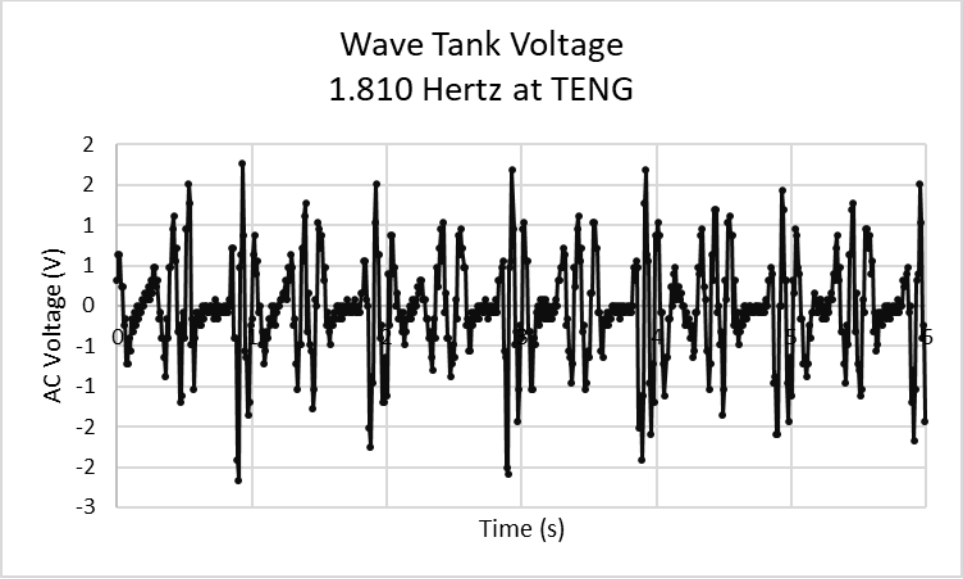
Wave Tank Voltage
1.810 Hertz at TENG
AC Voltage (V)
Time (s)

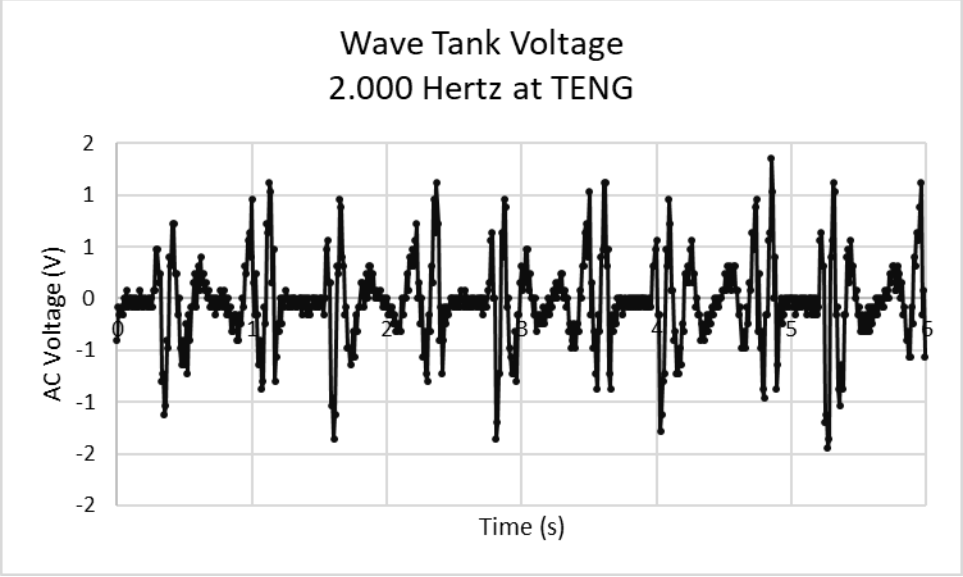
Wave Tank Voltage
2.000 Hertz at TENG
AC Voltage (V)
Time (s)

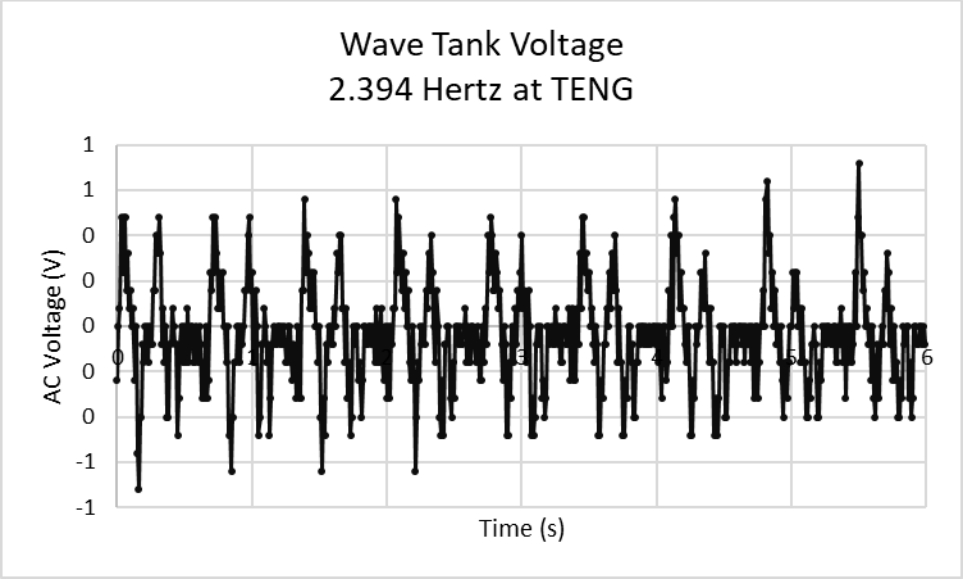
Wave Tank Voltage
2.394 Hertz at TENG
AC Voltage (V)
Time (s)

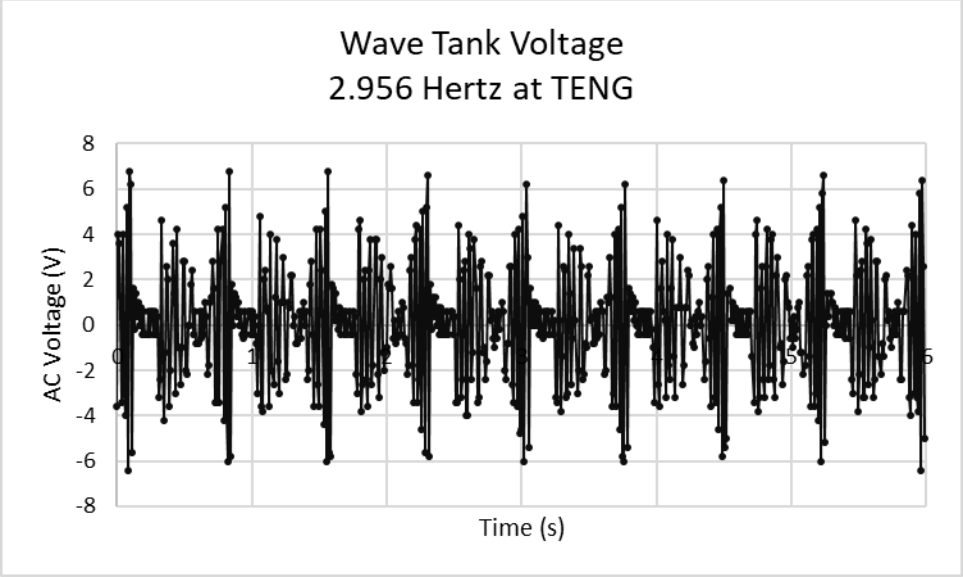
Wave Tank Voltage
2.956 Hertz at TENG
AC Voltage (V)
Time (s)

THIS PAGE INTENTIONALLY LEFT BLANK

LIST OF REFERENCES

[1] J. Chen, J. Yang, Z. Li, X. Fan, Y. Zi, Q. Jing, H. Guo, Z. Wen, K. Pradel, S. Niu, and Z. L Wang, "Networks of Triboelectric Nanogenerators For Harvesting Water Wave Energy: A Potential Approach Toward Blue Energy," ACS Nano, vol. 9, no. 3, pp. 3324–3331, Feb. 26, 2015.

[2] NASA Socioeconomic Data and Applications Center (SEDAC), "Gridded Population of the World v4." Accessed August 1, 2018, http://sedac.ciesin.columbia.edu/data/collection/gpw-v4

[3] Z. L. Wang, "Triboelectric Nanogenerators As New Energy Technology And Self-Powered Sensors – Principles, Problems And Perspectives," Faraday Discuss., vol. 176, pp. 447–458, Sept. 8, 2014.

[4] Z. L. Wang, "On Maxwell's Displacement Current For Energy And Sensors: The Origin Of Nanogenerators," Materials Today, vol. 00, no. 00, pp. 1–9, Jan. 2017.

[5] T. Jiang, Y. Yao, L. Xu, L. Zhang, T. Xia, and Z. Wang, "Spring-Assisted Triboelectric Nano Generator for Efficiently Harvesting Water Wave Energy,." Nano Energy, vol 31, pp.560-567, January 2017.

[6] Thethys, U.S. Department of Energy. "Annapolis Tidal Station." Accessed March 15, 2019. [Online]. Available: https://tethys.pnnl.gov/annex-iv-sites/annapolis-tidal-station

[7] M. Seol, Y. Choi, J. Han, S. Jeon, and M. Meyyappan, "Floating Oscillator-Embedded Triboelectric Generator for Versatile Mechanical Energy Harvesting," Scientific Reports, Nov. 10, 2015.

[8] L. Huang, W. Xu, G. Bai, M. Wong, Z. Yang, and J. Hao, "Wind Energy and Blue Energy Harvesting Based on Magnetic-Assisted Noncontact Triboelectric Nano Generator," Nano Energy, vol 30, pp.36-42, December 2016.

[9] Z. Lin, G. Cheng, X. Li, P. Yang, X Wen, and Z. Wang, "A Multi-Layered Interdigitive-Electrodes-Based Triboelectric Nano Generator for Harvesting Hydropower," Nano Energy, vol 15, pp.2211-2855, July 2015.

[10] L. Xu, Y. Pang, C. Zhang, T. Jiang, X. Chen, J. Luo, W. Tang, X. Cao, and Z. L. Wang, "Integrated Triboelectric Nanogenerator Array Based On Air-Driven Membrane Structures For Water Wave Energy Harvesting," Nano Energy, vol. 31, pp.351-358, Nov. 17, 2016.

[11] Z. L.Wang, L. Zhong, Y. Yao. T. Jiang, L. Zhang, Z. Chen, Z. Gao, "Charging System Optimization of Triboelectric Nanogenerator for Water Wave Energy Harvesting and Storage," ACS Applied Materials & Interfaces, vol. 8, pp. 21398−21406, 2016.

[12] Z-H. Lin, G. Cheng, L. Lin, S. Lee, and Z. L Wang, "Water-Solid Surface Contact Electrification And Its Use For Harvesting Liquid-Wave1 Energy," Angew. Chem., vol.52, pp. 12545– 12549, 2013.

[13] G. Cheng, Z-H Lin, Z-I. Du, and Z. L. Wang, "Simultaneously Harvesting Electrostatic And Mechanical Energies From Flowing Water By A Hybridized Triboelectric Nanogenerator," ACS Nano, vol. 8, no. 2, pp. 1932–1939, Jan. 27, 2014.

[14] Q. Jiang, Y. Han, W. Tang, H. Zhu, C. Gao, S. Chen, M. Willander, X. Cao, and Z Wang, "Self-Powered Seawater Desalination and Electrolysis Using Flowing Kinetic Energy," Nano Energy, vol. 15, pp. 266–274, July 2015.

[15] G. Zhu, Y. Su, P. Bai, J. Chen, Q. Jing, W. Yang, and Z. L. Wang, "Harvesting Water Wave Energy by Asymmetric Screening of Electrostatic Charges on a Nanostructured Hydrophobic Thin-Film Surface," ACS Nano, vol. 8, no. 6, pp. 6031–6037, Apr. 18, 2014.

[16] National Oceanic and Atmospheric Administration, "National Data Buoy Center." Accessed March 15 2018. [Online]. Available: http://www.ndbc.noaa.gov/rmd.shtml

[17] C. Wu, A. C. Wang, W. Ding, H. Guo, and Z. L. Wang, "Triboelectric Nanogenerator: A Foundation of the Energy for the New Era," Advanced Energy Materials, vol. 9, no. 1, pp. 1802906, 2019.

[18] A. F. Falcão, "Wave Energy Utilization: A Review Of The Technologies," Renewable and Sustainable Energy Reviews, vol. 14, no. 3, pp. 899–918, Oct. 22, 2008.

[19] S. Niu, Y. Liu, S. Wang, L. Lin, Y. Zhou, Y. Hu, and Z. L. Wang, "Theory of Sliding-Mode Triboelectric Nanogenerators," Advanced Materials, vol. 25, no. 43, pp. 6184–6193, 2013.

[20] Q. J. Liang, X. Yan, X. Liao, S. Cao, X. Zheng, H. Si, S. Lu, and Y. Zhang, "Multi-Unit Hydroelectric Generator Based On Contact Electrification And Its Service Behavior," Nano Energy, vol.16, pp. 329–338, Jul. 18, 2015.

[21] Q. Liang, X. Yan, X. Liao, and Y. Zhang, "Integrated Multi-Unit Transparent Triboelectric Nanogenerator Harvesting Rain Power For Driving Electronics," Nano Energy, vol. 25, pp. 18–25, Apr. 20, 2016.

[22] Q. Liang, X. Yan, Y. Gu, K. Zhang, M. Liang, S. Lu, X. Zheng, and Y. Zhang, "Highly Transparent Triboelectric Nanogenerator For Harvesting Water- Related Energy Reinforced By Antireflection Coating," Sci. Rep., vol. 5, pp. 9080, Mar. 13, 2015.

[23] Q. Zhang, Q. L. Liang, Q. Liao, F. Yi, X. Zheng, M. Ma, and F. Gao, Y. Zhang, "Service Behavior Of Multifunctional Triboelectric Nanogenerators.," Adv. Mater. vol. 29, pp. 1606703, 2017.

[24] X. Wang, Z. Wen, H. Guo, C. Wu, X. He, L. Lin, X. Cao, X. and Z. L. Wang, "Fully Packaged Blue Energy Harvester by Hybridizing a Rolling Triboelectric Nanogenerator and an Electromagnetic Generator," ACS Nano, vol. 10, no. 12, pp. 11369-11376, Nov. 22, 2016.

[25] S. Lee, J. Chung, D. Y. Kim, J-Y. Jung, S. H. Lee, and S. Lee, "Cylindrical Water Triboelectric Nanogenerator via Controlling Geometrical Shape of Anodized Aluminum for Enhanced Electrostatic Induction," ACS Applied Materials & Interfaces, vol. 8, no. 38, pp. 25014-25018, Sept. 13, 2016.

[26] Y. Xi, H. Guo, Y. Zi, X. Li, J. Wang, J. Deng, S. Li, C. Hu, X. Cao, and Z. L. Wang "Multifunctional TENG for Blue Energy Scavenging and Self-Powered Wind Speed Sensor," Advanced Energy Materials, vol. 7, no. 12, pp.1602397, 2017.

[27] Y. Su, X. Wen, G. Zhu, J. Yang, J. Chen, P. Bai, Z. Wu, Y. Jiang, and Z. L. Wang, "Hybrid Triboelectric Nanogenerator For Harvesting Water Wave Energy And As A Self-Powered Distress Signal Emitter," Nano Energy, vol. 9, pp. 186–195, Aug. 6, 2014.

[28] M-L. Seol, J-W. Han, D_I. Moon, K. J. Yoon, C. S. Hwang, and M. Meyyappan, "All-Printed Triboelectric Nanogenerator," Nano Energy, vol. 44, pp. 82–88, Nov. 28, 2017.

[29] S. Reilly, "Triboelectric Nanogenerator with Ocean Wave Energy," Calhoun Institutional Archive of the Naval Postgraduate School. June 2019.

THIS PAGE INTENTIONALLY LEFT BLANK

INITIAL DISTRIBUTION LIST

1. Defense Technical Information Center
   Ft. Belvoir, Virginia

2. Dudley Knox Library
   Naval Postgraduate School
   Monterey, California